Modulation of nuclear lamin-chromatin interactions by external cues

Anna Frida Forsberg

Thesis for the degree of Philosophiae Doctor (PhD)

Department of Molecular Medicine
Institute of Basic Medical Sciences
Faculty of Medicine
University of Oslo
Norway

2019

TABLE OF CONTENTS

ACKNOWLEDGMENT

First I would like to thank my main supervisor, Professor Philippe Collas. Thank you for giving me the opportunity to perform my PhD in your lab. I am grateful for the support and advice you have given which have helped me to develop as a scientist. I would also like to thank my co-supervisor Dr. Annaël Brunet. Your invaluable guidance have helped me become confident in my scientific reasoning and encouraged me to continue my scientific endeavor. In addition, I would like to thank my previous supervisors Dr Anja Oldenburg, and Professor Jan Øvind Moskaug who unfortunately no longer is with us.

I would like to thank my co-authors Tharvesh, Qiong and Thomas for fruitful discussions and help to complete and finish my papers. A special thanks goes to Sissel and Anita who have been invaluable in teaching me and helping me develop my technical skills in the laboratory.

For making life in the lab easier and for creating a movie and badminton club I would like to thank Torunn, Ninnin, Akshay, MO, Monika, Theresa and Rua. I would also like to thank new and old members of the Collas lab: Anja, Erwan, Coen, Nolwenn, Jonas, Sumithra, Kristin, Anna, Aurélie, Julia, Dunia and Louise.

To my sisters in science: Julia, Ida, Yvi, Vita and Madde I would like to say thank you. Even when we take very different paths within the science community, your sisterhood is what gives me hope for the future of Science.

A very special thanks to Brooke my dear friend and support network from down under. Thank you for our long skype conversations and whose advice has helped me stay on this path. In addition, I would like to thank my close friends Helene, Emelie, Elin and Therese you have been with me from the beginning and your encouragement has helped me all throughout this adventure. Finally, I would like to thank my family and especially my parents, you have supported me as I have traveled all over the world chasing my dreams and thanks to your unwavering support and love it has all been made into reality. Last, I would like to thank Jørgen whose support during the last sprint of my PhD has been priceless.

LIST OF PUBLICATIONS

Paper I

Frida Forsberg, Annaël Brunet, Tharvesh M. Liyakat Ali and Philippe Collas. Interplay of lamin A and lamin B LADs on the radial positioning of chromatin. *Nucleus* **10**, 7-20, 2019

Paper II

Annaël Brunet*, Frida Forsberg*, Qiong Fan, Thomas Sæther and Philippe Collas. Nuclear lamin B1 interactions with chromatin during the circadian cycle are uncoupled from periodic gene expression. *Frontiers in Genetics* **10**:917, 2019

*shared first authorship

LIST OF ABBREVIATIONS

3C	chromatin conformation capture
3D	three-dimensional
Ac	acetylated
BAF	barrier-to-autointegration factor
BMP	bone morphogenic protein
bp	base pairs
ChIP	chromatin immunoprecipitation
cLAD	constitutive LAD
CsA	cyclosporin A
CTCF	CCCTC-binding factor
DamID	DNA adenine methyltransferase identification
DNA	deoxyribonucleic acid
eGFP	enhanced green fluorescent protein
ER	endoplasmic reticulum
ESC	embryonic stem cell
FISH	fluorescence *in situ* hybridization
FPLD2	Dunnigan-type familial partial lipodystrophy
FRAP	fluorescence recovery after photobleaching
FTase	farnesyltransferase
FTI	farnesyltransferase inhibitor
H3K4me1	histone 3 lysine 4 mono-methylation
HAT	histone acetyltransferase
HGPS	Hutchinson-Gilford progeria syndrome

HP1	heterochromatin protein 1
Ig	immunoglobulin
INM	inner nuclear membrane
K	lysine
KASH	Klarsicht, Anc-1, Syne-1 homology
LAD	lamina associated domain
LAP	lamina-associated polypeptide
LAS	lamina-associated sequence
LBR	lamin B receptor
LEM	LAP2, emerin, MAN1
LINC	linker of nucleoskeleton and cytoskeleton complex
^{m6}A	adenine-6-methylation modification
me1	monomethylated
me2	dimethylated
me3	trimethylated
Mb	megabases
MNase	micrococcal nuclease
NAD	nucleolus associated domain
NET	nuclear envelope transmembrane protein
ONM	outer nuclear membrane
PcG	Polycomb group
PML	promyelocytic leukemia
PRC	Polycomb repressor complex
PTM	post-translational modification

R	arginine
RNA	ribonucleic acid
RNA pol II	RNA polymerase II
SCN	suprachiasmatic nucleus
S	serine
SUN	Sad1 Unc-84
TAD	topologically associated domain
TGFβ	transforming growth factor beta
TSS	transcription start site
vLAD	variable LAD
W	tryptophan

1. INTRODUCTION

In a eukaryotic cell, the nucleus is separated from the cytoplasm by the nuclear envelope, a protective barrier and regulator of the nuclear genome. The nuclear envelope is composed of a double nuclear membrane perforated by nuclear pores allowing import and export of proteins from and into the cytoplasm, and export of ribonucleic acids (RNAs). The outer nuclear membrane (ONM) contains many proteins also found in the endoplasmic reticulum, with which it is continuous. The inner nuclear membrane (INM), in contrast, harbors a unique set of proteins, some of which can interact with chromosomes. Subjacent to the INM is the nuclear lamina, a meshwork of A- and B-type nuclear lamins. The nuclear lamina regulates many nuclear functions including replication of deoxyribonucleic acid (DNA), gene expression and signaling pathways, and contributes to the radial (center-to-periphery) arrangement of the genome through interactions with chromatin. Interactions of both A- and B-type lamins with chromatin establish heterochromatic chromatin domains called lamina-associated domains, or LADs. LADs are overall well conserved between cell types, while others are more variable. Interestingly, LADs formed by chromatin interactions with A-type lamins (referred to here as A-LADs) and B-type lamins (B-LADs) display distinct characteristics and dynamics. Several studies, including our own, indicate that LADs are dynamic and may be detected at the nuclear periphery and in the nuclear interior. However, the interplay between A-LADs and B-LADs in chromatin organization has not been explored until work presented in this thesis was initiated (**Paper I**).

Moreover, recent although scarce evidence suggests that a subset of interactions of chromatin with the nuclear lamina could be regulated in a circadian manner – that is, with a 24 h periodicity, potentially adding a temporal component to the regulation of lamin-chromatin interactions. We have investigated whether LADs display periodic interactions with nuclear lamins during the circadian cycle, a central regulator of many physiological processes in mammals (**Paper II**).

1.1 CHROMATIN ORGANIZATION IN THE EUKARYOTIC NUCLEUS

Hereditary genetic information is contained in the genome, of which ~2% are sequences (genes) encoding RNAs translated into proteins necessary for all cellular processes. Approximately ~98% of the genome contains non-protein-coding sequences such as regulatory elements

(promoters and enhancers) that regulate gene expression, DNA repeats and sequences encoding RNAs not translated into proteins (noncoding (nc)RNAs), including small interfering RNAs, enhancer RNAs and long noncoding RNAs. Importantly, regulatory elements and other inter-genic sequences harbor a multitude of DNA motifs acting as binding sites for transcription factors, which also contribute to the regulation of gene expression[1].

Genome organization is an important component of gene regulation. The most basic mammalian genome organization is along the linear genome. The genome can be divided into distinct regions depending on DNA base composition. Stretches of sequences are adenine- and thymidine- (AT)-rich or guanine- and cytosine- (GC)-rich compared to the average base composition along the genome[2,3]. Typically, AT-rich regions are of low gene density while GC-rich areas harbor a higher gene density than genome average (which is ~8 genes/Mb in the human genome). Genes in gene-dense areas are also overall more actively transcribed than genes in gene-poor areas[4,5]. This highlights that DNA sequence plays an important role in the global organization of the genome and gene expression output.

In the eukaryotic nucleus, the genome is organized in chromatin, an assembly of DNA and proteins, which adopts a conformation enabling packaging of all chromosomes into the nucleus. Chromatin is a flexible structure, enabling DNA replication and transcription. The basic building block of chromatin is the nucleosome, a unit consisting of 147 base pairs (bp) of double-stranded DNA wrapped around a protein octamer made up of two copies of the histone proteins H2A, H2B, H3 and H4[6–8] (**Fig. 1A,B**). Each chromosome is built as an array of multiple nucleosomes connected through 10-90 bp of linker DNA. To stabilize DNA wrapped around the histone octamer, linker histone H1 (or H5 in ovarian species) bind to the linker DNA (**Fig. 1B**). These linker histones enable a folding of chromatin resulting in the organization of nucleosome arrays into a ~30 nm thick chromatin fiber[9,10] (**Fig. 1B**). During the cell cycle, chromatin exists in various forms of compaction: interphase chromatin is the least condensed whereas during prophase and throughout mitosis chromatin compacts to an extent that resolves each individual chromosome in metaphase[1].

Chromatin compaction is modulated by two main classes of epigenetic modifications – that is, chemical modifications of DNA and histones which regulate gene expression without altering DNA sequence; these include DNA methylation, the addition of a methyl (-CH3) group on cytosines in CG dinucleotides, and post-translational modifications (PTMs) of histones. Histones can be modified in the core, the C-terminal domain, and the N-terminal tail which protrudes from nucleosomes. Over 100 different histone PTMs have been reported to occur on

specific amino acids, including acetylation, phosphorylation, methylation and ubiquitination, perhaps the best characterized PTMs to date[11]. In particular, histones H3 and H4 can be acetylated (ac) or mono-, di- and trimethylated (me1/2/3) at several lysine (Lys, or K in single-letter amino acid code; such as K4, K9, K16 or K27) (**Fig. 1A**) and arginine (e.g. Arg2, or R2) residues[12]. Importantly for the regulation of chromatin compaction and gene expression, histone PTMs are combinatorial[13]; these PTM combinations can be highly complex and interestingly have led to the development of machine learning algorithms aiding in the definition of so-called "chromatin states", i.e. recurrent combinations of histone PTMs along the genome[14]. Moreover, cross-talks between neighboring PTMs regulate either other PTMs and/or binding of chromatin remodeling enzymes and transcription factors[15,16]. Changes in histone acetylation and methylation can affect transcriptional activity by inhibiting or allowing transcription factor access to gene regulatory elements. Histone PTMs (as does DNA methylation) can also affect chromatin conformation by allowing binding of chromatin modifiers that elicit chromatin decompaction or compaction, in turn leading to promotion or inhibition of transcription[15,17]. Histone PMTs have been extensively profiled throughout the genome by chromatin immunoprecipitation (ChIP) using antibodies specific to these PTMs (e.g. antibodies to histone H3 lysine 4 trimethylated [H3K4me3]) and high-throughput sequencing of the precipitated DNA. Histone PTM profiling has resulted in integrative analyses of epigenomes (an ensemble of epigenetic PTMs) in well over 100 different cell types from a variety of tissues[18–20]. Mapping of epigenomes constitutes an important milestone in our understanding of genome function, because, through annotations of genomic elements (such as enhancers, active enhancers, potentially active enhancers, enhancers in gene bodies and bivalent promoters), one can ascribe functionality to these genomic elements.

In the interphase nucleus, chromatin can be divided into two major levels of compaction distinguishable by electron microscopy (**Fig. 1C**). Euchromatin is not electron-dense because it is predominantly non-compacted and accessible to e.g. nucleases[21] (which can cut DNA within these regions) and transcription factors. Euchromatin is mainly gene-rich and transcribed or shows potential for transcription; it is promptly decondensed when cells exit mitosis in early G1-phase and is replicated early in S-phase[22,23]. Histone PTMs characterizing euchromatin are generally found in regions that regulate transcription. For example, H3K4me1 characterizes enhancers, while active enhancers (enhancers of transcriptionally active cognate genes) are also marked by H3K27ac[24]. H3K4me3 is found at the transcription start site (TSS) and promoter of active genes[25] (**Fig. 1D**) and interestingly, co-enrichment of promoters with the repressing PTM

H3K27me3[26] generates a "bivalent" promoter state which marks inactive developmentally-regulated genes that can be activated later in development or during cell differentiation[27,28]. In contrast to euchromatin, heterochromatin mainly consists of electron-dense compact regions (**Fig. 1C**) and are replicated in late S-phase. Most heterochromatin contains gene-poor regions with a limited number of transcribed genes[22,23]. It largely consists of nucleosomes that are hypoacetylated (favoring tight electrostatic interactions between the negatively charged DNA and positively charged histones) and enriched in H3K9me2 or H3K9me3, hallmarks of constitutive heterochromatin[11,23]. H3K27me3 in contrast characterizes facultative heterochromatin, which corresponds to regions that can be transcribed after losing this PTM[29], for example in the promoters of developmentally regulated genes (**Fig. 1D**). Chromatin accessibility, or the lack thereof, is dependent on histone modifications and of numerous proteins, such as genome structural proteins (e.g. CCCTC-binding factor [CTCF] and cohesin), transcription factors, histone modifiers and chromatin remodeling enzymes that can bind to and alter how compact nucleosomes are arranged along the chromatin fiber.

Chromatin assembly therefore plays an important role in the regulation of gene expression[30,31]. In addition, gene expression is affected at a higher order by how chromatin is organized in the three-dimensional (3D) nucleus space.
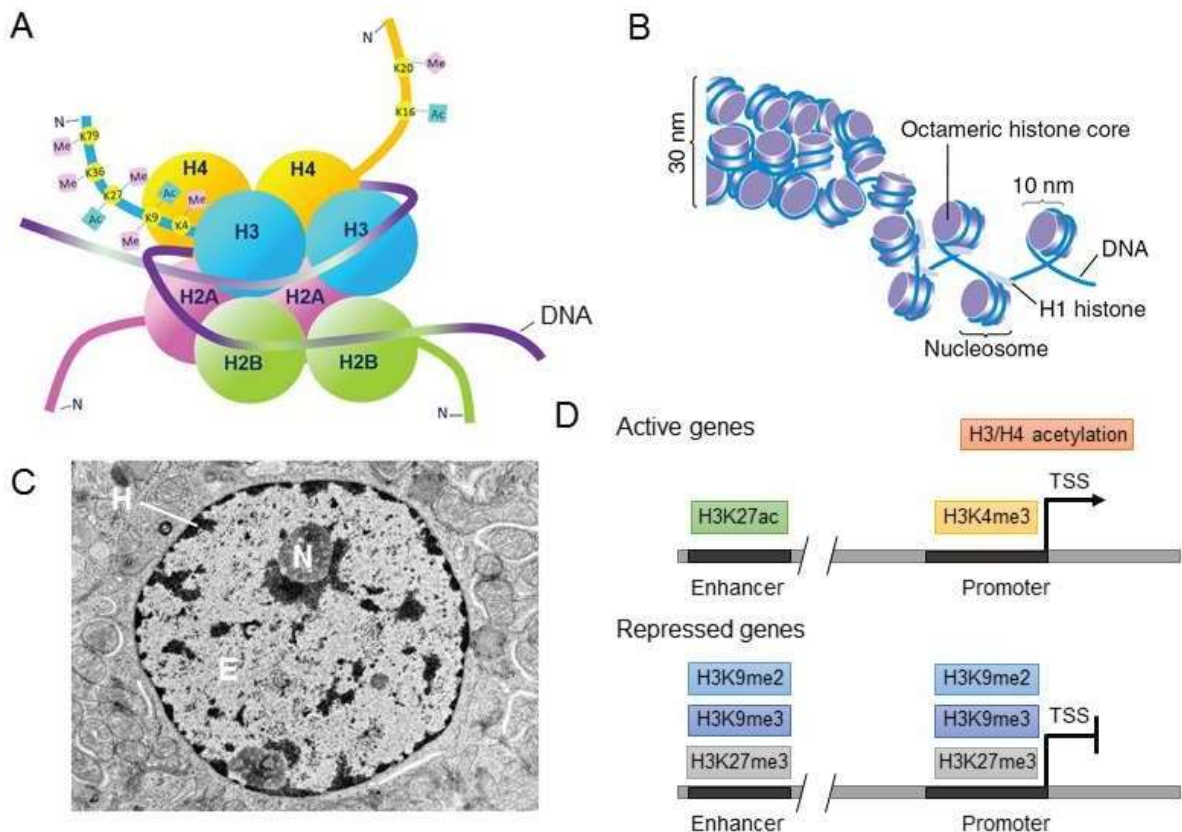
Figure 1. Chromatin assembly. A. Schematic representation of a nucleosome. Lysine (K) residues in the N-terminal tails of, here, H3 and H4, are represented with PTMs such as the addition of acetyl (Ac) and methyl (Me) groups. From[8] by permission of Oxford University Press. **B.** Chromatin compaction levels. Adapted from[1] with copyright permission. **C.** Electron micrograph of an interphase human cell nucleus; N, nucleolus; H, heterochromatin; E, euchromatin. Adapted from http://medcell.med.yale.edu/histology/cell_lab/euchromatin_and_heterochromatin.php. **D.** Overview of histone modifications enriched in the enhancer and promoter of active (arrow) and repressed (bar) genes. The gray bar represents the DNA sequence.

1.2 HIERARCHICAL ORGANIZATION OF CHROMATIN IN THE MAMMALIAN NUCLEUS

Chromatin organization in the nucleus is paramount for the regulation of gene expression. The genome is intricately 3-dimensionally folded in the nucleus. 3D folding of chromatin is critical for the proper orchestration of gene expression during development, for physiological processes and for tissue homeostasis, both at the gene locus level and at a larger, nucleus-wide, scale. In addition, it is essential for keeping the balance between healthy and pathological states[32]. Studies involving various cell types and ensemble vs. single-cell molecular analyses, together with combinations of methods such as high-throughput sequencing, bioinformatics, microscopy imaging[33–35] and computational modeling[36,37] provide a comprehensive picture of genome conformation over a range of scales (from gene locus to whole genome level) and resolutions (from megabase down to kilobase resolution)[38–41]. Moreover, these studies reveal variations in

chromatin topologies between cell types and between cells in a population, attesting of underlying dynamic processes[42,43]. So clearly, chromatin is not static.

An overall feature of spatial genome organization is a hierarchical and modular conformation. In mammalian nuclei, individual chromosomes occupy well-defined territories and a radial (nuclear center-to-periphery) placement which is strikingly rather well conserved between cell types[44]. Spatial chromatin organization is also dependent on multiple factors, which occupy space (molecular crowding) and generate "bulk", physically excluding chromatin from certain regions in the nucleoplasm and/or act as anchors for chromatin. Some of these factors assemble into foci or nuclear bodies, which carry out specific functions. One example is nuclear speckles, which by concentrating mRNA splicing factors, play a role in the regulation of gene expression through facilitation of constitutive and alternative splicing[45]. Another example is promyelocytic leukemia (PML) nuclear bodies, which contain up to one hundred proteins and are involved in many nuclear functions including regulation of cell growth, tumor suppression, protein processing and anti-viral immune functions[46]. The largest and perhaps best characterized nuclear body is the nucleolus, where ribosomal DNA is transcribed, and ribosome units are assembled[47].

A role of PML bodies and nucleoli as chromatin anchors comes from evidence that chromatin domains, with specific characteristics, are associated with these structures. Work from our laboratory has shown that PML proteins (not necessarily in the form of PML bodies *per se*) organize large H3K9me3-rich heterochromatic domains referred to as PML-associated domains (or PADs)[48]. Furthermore, heterochromatin enriched in H3K9me2 and H3K9me3 associates with the nucleolus in the form of nucleolus-associated domains, or NADs[49–52]. The existence of nuclear bodies suggests that it is more efficient for a cell to concentrate factors necessary for specific functions into foci. In addition, it suggests that it may similarly be more efficient to concentrate parts of chromatin at or near foci to carry out functions such as transcription or splicing than spreading proteins in charge of such processes along chromatin. Nuclear bodies may have evolved as physical entities where chromatin regions of similar characteristics (homotypic domains) can aggregate (e.g. by phase separation[53–56]) and form defined domains in the genome. Additional chromatin domains, which anchor chromatin primarily at the nuclear periphery, are lamina-associated domains (LADs). Given the importance of LADs in the work presented in this thesis, these are discussed in a separate section.

1.2.1 Chromosome territories

Chromatin positioning in the 3D nuclear space is not random. Electron microscopy, high-resolution light microscopy and fluorescence *in situ* hybridization (FISH) show that chromatin belonging to the same chromosome is preferentially confined into discrete regions forming chromosome territories[33,44,57] (**Fig. 2**). Using 24 chromosome paint probes in FISH experiments, it has been possible to label all chromosomes in human fibroblast nuclei[33] (**Fig. 2A,B**). This revealed not only chromosome territories, but also that these territories are radially arranged in the nucleus[33]. Strikingly, they are organized depending on size, with large and more gene-poor chromosomes positioned towards the nuclear periphery while smaller and more gene-rich chromosomes are more centrally placed (**Fig. 2**). One exception is human chromosome 18, which is small, gene-poor and located towards the periphery[33,57,58] (**Fig. 2C**). Thus, not only size but also gene density seems to be indicative of the radial positioning of chromosomes. Due to the current lack of fixed reference points in the mammalian nucleus (unlike in yeast where the spindle pole body and nucleolus have been used as such in genome modeling studies[59]), the absolute positioning of chromosome territories has yet been elucidated. Nevertheless, the radial placement of chromosome territories creates topological configurations that allow a regulation of nuclear processes in space and time, such as regulation of chromosomal interactions (described below), regulation of chromosome interactions with intranuclear structures (such as the nuclear envelope), DNA replication (early S-phase replication in the nuclear center vs. late S-phase replication at the nuclear periphery) and gene expression (overall repressed domains at the nuclear periphery and overall active domains in the nucleus center)[60].
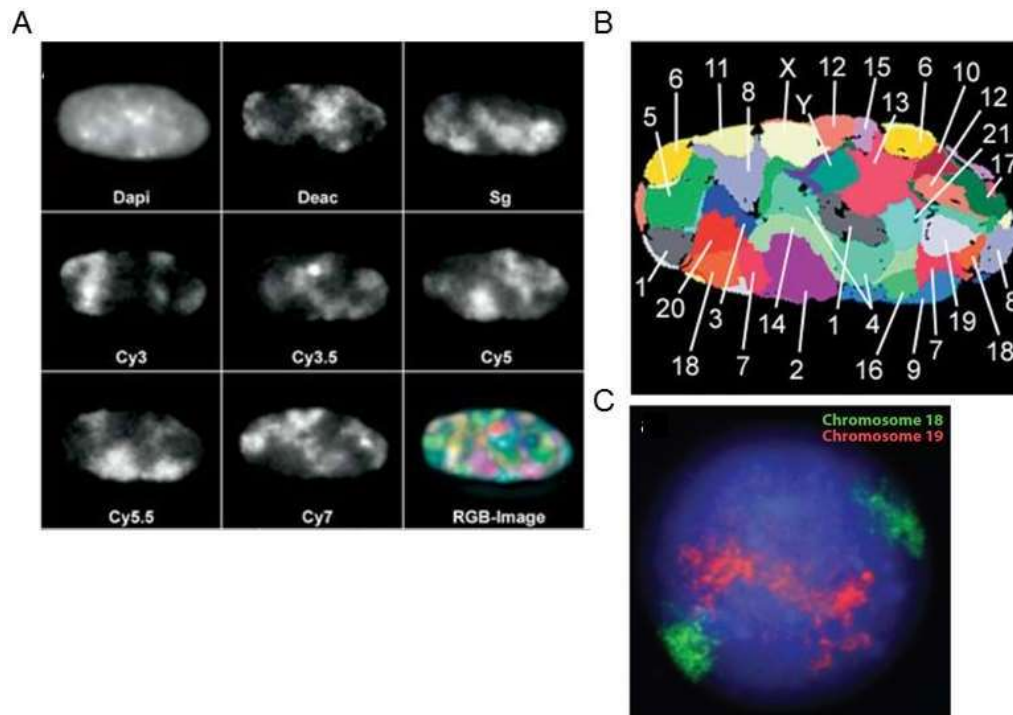
Figure 2. Chromosome territories in the interphase nucleus. A. Seven channels (diethylaminocoumarin (Deac), Spectrum Green (SG), and the cyanine dyes Cy3, Cy3.5, Cy5) each showing a subset of chromosome territories. Bottom right: RGB image of the superposition of all seven channels show chromosome paints of all 24 chromosomes in a human fibroblast nucleus. Republished from[33] with copyright permission under the creative commons attribution (CC BY) license. **B.** Color representation of all chromosome territories detectable in a human fibroblast nucleus**.** Republished from[33] with copyright permission under the creative commons attribution (CC BY) license. **C.** FISH image of chromosome 18 (green) and chromosome 19 (red) in a human nucleus. Note the striking peripheral and central localization of chromosomes 18 and 19, respectively. Republished with permission of Annual Reviews, Inc from[58]**.**

1.2.2   Compartments and topologically associated domains

Due to advancements in chromatin conformation capture (3C) methods, multiple studies have been able to interrogate genome-wide chromosomal interactions. 3D techniques aim to capture snapshots of interactions between genome regions in a cell population[61] and more recently, in single cells[62]. One 3C-based technique is Hi-C[61]. In Hi-C, chromatin is crosslinked and digested with a restriction enzyme (a four- or six-base pair cutter) which generates restriction fragments. The 5' ends of these fragments are filled with biotin and ligated under dilute conditions. The ligated DNA is sheared, proteins are digested and the biotin containing fragments are affinity-isolated with streptavidin beads and sequenced[61]. Paired-end sequencing and mapping to a reference genome enables identification of pair-wise chromosomal interactions, reflecting regions that are in close spatial proximity. The result of a Hi-C experiment is a large matrix of interaction frequencies, often shown as a heat map, between all regions of the genome in the cell population studied (**Fig. 3A**). Hi-C data concur in that

8

proximal interactions are statistically more frequent than long-range interactions, and intrachromosomal contacts largely dominate over inter-chromosomal contacts[38,39,61].

Analysis of Hi-C data, supported by microscopy studies[34,35,40,41,63], suggests a hierarchical organization of the genome. At the multi-megabase scale, the genome can be classified into two types of compartments based on principle component analysis of Hi-C data, where chromatin in each compartment preferentially interacts with chromatin within the same compartment[38,61,64] (**Fig. 3 A,B**). Depending on chromatin compaction, compartments have been divided into accessible ("open") and transcribed A compartments, and into dense ("closed") and inactive B compartments[42,65]. Several subtypes of B compartments (B1, B2, B3 and B4) have also been reported based on their composition in histone modifications (including H3K9me3 and H3K27me3) and their enrichment in RNA polymerase II (RNA pol II)[65]. B1 compartments are characterized by H3K27me3 and replicate during the middle of S-phase and are considered as facultative heterochromatin. B2 compartments lack H3K27me3 marks but are enriched in LADs and NADs. B3 compartments lack H3K27me3, nuclear lamina and NAD enrichment. The B4 compartment represents only a handful of chromatin regions and are enriched in both active (H3K36me3) and repressive (H3K9me3 and H3K20me3) chromatin marks[65]. Similarly, A compartments can be divided into A1 and A2 sub compartments. Both A-compartments are depleted of the nuclear lamina and NADs and are enriched in H3K36me3, H3K79me2, H3K27ac and H3K4me1. A1 compartments finish replicating during early S-phase whereas A2 compartments replicate until the middle of S-phase. In addition, A2 compartments can be associated with H3K9me3 and harbor a lower GC content compared to A1 compartments[65]. Within A and B compartments, topologically associated domains (TADs) (**Fig. 3A,B**) are defined as regions with a high frequency of chromosomal contacts, while contacts are less frequent between adjacent TADs; these observations have been corroborated by FISH[38,39,61,64]. In mouse and human cells, the linear size of TADs ranges from 500 to 1000 kb, with an average of 800 kb[38,61]. Notably, by showing that chromatin preferentially interacts with chromatin within the same chromosome, Hi-C data recapitulate the notion of chromosome territories[61](**Fig. 3A,B**).

Along the linear genome, TAD boundaries are relatively well defined and are overall conserved between cell types[38,42,61]. TAD boundaries are depleted of chromatin interactions and enriched in the insulator protein CTCF, cohesin and in expressed genes[38,39,66]. The insulator property of TAD boundaries is believed to play an important role in the co-regulation of gene expression within TADs[42] by favoring promoter-enhancer contacts within them[43]. Moreover, as shown in

Paper I[67] and in other work from our laboratory[68] radial TAD positioning in the 3D nucleus can vary between cells in a population and between cell types[36,68], also likely contributing to the regulation of gene expression at the nucleus scale[68]. These higher-order topological changes in chromatin conformation, through long-range TAD-TAD interactions[41,68–73] or interactions between other chromatin domains[74], and switching of TADs between A and B compartments, coincide with general changes in gene expression[42,75].

These observations altogether indicate that cell type-specific gene expression programs entail multiple levels of chromatin conformation changes, at the gene locus level (within TADs), and at the nucleus level through dynamic TAD-TAD interactions. An additional important component in higher-order level gene regulation is the radial positioning of TADs, which is largely governed by interactions with the nuclear envelope.
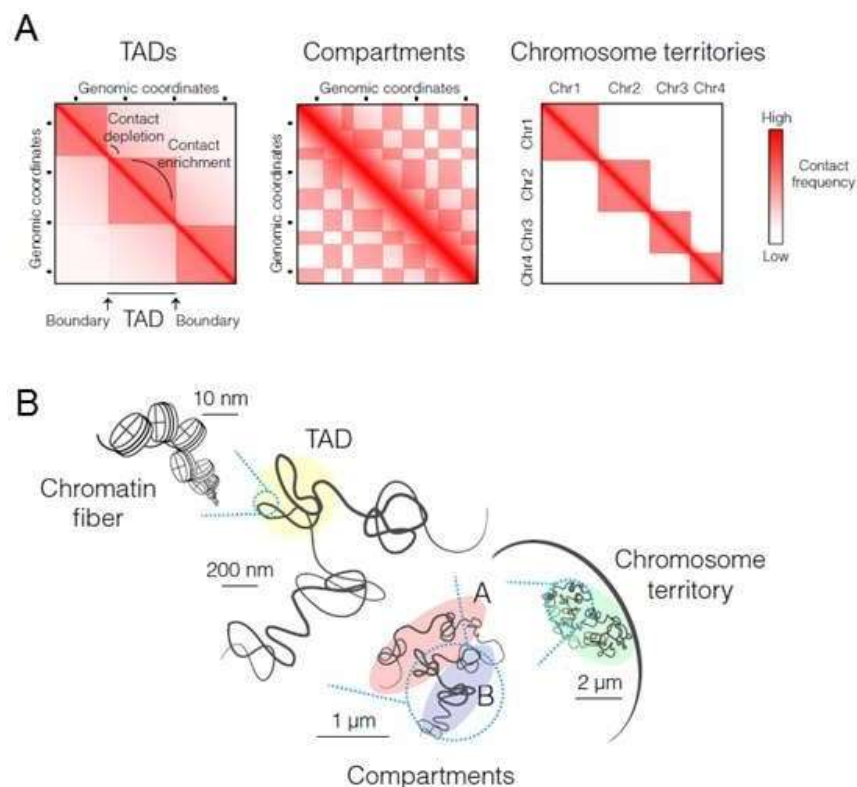
Figure 3. Three-dimensional genome organization in the nucleus. A. Schematic representation of Hi-C matrices (shown as heatmaps) at different genomic scales, reflecting the different layers of higher-order chromosome folding. Topologically associated domains (TADs) are regions of chromatin which have high contact frequency. Compartments A and B are formed by multiple TADs in contact with each other. Multiple compartments co-exist in the same chromosome; interactions between compartments occur within a chromosome territory. Increasing red intensity in the squares corresponds to an increasing number of contacts. From[76], reprinted with permission from AAAS. **B.** Hierarchical chromosome folding inside the nucleus, illustrating the chromosome territory, compartment and TAD concepts. From[76], reprinted with permission from AAAS.

1.3 ORGANIZATION OF THE NUCLEAR ENVELOPE

The nuclear envelope consists of an inner and outer nuclear membrane spanned by nuclear pore complexes (NPCs)[77] (**Fig. 4**) which enable import and export of proteins and export of RNAs[78–82]. The outer nuclear membrane (ONM) is continuous with the ER and shares properties of the ER[79,80]. The ONM harbors a family of proteins called nesprins. Nesprins contain a KASH (for Klarsicht, Anc-1, Syne-1 homology) domain which resides in the perinuclear space between the nuclear membranes. The KASH domain can interact with the SUN (Sad1 Unc-84) domain family of proteins anchored in the INM, together forming the linker of nucleoskeleton and cytoskeleton (LINC) complex[83,84] (**Fig. 4**) which acts as a mechanotransduction relay (or a force transmitter) between the cytoplasm and the nucleus[85]. Recent studies of the composition of the nuclear envelope in various tissues have identified an increasing number of nuclear envelope transmembrane proteins (NETs), some that are tissue-specific[86–89].

A set of well characterized NETs include lamina associated polypeptide (LAP)1/A/B/C, LAP2β, emerin, MAN1 and lamin B receptor (LBR)[90] (**Fig. 4**). LAP2β has been implicated in the control of DNA replication initiation and transcription regulation[91,92]. Emerin may be considered as a peripheral component in the LINC complex, as emerin can interact with nesprins[93–95] and emerin deficiency leads to impaired mechanotransduction[96]. Furthermore, NETs are involved in the regulation of cell signaling. Indeed, emerin has been suggested to influence WNT signaling by regulating the flux of β-catenin into the nucleus[97] and MAN1 influences transforming growth factor beta (TGFβ) and bone morphogenic protein (BMP) signaling by binding to SMAD2 and SMAD3[98,99]. This leads to disrupted SMAD phosphorylation and heterodimerization and subsequent signaling interference[98,99].

Importantly, LAP2β, MAN1, emerin and LBR all interact with chromatin and thus take part in the radial organization of chromatin[82,90]; this is further discussed in section 1.4.1. Subjacent to the INM lays the nuclear lamina. The lamina plays an important role in signal transduction but also in the spatial organization of chromatin, and mutations in nuclear lamins cause several diseases commonly referred to as laminopaties[100,101]. This thesis focuses on the importance of the nuclear lamina in genome organization.
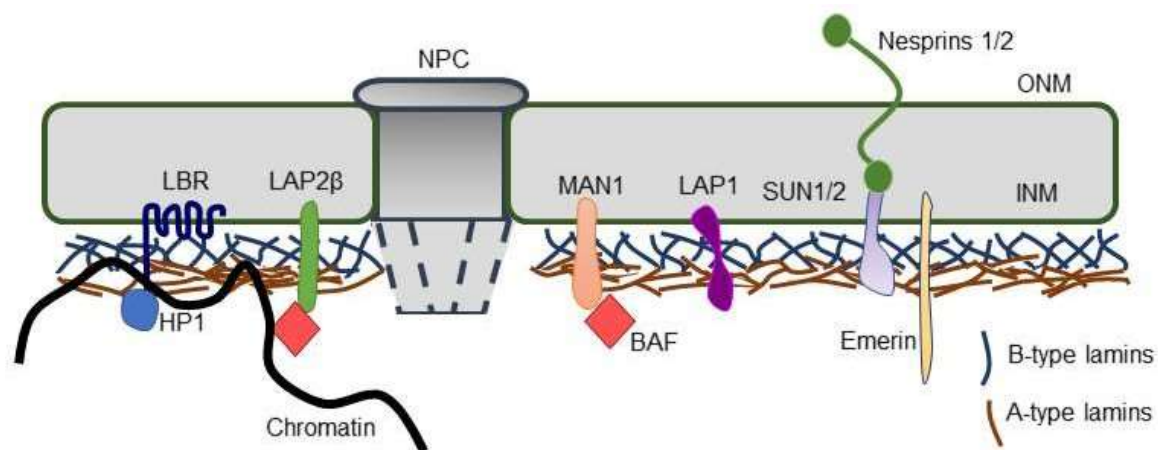
Figure 4. Nuclear envelope organization. The inner nuclear membrane (INM) and outer nuclear membrane (ONM) are perforated by nuclear pore complexes (NPCs). The INM is spanned by multiple nuclear envelope transmembrane proteins, including LBR, LAP2β, MAN1, LAP1, emerin and others. Below the INM, inside the nucleus, is the nuclear lamin, a polymer of A- and B-type lamins. A subset of INM transmembrane proteins, as well as the nuclear lamina, are able to interact with chromatin and as such anchor chromatin at the nuclear periphery.

1.3.1 Organization of the nuclear lamina

The nuclear lamina is made of an interwoven meshwork of type-V intermediate filaments called A- and B-type lamins[100] (**Fig. 5A**) which play an important role in the structural organization of the nucleus. Nuclear lamins consists of an N-terminal head domain, a coiled-coil central rod domain and a globular C-terminal tail domain. The tail domain harbors an immunoglobulin (Ig)-like beta fold that contains a nuclear localization sequence[102–104]. Assembly of the nuclear lamina occurs by a multi-step polymerization process. This entails homodimerization, head-to-tail assembly of homodimers and antiparallel assembly of the head-to-tail polymers into non-polar protofilaments. These congregate to construct intermediate filaments with approximately 3-5 protofilaments per 10 nm filament (**Fig. 5B**). Filaments are approximately 3.5 nm thick and form a meshwork which varies in density, forming the nuclear lamina[104,105]. Lamin filaments occupy roughly 12.5% of the meshwork that makes up the nuclear lamina, while spaces between filaments are occupied by various proteins and chromatin[105]. Structural assemblies of individual A- and B-type lamin together contribute to the radial organization of chromatin in the nucleus[105,106]. A- and B-type lamins share similar properties but also display significant structural and functional differences.

1.3.1.1 A-type lamins
There are two types of A-type lamins, lamins A and C (often referred to as lamin A/C), that are splice variants of the *LMNA* gene[100,107] (**Fig. 5A**). Lamins A and C do not form heterodimers

but homodimers and distinct filamentous meshworks[108]. A-type lamins are expressed at very low levels in embryonic stem cells (ESCs)[109]. However, A-type lamin expression, is not synchronous during embryonic development and is dependent on tissue and cell type[110,111]. Thus, expression of lamin A/C is developmentally regulated and shows some mosaicism in adult tissues.

Lamins contribute to the structural stability of the nucleus[112] and are involved in stabilizing several of NETs and INM proteins at the nuclear envelope, including emerin[89,113–115]. In addition, A-type lamins play an important role in mechanotransduction by contributing to the ability of the nucleus to register and act towards outside forces[116]. A-type lamins interact with SUN proteins[117] and together with emerin can bind to nesperins[93,114], thus assisting in connecting the nucleus with the cytoskeleton[116,117]. Force to the cell, and consequently to the nucleus, leads to recruitment of A-type lamins and nuclear stiffening while reduced tension leads to degradation of A-type lamins and reduced nuclear stiffness[118,119]. Whereas A-type lamins correlate with nuclear stiffening, B-type lamins correlate with nuclear softness; accordingly, the ratio between A-type and B-type lamins differ depending on tissue stiffness[119]. Long-term force on the nucleus can thus affect large-scale chromatin organization with an increase of heterochromatin[120].

A-type lamins not only exist at the nuclear lamina but also in the nucleoplasm where they have been reported as a detergent-soluble pool[121,122]. About 10 % of lamin A/C is soluble in non-ionic detergent (0.5% NP-40) and phosphorylation on serine 22 (S22) and S392 is involved in depolymerization of lamin A/C[108,123]. Fluorescence recovery after photobleaching (FRAP) experiments in hamster ovarian (K1-CHO cells)[124] and human fibrosarcoma (HT1080)[125] cells show that lamin A/C at the nuclear lamina is immobile and do not recover after bleaching[124,125]. In contrast, nucleoplasmic lamin A/C is more mobile, with ~50% of lamin A/C being recovered within seconds after photobleaching[124,125]. However, the remaining 50% show little to no recovery after photobleaching, indicating that part of lamin A/C in the nucleoplasm is immobile[124–126]. It has also been proposed that nucleoplasmic lamin A/C structurally differs and from the filamentous structure at the nuclear lamina since these exhibit differential solubilization properties[104,108,127]. Nucleoplasmic lamin A/C may exist as short polymers and dimers[104,108,126,127]. However, to our knowledge this has not been shown, likely because it remains challenging to isolate nucleoplasmic lamins without affecting nuclear architecture, and hence the lamina meshwork.

One key feature of A-type lamins in the nucleoplasm are that they interact with LAP2α[121]. Knockdown of LAP2α results in a decrease of A-type lamins in the nucleoplasm[122], and as we address later, a redistribution of LADs[122], indicating that nucleoplasmic A-type lamins are dependent on LAP2α. Nucleoplasmic A-type lamins are important for cell cycle progression[127–129]. LAP2α and A-type lamins can interact with retinoblastoma (Rb), which regulates the cell cycle, and knockdown of LAP2α or lamin A results in displacement of Rb and cell cycle arrest[128,129].

A-type lamins have been suggested to be involved in the assembly of certain nuclear bodies. Lamin A interacts with proteins of the Polycomb repressor complexes PRC1 and PRC2[130]. Depletion of A-type lamins correlates with a decrease in size of Polycomb group (PcG) foci[130,131], suggesting that they assist in the assembly of PcG foci. They are also involved in proper recruitment of EZH2, the H3K27 methyltransferase component of the PRC2 complex[132], to PRC2 target genomic regions, and deletion of A-type lamins impairs this recruitment[130]. Moreover, work from our laboratory has shown that an intranuclear wild-type lamin A/C network is involved in proper association of PRC2 and H3K27me3 at important gene loci involved in mesodermal induction in differentiated pluripotent stem cells[133] and in adipocyte differentiation in pre-adipocytes[134]. A mutation in the immunoglobulin (Ig)-like fold of lamin A (Arg482Trp, or R482W) causing Dunnigan-type familial partial lipodystrophy (FPLD2) impairs lamin A binding to these loci and/or PCR2 recruitment and H3K27me3 at these sites[133,134]. These studies reveal the importance of A-type lamins in the proper distribution of PRC2 throughout the genome[135]. These studies together highlight a central role of A-type lamins in the large-scale regulation of chromatin composition and organization.

1.3.1.2 B-type lamins

B-type lamins consist of lamins B1 and B2, transcribed from the *LMNB1* and *LMNB2* genes[136–138] (**Fig. 5A**). B-type lamins are ubiquitously expressed in stem cells and differentiated cells[139], and have been suggested to be essential for development and cell function[115,140]. B-type lamins are mainly enriched at the nuclear lamina[100,105,106], however lamin B1 has also been reported in the nucleoplasm[106,141,142].

B-type lamins are involved in different aspects of transcription. During S-phase, lamin B1 coincides with sites of DNA replication[142]. The lamin Ig fold is able to bind to proliferating cell nuclear antigen and disruption of this binding correlates with inhibition of DNA replication[143]. In addition, downregulation of lamin B1 correlates with splicing deregulation and an increase in enlarged nuclear speckles[144]. In addition, it leads to slower proliferation and cellular

senescence[115,144–146]. Intriguingly, induction of senescence correlates with loss of lamin B1 expression and activation of p53 or pRb pathways is sufficient to induce lamin B1 downregulation[145,146]. Moreover, lamin B1 has been suggested to be involved in chromatin condensation in interphase since the downregulation of lamin B1 correlates with diffusion of chromosome territories[144]. Altogether, these studies indicate that B-type lamins are involved in multiple cellular processes and highlight their importance in cell fitness.
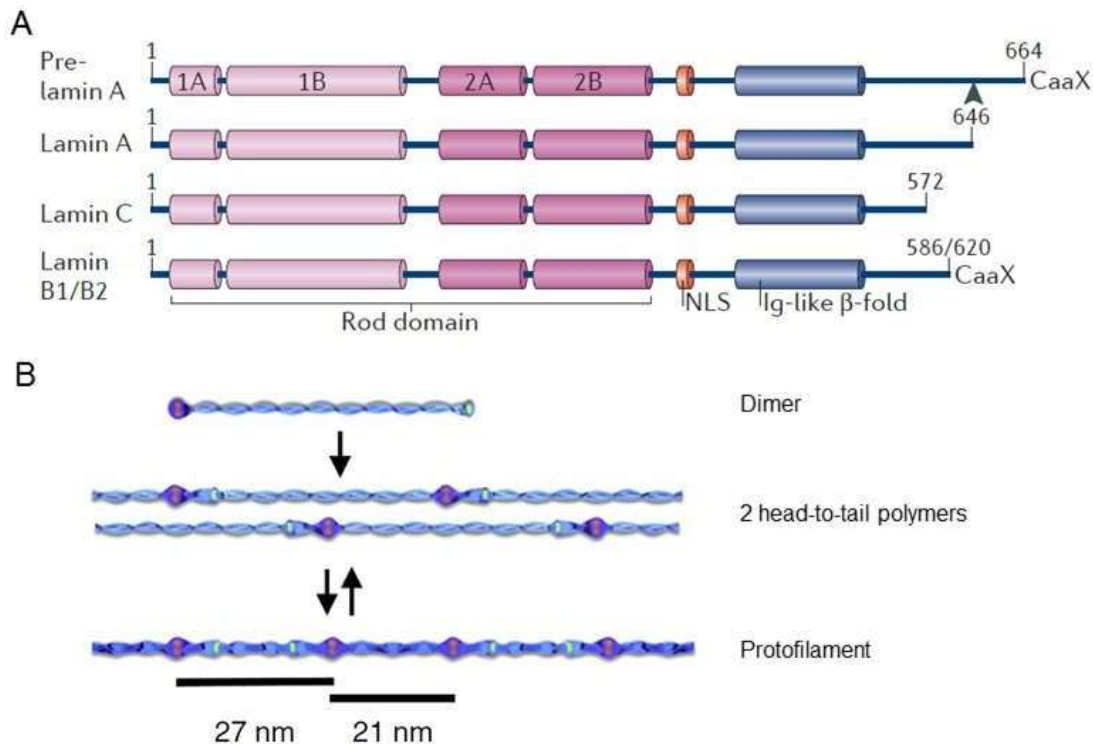
Figure 5. Structure and assembly of nuclear lamins. **A.** A-type and B-type lamins contain a rod domain, a nuclear localization signal (NLS) and an Ig-fold in the N-terminal region. Reprinted with copyright permission by Springer Nature from[100]. **B.** Lamin polypeptides assemble into dimers and associate to form head-to-tail polymers. Two head to-tail polymers reversibly form protofilaments. Reprinted from[104] with permission from Elsevier.

1.3.2 Maturation of A and B-type lamins

After synthesis, both A- and B-type lamins undergo a maturation process. The C-terminus of B-type lamins and prelamin A harbors a CAAX motif (C, cysteine; A, alpha residue and X, any residue) which is processed in a step-wise manner[100,147]. The first step in lamin processing is farnesylation by the soluble enzyme farnesyltransferase (FTase) (**Fig. 6A**). Farnesylation makes the C-terminus hydrophobic and consequently lamins are targeted to the INM[100,147–149]. Of note, lamins are periphery membrane proteins, so as opposed to integral membrane proteins (such as e.g. LAP2β, emerin or LBR), they do not traverse the lipid bilayer. Farnesylation is required for subsequent lamin processing, suggesting that for maturation, lamins may need to be at the

nuclear membrane. Inhibition of farnesylation using farnesyl transferase inhibitors (FTIs) re-localizes B- and A-type lamins to the nucleoplasm and long-term treatment by FTIs induces senescence[150]. Thus, farnesylation and location of lamins at the nuclear envelope seems to be essential for lamin maturation and cell fitness.

Next, the AAX motif is cleaved from the C-terminus by the INM integral proteins RCE1 and ZMPSTE24[100,151] (**Fig. 6B**). Interestingly though, RCE1 knockout does not affect prelamin A processing, likely due to redundancy of these enzymes[152]. Accordingly, ZMPSTE24 knockdown has no major impact on B-type lamin processing[100,152,153]. However, it impairs prelamin A processing not due to the lack of C-terminal cleavage but due to other roles of ZMPSTE24 in prelamin A processing (discussed in the next paragraph). After AAX motif removal, the exposed carboxyl group at the C-terminal cystine is methylated by isoprenylcysteine carboxyl methyltransferase (ICMT)[100] (**Fig. 6C**). ICMT is located in the INM and uses S-adenosyl-L-methionine as methyl donor. ICMT is vital in lamin processing and its inhibition correlates with inhibition of cell proliferation and cell cycle arrest in cancer cells[100,147,154,155]. Thus, proper lamin processing is essential for cell fitness.

Whereas B-type lamins are stably farnesylated and incorporated in the INM, cleavage of 18 amino acids in the C-terminus of lamin A by ZMPSTE24 leads to release of lamin A from the membrane[100,152,156] (**Fig. 6D**). Inhibition of ZMPSTE24 ability to cleave prelamin A leads to an accumulation of prelamin A which is detrimental to nuclear organization and has been tied to multiple disease[152,157]. One well known disease which disrupts lamin A processing is Hutchinson-Gilford progeria syndrome (HGPS)[158] (a laminopathy) which is further discussed in section 1.4.4.
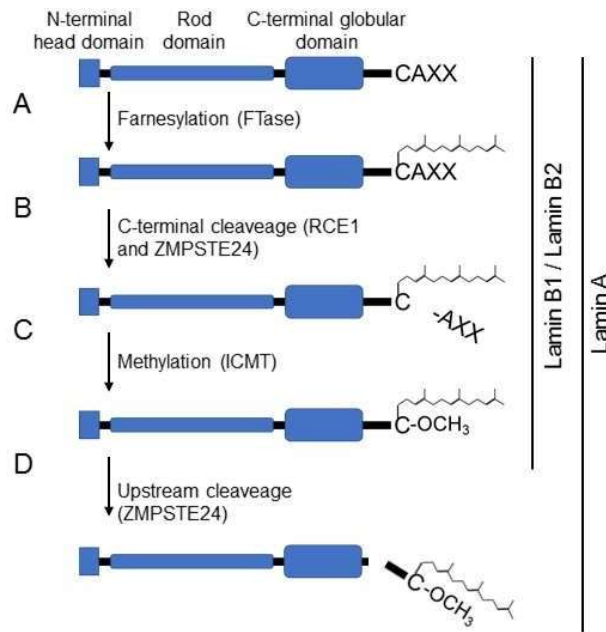
Figure 6. Lamin maturation process. **A.** Farnesylation of lamins on the cysteine (C) residue in the C-terminal CAAX motif by FTase **B.** Proteolysis of the AAX residues by RCE1 and ZMPSTE24. **C.** Carboxymethylation of the cysteine residue by ICMT after cleavage of the AAX motif. **D.** ZMPSTE24-mediated cleavage of lamin A removes an additional 15 amino acids at the C-terminal end, including the farnesylated cysteine.

1.4 CHROMATIN INTERACTIONS WITH THE INNER NUCLEAR MEMBRANE

Organization of chromatin at the nuclear periphery is complex because chromatin is able to interact with a subset of NETs and with the nuclear lamina. The INM protein LBR can bind to nuclesomal DNA and together with lamin A/C tethers heterochromatin at the nuclear periphery[159,160]. LBR binds heterochromatin protein 1(HP1) (**Fig. 4**)[161], which in turns binds H3K9me3-marked heterochromatin[162]; thus, through its interactions with LBR, HP1 may potentially act as an indirect mediator of heterochromatin anchoring at the INM. In addition, DNA-bound barrier-to-autointegration factor (BAF) can bind proteins that contain a LEM[163,164] ("LAP2, emerin, MAN1"[165]) domain and constitutes an interface between the genome and the nuclear envelope[163–165] (**Fig. 4**).

INM proteins are critical for maintaining a repressive environment at the nuclear periphery. LAP2β interacts with the histone deacetylase HDAC3[166]. HDAC3 plays a part in composing the gene repression environment at the nuclear periphery by ensuring that, through histone deacetylation, chromatin states at the periphery remain repressive[167]. One possible mechanism may involve deacetylation of histone H4[166]. In addition, HDAC3 may play a part in tethering chromatin to the nuclear periphery since deletion of HDAC3 in *Drosophila melanogaster* Schneider 2 cells results in displacement of genes away from the nuclear periphery[167].

The nuclear periphery is a dynamic area where several NETs interact with the lamina (**Fig. 4**). LAP2β, emerin, MAN1 and LBR are lamin-binding proteins and form tissue-specific

complexes with the nuclear lamina[89,159,168–170]. INM proteins and the lamina, in these complexes, work together to organize chromatin. For example, during myogenesis, the tissue-specific NETs NET39, Tmem38A and WFS1 target myogenic genes to the nuclear lamina where they are repressed[171]. However, it is unclear whether the chromatin-binding ability of NETs is modulated by their binding to the lamina.

1.4.1 Chromatin interaction with the nuclear lamina: lamina-associated domains

The nuclear lamina plays a fundamental role in the radial organization of chromatin by interacting with chromatin through LADs[172]. LADs have been identified using three main approaches[172–174].

(i) The first report of LADs used DNA adenine methyltransferase identification (DamID) to investigate genome-wide contacts of lamin B1[172] (**Fig. 7A**). DamID utilizes adenosine methylation, which does not naturally occur in eukaryotes. Expression of a DNA adenine methyltransferase (Dam) and lamin B1 fusion protein results in an adenine-6-methylation modification (^{m6}A) of DNA in regions close to where the fusion protein is expressed. Genomic regions containing the ^{m6}A modification can then be selectively amplified by methyl-specific PCR. In methyl-specific PCR genomic DNA is digested with *Dpn*I which recognizes sequences of $G^{m6}ATC$. The ends are ligated to adapters with a known sequence and the ligation products are digested with *Dpn*II which recognizes unmethylated GATC sites. The products are amplified with primers to the known adapters leading to amplification of regions flanked by $G^{m6}ATC$. The amplified products can then be identified by hybridization to microarrays or sequencing[172,175].

(ii) LADs have also been identified by chromatin immunoprecipitation (ChIP) and sequencing (ChIP-seq) of A- or B-type lamins[122,173,176] (**Fig. 7B**). Despite difference in approaches, LADs mapped by DamID strikingly overlap with those identified by ChIP-seq[173], reciprocally validating these methods for LAD identification. Arguably, an advantage of ChIP over DamID is that the latter requires overexpression of the lamin fusion protein, limiting its application in cell systems where transfection or induction of a stably integrated transgene is not possible. Another limitation of DamID lies in the nature of its negative control (expression of the Dam protein alone), which diffuses in the nucleoplasm where it can non-specifically bind DNA. Since these interactions are subtracted in lamin DamID analyses, interactions of lamins with chromatin in the nuclear interior[122,127,176,177] can be overlooked.

(iii) A third approach to identify LADs is by imaging using an [m6]A tracer (**Fig. 7C**). The [m6]A-tracer is a truncated part of the *Dpn*I protein that is fused to an enhanced green fluorescent protein (eGFP) tag. The [m6]A tracer technology facilitates the study of genome-nuclear lamina interactions in single cells[174]. Additional information provided by the m[6A] tracer approach is that it enables the detection of any DNA sequence that has been, at some point, in contact with the lamina, even though this physical interaction is no longer present at the time of observation[174]. Therefore, it provides a temporal aspect of chromatin interaction with the nuclear lamina at the single-cell level[174].
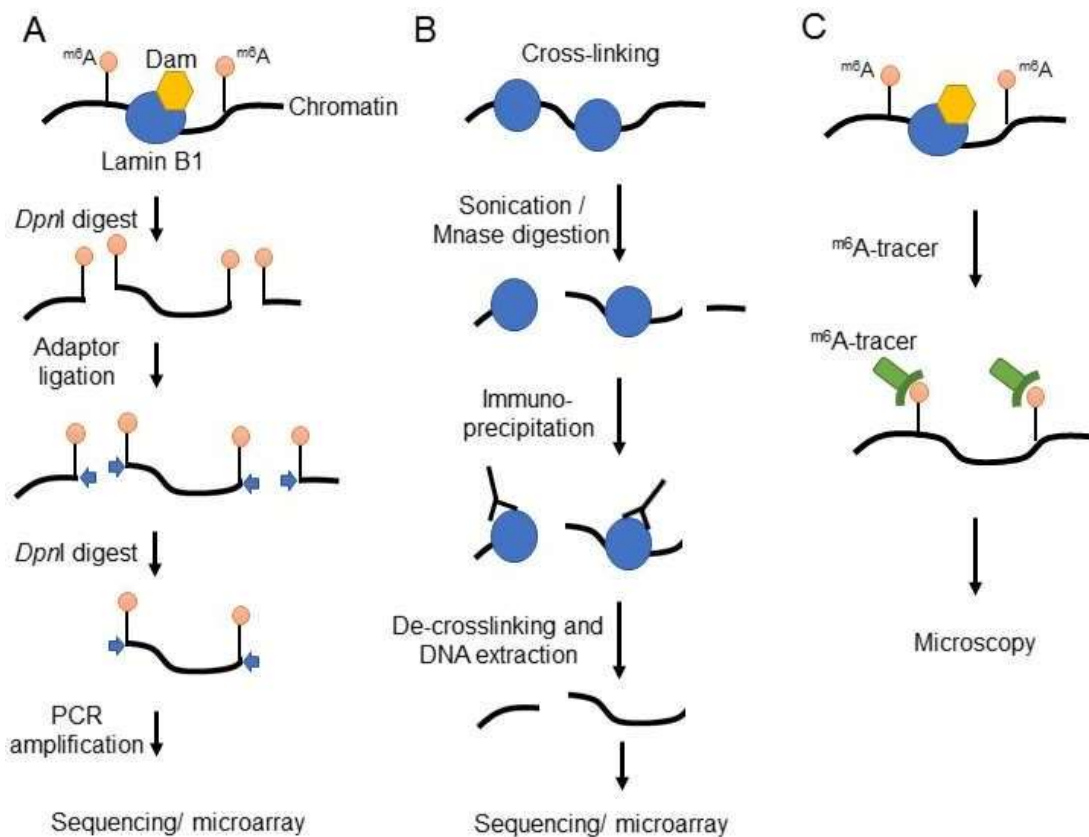
Figure 7. Methods of LAD detection. A. DNA adenine methyltransferase identification (DamID): the fusion protein of Dam and lamin B1 methylates adenosine in its proximity. DNA is digested with *Dpn*I (recognizes sequences of G[m6]ATC). The ends are ligated to adapters with a known sequence and the ligation products are digested with *Dpn*II. The products are amplified with primers to the known adapters leading to amplification of regions flanked by G[m6]ATC. **B.** Chromatin immunoprecipitation (ChIP): Samples are crosslinked with formaldehyde and sonicated. The samples are immunoprecipitated with antibodies against lamin B1. Samples are de-crosslinked and the DNA is extracted. **C.** [m6]A tracer: Dam-lamin B1 fusion protein methylates adenosine. The methylated adenosine is bound by the m[6]A tracer which is fused with an eGFP tag which can be detected through microscopy.

Regardless of genomics approach used, common features of LADs have emerged. LADs are present on all chromosomes, albeit at different densities, as domains ranging from 0.1 to 10 Mb[122,172–174,176,178]. Ensemble analysis such as DamID or ChIP-seq (that is, analyses from an

ensemble of typically millions of cells) indicates that LADs make up about 30% of the genome; further, both A- and B-type lamins can form LADs[172,177,178]. LADs overlap with regions of low gene density, replicate in late S-phase, are largely heterochromatic and strongly overlap with B-compartments[36,172,176,179,180]. The nuclear lamina is a repressive environment and in concordance gene expression within LADs is low[172,176,178]. LADs are enriched in the repressive PTMs H3K9me2 and H3K9me3[172,177]. Along the linear genome LADs are distinguished by distinct borders[172]. LAD borders are enriched in H3K27me3 and tend to be flanked by GC rich regions[172]. Motif searches in LAD borders reveal enrichment in binding motifs for YY1 transcription factors, CTCF and BTB/POZ domain proteins[181]. Some of these proteins may be implicated in targeting and/or anchoring LADs to the nuclear lamina (see below).

LADs are usually conserved between cell types but can also be cell type-specific. Constitutive LADs (cLADs) can be conserved between species; e.g., there is a striking 91% overlap of cLADs in human and mouse ESCs[182]. cLADs are AT-rich to the extent that AT content across the genome can predict cLADs[183]. cLADs can interact with both A- and B-type lamins[183], indicating that LAD conservation does not seem to depend on a specific lamin subtype. In **Paper I**, we address this issue in an analysis of LADs interacting with A- and/or B-type lamins. In contrast to cLADs, variable LADs (vLADs) are more cell type-specific and may vary during differentiation[176,182]; they are often found in regions containing cell type-specific genes important for development[171,177,182]. The existence of cLADs and vLADs suggests distinct modes of regulation of chromatin interaction with nuclear lamins.

LADs are not fixed at the nuclear envelope and only occasionally contact the nuclear lamina[36,174,179]. Contact frequency of a LAD with the nuclear lamina is a good indicator of how stably a genomic area is associated with the nuclear lamina[174,179]. cLADs are consistently positioned at the nuclear lamina, even within single cells of the same cell population, and have a high contact frequency with the nuclear lamina[179]. This correlates with H3K9me3 and low gene expression in these LADs[179]. In contrast, vLADs displays lower interaction frequency with the nuclear lamina[174,179]. **Paper II** in this thesis provides an account of the proportion of cLADs and vLADs upon entrainment of the circadian clock in mouse liver.

Analysis of sequencing reads in lamin A/C LAD ChIP-seq data interestingly reveals that pockets of chromatin within lamin A/C LADs are not enriched in lamin A/C[178], suggesting that all regions within a LAD do not necessarily associate with the nuclear lamina. The [m6]A tracer approach in combination with FISH has enabled the study of LAD-nuclear lamina contacts in single cells, over time. Strikingly, only ~30% of LADs identified by DamID-sequencing are

found at the nuclear periphery in a given cell[36,179]. This may be due to certain regions only transiently associating with the lamina. LAD positioning in the nuclear space seems to be stochastic. Following LADs throughout mitosis shows that LADs in daughter cells do not necessarily relocate to the nuclear lamina[174]: some LADs interact with the nucleolus while some NADs relocate to the lamina[184]. Both NADs and LADs are AT-rich, gene poor and overall repressed[51,172,173,184]. The apparent stochasticity of the positioning of genomic regions between the nuclear lamina and nucleolus argues that the overall position of a genomic region is secondary to the chromatin environment it is located in.

The mechanism that determines which LADs are at the nuclear periphery remain poorly understood. It has been suggested that targeting of genomic regions may be due to genome organizers such as CTCF, YY1 and EZH2[181]. Accumulation of YY1 at a genomic sequence followed by H3K27me3 is enough to target the sequence to the nuclear periphery[181]. Since YY1 is not enriched at the nuclear lamina *per se*, it may only play a role in repositioning loci towards the periphery rather than maintaining them at the periphery. Moreover, insertion of a LAD border sequence into an ectopic genomic region is enough to elicit repositioning to the nuclear periphery[181]. In addition, LADs contain lamina-associating sequences (LASs) which are sufficient to localize regions to the nuclear lamina[185]. LASs is enriched in a GAGA motif[177,185] which is bound by the cKROX transcription factor in a complex with HDAC3 and LAP2β[185]. cKROX and HDAC3 seem to tether chromatin to the lamina since knockdown of either protein promotes disassociation of chromatin from the lamina[185,186].

cLADs that remain at the nuclear lamina are enriched in H3K9me2[174] and depletion of H3K9me2/me3 methyltransferases G9a and Suv39H1 weakens and in some cases detaches LADs from the nuclear lamina[174,181,187,188]. In addition, in *Caenorhabditis elegans*, recruitment of loci to the nuclear periphery is driven by successive mono, di and trimethylation of H3K9[189]. Further, FISH-based screening reveals that multiple factors are implemented in targeting chromatin to the nuclear lamina, including NETs, chromatin remodelers and DNA replication factors[190]. Thus, more work is needed to identify factors that are implicated in targeting and anchoring specific genes and genomic regions to the nuclear lamina. The results are expected to be complex as results to date suggest that several factors can be involved in targeting a given locus to the nuclear lamina, and conversely, one factor is able to target multiple loci to this nuclear domain[190].

1.4.2 The role of LADs in nuclear organization

The nuclear lamina is a heterochromatin environment and repositioning of genes to the nuclear lamina can lead to their repression[172,177,185,191]. However, not all genes within LADs are inactive[172,177,182], in particular if the gene is not associated with lamins directly but lay within a LAD[177] (**Fig. 8A**). Nonetheless, genes that are more permanently associated with the lamina tend to be more repressed[179].

LAD organization plays a part in the regulation of gene expression, with a subset of genes that are detached from the lamina becoming upregulated, and vice versa[171,176,177,182]. During differentiation of mouse ESCs into astrocytes, genes that lose lamina association, as determined by DamID analysis of lamin B1, during differentiation are often "unlocked"(**Fig. 8B,C**) for activation during a later stage in the differentiation process[182] (**Fig. 8C (G1)**). The genes that are "unlocked" are often dependent on what cell type the ESCs are differentiated into[182]. This is also observed during myogenesis, adipocyte differentiation and T-cell activation[171,177,192]. Regions that detach from the lamina during differentiation lose their repressive histone marks and gain marks of active chromatin such as H3K4me3 and H3K9ac[171]. However, not all genes that dissociate form the lamina become active[171,177,182,192,193] (**Fig. 8C(G2)**), so other mechanisms are involved in regulating gene expression at loci able to associate with nuclear lamins.
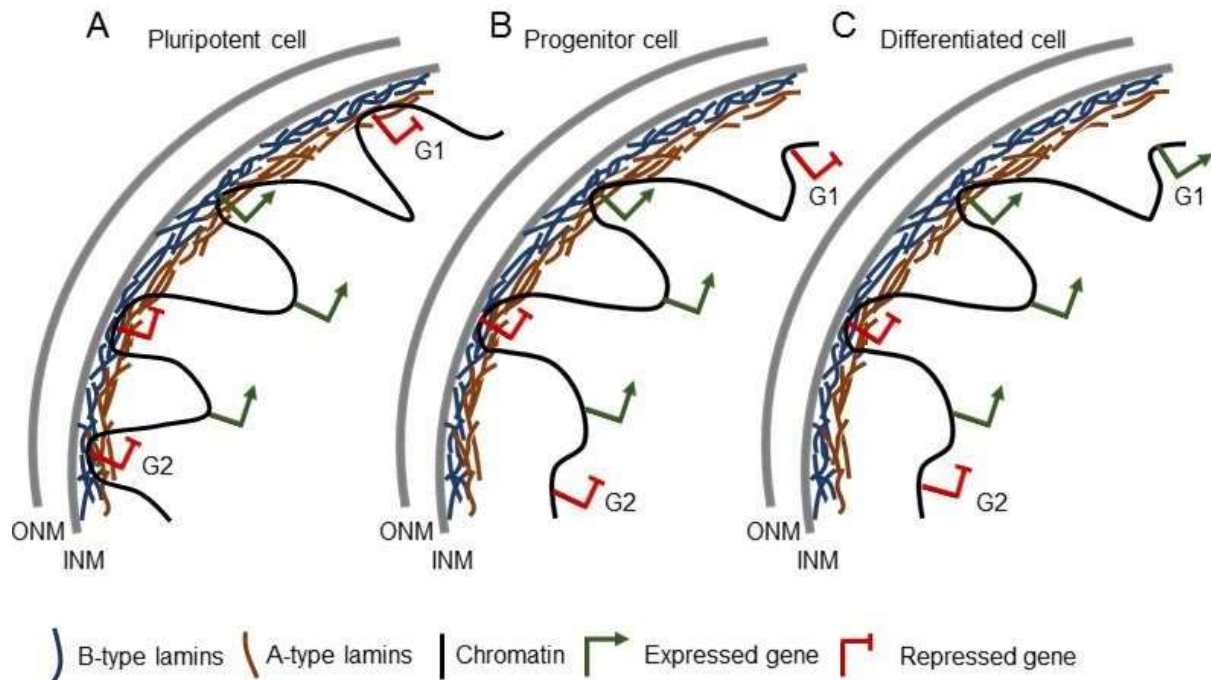
Figure 8. LAD re-organization during cellular differentiation. A. The nuclear periphery mainly consists of heterochromatin containing repressed genes, and a minor proportion of expressed genes. **B.** LADs are released from the lamina during differentiation from a pluripotent stem cell towards a terminally differentiated cell. **C.** Dissociation of LADs from the nuclear lamina is accompanied expression of some of the genes, but not all.

Indeed, association of the TSS and promoters of genes with nuclear lamins tends to correlate with transcriptional repression[177,193]. However, positioning promoters at the nuclear lamina is not sufficient for repression; a change in chromatin state is also necessary[177,179]. Experimental inclusion of promoters to distinct LADs has enabled a classification of promoters: i) promoters repressed by the nuclear lamina which can be activated if released, ii) promoters repressed independently of nuclear lamina association and, iii) promoters that escape repression even if they are within LADs[193]. The third class of promoters, although within LADs, are not always associated with the nuclear lamina and are less enriched in H3K9me2 and H3K9me3[193], which could be one of the reasons why they can escape repression. Similar classes have also been applied to enhancers within LADs[193]. This altogether hints to a functional heterogeneity of the chromatin environment in the nuclear lamina neighborhood.

Changes in LAD-lamina association have been linked to changes in large-scale chromatin conformation. Lamin B1 knockdown in mouse ESCs, even though it does not alter overall TAD structure, has been correlated with changes in TAD-TAD interactions[180]. During T-cell activation, loss of lamina association has been linked to altered compartment affinity with B-compartments changing into A-compartments. This has been correlated with a shorter distance

between enhancers and genes[192]. In addition, work from our laboratory shows that, during adipocyte differentiation, long-range TAD-TAD interactions have been seen to increase when TADs are displaced towards the nuclear periphery and gain lamin association[68]. Taken together, this indicates that the nuclear lamina helps maintain global chromatin conformation. What remains unclear, however, is how heterochromatin domains migrate towards the nuclear periphery as they segregate from euchromatic regions. This question is to date an active area of research.

A role of A-type lamins in the global organization of chromatin and in chromatin dynamics has been demonstrated by investigating telomere diffusion in the nuclear center[126]. Telomeres are generally constrained[194] and display slow diffusion[126]. Knockout of *Lmna* in mouse embryonic fibroblasts (MEFs) leads to faster telomere diffusion[126,195,196]. However, knockout or knockdown of several proteins important for genome organization, including lamin B1, lamin B2, emerin, CTCF, cohesin, LAP2α and BAF, show that BAF was the only other protein (besides lamin A) which changed the diffusion pattern of telomeres[126,196]. Moreover, knockdown of BAF in *Lmna* knockout cells lead to increased chromatin dynamics[196]. Together, these studies indicate that A-type lamin interaction with chromatin is necessary for maintenance of genome organization.

1.4.3   Lamin interaction with euchromatin

In general, the lamina is a repressive nuclear environment. However, in rod cells of nocturnal animals such as mice the nucleus is inverted with heterochromatin at the center of the nucleus and euchromatin at the periphery[197]. Whether lamins are able to interact with euchromatin has been a source of debate and in recent years, evidence supporting this view has emerged.

Not only A-type lamins, but also lamin B1 have been found in the nuclear interior, away from the periphery[106,121,122,141]. These nucleoplasmic lamin pools are likely able to interact with chromatin. One of the first indications that A-type lamins could interact with euchromatin was a study that compared sonication and micrococcal nuclease (MNase) digestion for chromatin fragmentation in lamin A/C ChIP in HeLa cells. This led to the detection of lamin A/C LADs ("A-LADs") in regions sensitive to MNase, and thus euchromatic[178]. In addition, a study testing a lower number of sonication cycles for chromatin fragmentation in fibroblasts reported A-LADs able to interact with euchromatin[122]. Gene density of LADs interacting with euchromatin is higher compared to heterochromatic LADs, which is in par with the higher gene density often seen in euchromatin. However, histone PTMs of euchromatic A-LADs do not differ from A-

LADs formed at heterochromatin, and are enriched in H3K9me3, H3K27me3 and EZH2[122,178]. Thus, A-LADs globally found in euchromatin may still be in a repressive chromatin environment. A-LADs that associate with euchromatin interact with LAP2α and in LAP2α-deficient cells A-type lamin association with chromatin is re-localized to heterochromatin regions[122]. This however is not correlated to changes in gene expression[122]. In general, euchromatin A-LADs have a lower overlap with B-LADs compared to heterochromatin A-LADs[122,178]. On a side note, the discovery of A-LADs within euchromatin regions highlights the importance of the methodology used to determine lamin-chromatin interactions.

These studies provide rather compelling evidence for the existence of A-LADs in euchromatic regions. Interestingly, recent work also reports euchromatic lamin B1 LADs (B-LADs). B-LADs were mapped during epithelial-to-mesenchymal transition (EMT) using ChIP-seq with only few sonication rounds. Euchromatic B-LADs are dynamic and can change during EMT indicating that they consists of vLADs[198]. In contrast to heterochromatin B-LADs, euchromatin B-LADs are associated with GC-rich chromatin, are gene-rich and are found in A-compartments[198]. Evidence for euchromatin LADs is increasing; however their significance in chromatin organization remains to be examined. The spatial localization of these euchromatic LADs, although presumed to be in the nuclear center based on the nature of the chromatin domains they encompass, also remains to be determined.

1.4.4 Mutations in lamin A/C affect large-scale genome organization

Mutations in nuclear lamins, and lamin A/C in particular, lead to systemic diseases that affect multiple tissues[100,199]. The laminopathy HGPS is caused by a mutation in exon 11 of the *LMNA* gene which leads to a cryptic splice site. This leads to a loss of 50 amino acids in the non-helical lamin A tail domain, including the ZMPSTE24 cleavage site[158,200]. The resulting protein, progerin, undergoes normal AAX removal and carboxyl methylation. However, due to the inability of ZMPSTE24 to cleave the protein it remains permanently farnesylated which leads to a permanent residence of lamin A at the nuclear periphery[158]. Progerin exhibits a dose-dependent effect on nuclear architecture with increasing amount leading to nuclear blebbing and disruption in nuclear organization[201]. Increasing amounts of progerin also leads to progressive loss of heterochromatin at the nuclear periphery[201]. These processes correlate with a global loss of heterochromatin markers in HGPS cells, including H3K27me3 and H3K9me3, compared to *LMNA* wild-type cells[202]. The reduction of H3K27me3 has been detected mainly in gene-poor regions[203] and could be due to lower global levels of EZH2 in HGPS cells[202,203].

Investigation of A-LADs in HGPS cells showed a decrease of lamin association in regions of reduced H3K27me3[203]. Interestingly, FTIs have been seen to reduce nuclear blebbing and the number of misshapen nuclei in HGPS cells and might be a basis for treatment for patients suffering from progeria[204].

FPLD2 patient cells have an abnormal nuclear shape and morphology,[205] indicating that the R482W mutation can effect nuclear and chromatin organization. A-LADs in FPLD2 patient and wild-type fibroblasts largely overlap; however 3D genome modeling suggests that A-LADs specific to FPLD2 patients are more centrally positioned compared to wild-type-specific A-LADs[36]. In lamin A R482W patient fibroblasts the T/Brachyury locus lacks lamin A binding and is displaced towards the nuclear center relative to wild-type fibroblasts[133]. T/Brachyury is important for mesoderm differentiation[206] and induced pluripotent stem cells derived from FPLD2 fibroblasts show altered mesodermal and endothelial differentiation[133]. The R482W mutation corelates with impaired PRC2 repression of the *T/Brachyury* locus and an overexpression of T/Brachyury target genes[133]. In addition, the R482W mutant has been tied to the deregulation of an anti-adipogenic micro-RNA, miR-335[134]. FISH studies into the locus positioning of *MIR335* during adipocyte differentiation of wild-type and R482W mutant cells have revealed that the *MIR335* locus remains in the nuclear interior as compared to wild-type cells where it is repositioned to the nuclear periphery[134]. Altogether, these studies indicate pathological mutations in lamin A/C can have marked effects on chromatin organization at the whole-nucleus level and at the gene locus level.

The aforementioned studies provide compelling evidence that nuclear lamins play a fundamental role in the spatial and functional organization of the mammalian genome. While by their stability, cLADs seem to play a structural role in nuclear architecture, vLADs may play a more regulatory function in genome activity than mere chromatin anchoring. There is also mounting evidence that some of lamin-chromatin interactions are under the influence of environmental cues, such as differentiation cues[176,182], and, as recently shown, circadian rhythms. The following section describes how gene expression, epigenetic modifications of chromatin and interaction of specific loci with the nuclear lamina are under circadian control.

1.5 THE CIRCADIAN RHYTHM AND ITS IMPACT ON GENOME ORGANIZATION

All mammals follow an evolutionary maintained adjustment to the environment, the 24-h circadian rhythm. The circadian rhythm is governed by environmental cues, often called

Zeitgebers, that partition periods of rest and activity and of fasting and feeding[207–209]. In mammals, the main Zeitgeber for circadian oscillation is light which entrains the central clock[210–212]. Retinal photoreceptors register light entrainment and convey this information to the suprachiasmatic nucleus (SCN) in the hypothalamus[213,214]. The SCN converts light information into various hormonal secretions which influence metabolic output, temperature and gene expression[210–212]. The circadian rhythm is also governed by patterns of dietary intake; these cues affect so-called peripheral clocks found in virtually all organs including liver, intestine, pancreas, lungs and adipose tissue[207,208]. Consistent patterns of feeding and fasting maintain the circadian oscillation of metabolites and normal circadian physiology[215,216]. Abnormal fasting/feeding patterns, such as those occurring during day/night shiftwork or caused by jetlag, lead to disturbed circadian oscillations of gene and protein expression and may underline metabolic diseases[217,218]. Proper control of circadian rhythms is therefore essential to a healthy condition.

1.5.1 The molecular clock of circadian rhythms

In mammals, the molecular clock of the circadian rhythm is governed by a transcriptional-translational feedback loop. The core clock transcription factors CLOCK and BMAL1 dimerize and bind to E-box motifs (CACGTG) to initiate transcription of circadian genes, including *Cry* and *Per*[219,220]. CRY (CRY1 and CRY2) and PER (PER1, PER2 and PER3) in turn bind to regulatory elements on *Clock* and *Bmal1* (note: the official *Bmal1* gene name is *Arntl*, but *Bmal1* is still most often used in the literature) to repress their expression, thereby inhibiting their own expression[221–224]. In addition, the CLOCK:BMAL1 complex activates the retinoic acid-related orphan receptors (RORs) RORα, RORβ and RORγ. REV-ERB proteins (REV- ERBα and REV-ERBβ) compete for binding to the retinoic acid–related orphan receptor response element (RORE) in the promoter of *Bmal1*[225,226]. While REV-ERB proteins inhibit *Bmal1* expression, RORs acts as transcriptional activators of *Bmal1*[225,226]. In turn, *Nr1d1* (*Rev- erbα*) is inhibited by the decrease in CLOCK:BMAL1[224,226] (**Fig. 9**).

The circadian clock is present in every cell in the body[227–230]. However, comparing cycling gene expression between different tissues reveals that the nature of genes displaying circadian expression patterns differs between tissues[231,232], thus the core clock components interact with tissue-specific factor to drive tissue-specific circadian gene expression. Another way by which the core molecular clock may maintain tissue specificity is through paralogs and homologs. For example, in the mammalian forebrain, BMAL1 form complexes with the CLOCK paralog

NPAS2[233]. In addition, the ROR homolog RORα is expressed in neural tissue whereas RORγ is expressed in peripheral tissues[225]. This diversity in core clock transcription factors implicated in various tissues contributes to a striking 5-20% of genes expressed in any tissue following circadian expression patterns[231].
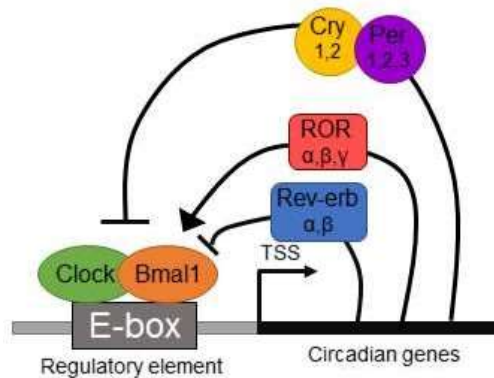
Figure 9. Overview of the molecular clock controlling circadian gene expression. The CLOCK:BMAL1 complex binds to E-box elements in the promoters of circadian genes (clock regulatory elements), which include *Cry* and *Per*. In turn, the CRY and PER transcription factors bind to regulatory elements of inhibit their expression. This results in self-regulation of CLOCK and BMAL1 proteins and *Cry* and *Per* transcription, which ultimately leads to transcriptional up-regulation of *Clock* and *Bmal1*, and a new cycle starts. ROR and REV-ERB proteins compete with each other for either activation or repression of *Bmal1*.

1.5.2 Influence of the circadian rhythm on gene expression

Binding of circadian transcription factors to regulatory regions of their target genes is essential in driving circadian gene expression[234,235]. The circadian transcriptional landscape, for each cycle, follows distinct phases of activation, transcription and repression.

During the activation phase, CLOCK and BMAL1, together with the histone acetyltransferases (HATs) p300 and CBP, are recruited to E-boxes in regulatory elements of circadian genes[236–238], increasing accessibility for the transcription machinery (**Fig. 10**). p300 co-precipitates with CLOCK in mouse liver nuclei, indicating that it is part in the activation complex of CLOCK:BMAL1[236]. CBP is dependent on its interaction partners to be able to affect circadian transcription[236–238]. Interestingly, CBP seems to have a dual function governed by its interaction partners. Overexpression of CBP leads to repression of CLOCK:BMAL1-mediated transcription when it interacts with pCAF[237,238]. However, when CBP interacts with HDAC3 it leads to increased CLOCK:BMAL1 transcriptional activity[237].

Binding of CLOCK:BMAL1 is accompanied by enrichment of H3K4me3 and H3K9ac at promoters and TSSs[234]. ChIP experiments show circadian patterns of H3K4me3 enrichment at promoters of circadian genes, that have been linked to the methyltransferases MLL1 and MLL3[239,240]. MLL1 recruitment is dependent on interaction with CLOCK:BMAL1. In addition, this interaction occurs in a circadian manner to enable oscillating recruitment of MLL1 to circadian gene promoters[239]. In contrast to MLL1, MLL3 is able to bind independently to DNA. However, MLL3 expression is under circadian regulation, ensuring that H3K4me3 enrichment occur in a circadian manner[240]. Moreover, CLOCK harbors intrinsic HAT activity and can acetylate H3K9[241], arguing that components of the clock machinery are directly able to epigenetically modify chromatin.

During the transcription phase, recruitment of the CLOCK:BMAL1 complex to target genes in liver is governed by multiple coactivators which can induce locus-specific gene expression. These include the NAD$^+$-dependent HDACs SIRT1 and SIRT6[242,243]. SIRT1, through its interaction with CLOCK, binds to E-boxes in a circadian manner concurring with binding to CLOCK:BMAL1[243,244]. In addition, SIRT1 knockout in MEFs correlates with a lengthening of the transcription phase[243]. SIRT6 can recruit the transcription factor SREBP-1 which is involved in the circadian regulation of a subset of genes involved in fatty acid and lipid metabolism in liver[242]. Moreover, ChIP experiments, in mouse liver, reveal that the histone lysine demethylases JARID1A and LSD1 can interact with the CLOCK:BMAL1 complex in the *Per2* E-box and enhance CLOCK:BMAL1-mediated transcription of *Per2*[245,246]. Together, these factors prime circadian chromatin for transcription and RNA Pol II is recruited in a circadian manner to circadian genes to start transcription[234,247] (**Fig. 10**).

In the repression phase, CRY and PER bind to E-box elements in the *Clock* and *Bmal1* promoters to repress their expression[234] (**Fig. 10**). Repressors in the core clock machinery interact with a multitude of proteins and repressor complexes. PER complexes associate with SIN3-HDAC which deacetylates H3K9, leading to transcriptional repression[248]. In addition, SUV39H methylates H3K9 to repress gene expression. SUV39H activity is dependent on PER complex interaction and is abolished in *Per* knockout cells[249]. In addition, REV-ERBα binds to regulatory elements of its target genes, including *Bmal1,* and recruits HDAC3, leading to the H3K9 deacetylation and down-regulation of gene expression[250–252]. This results in the decrease in the protein level of CLOCK:BMAL1, followed by a decrease in the level of their transcriptional repressors (CRY and PER). As a result, *Clock* and *Bmal1* expression increases again and a new activation phase is initiated (see **Fig. 9**).
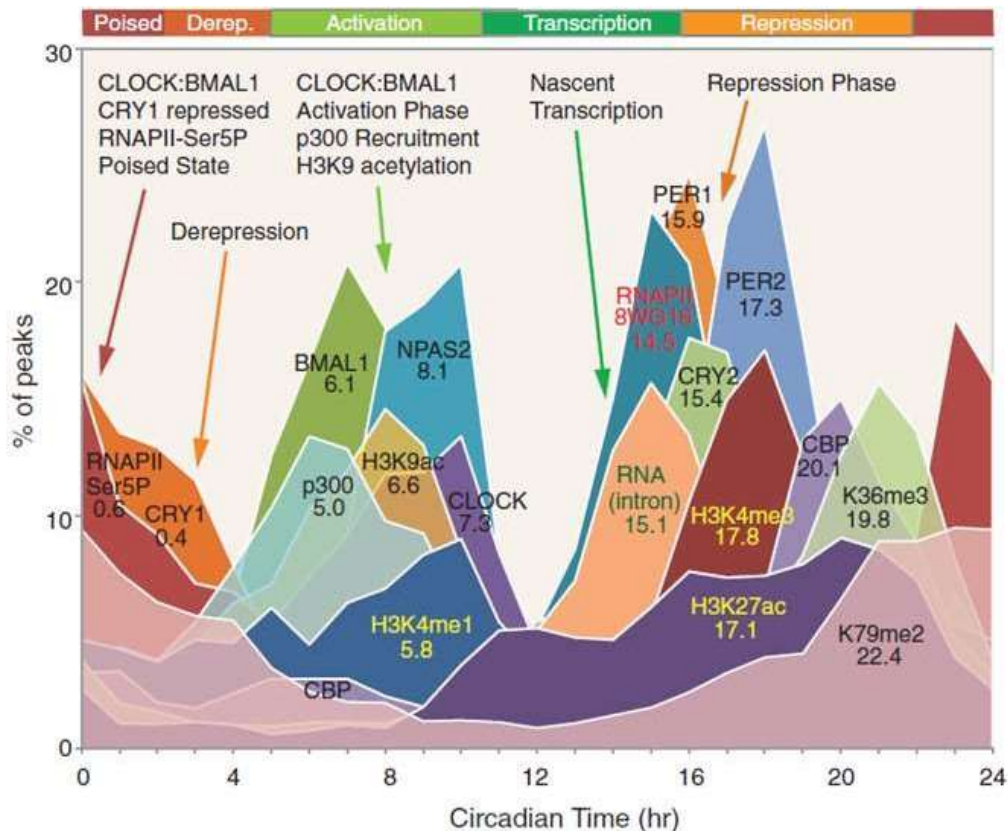
Figure 10. The circadian cistrome and epigenome in liver. Histogram of the percentage of peak enrichment of circadian transcriptional regulators, histone modifications and RNA transcripts, over time, show the circadian phase distribution in mouse liver. The results are an interpretation of ChIP-seq datasets for the various histone PTMs and transcription regulators. From[234], reprinted with permission from AAAS.

1.5.3 Impact of the circadian rhythm on genome organization

Accessibility to regulatory elements is requisite for circadian transcription factors to drive rhythmic gene expression. Recent studies have revealed that chromatin conformation also undergoes rhythmic changes during the circadian cycle. In particular, 4C-seq and Hi-C investigations show that whereas overall TAD structure and boundaries do not change during the circadian cycle[253], a subset of sub-TAD chromosomal interactions, including promoter-enhancer interactions, are subject to circadian rhythmicity[252–256].

Supporting this view, dynamic chromatin reconfiguration within TADs is affected by drivers and repressors of the circadian clock. BMAL1 target gene expression correlates with rhythmical chromosomal interactions[254,256]. This circadian interactome is lost in *Bmal1* knockout cells, indicating that at least some circadian chromatin interactions are dependent on BMAL1 binding to chromatin[254,256]. Moreover, REV-ERBα obstructs circadian chromatin interactions between

enhancers regulated by REV-ERBα and circadian gene promoters[253]. This occurs through recruitment of the NCoR-HDAC3 co-repressor complex to the regulatory elements by REV-ERBα, resulting in histone deacetylation and removal of the chromatin looping factor MED1[253]. To study how tissue-specific CLOCK:BMAL1 chromatin interactions might promote tissue-specific circadian gene expression, a ChIP-seq analysis of BMAL1 was done in mouse liver, kidney and heart[254]. Interestingly, the data show that BMAL1 binds to DNA in a tissue-specific manner, which is regulated by tissue-specific chromatin accessibility. In addition, these DNA binding sites are enriched in motifs for tissue-specific transcription factors, suggesting that these may mediate some of these circadian BMAL1-DNA interactions. This tissue-specific binding is accompanied by tissue-specific chromatin looping between regulatory elements, which is lost in *Bmal1* knockout cells[254,255].

Few studies have investigated how the nuclear envelope may contribute to organizing circadian genome conformation and gene expression. The INM protein MAN1 (see **Fig. 3**) has been shown to directly bind the *BMAL1* promoter to promote *BMAL1* transcription *in vitro*[257]. The question remains however of whether MAN1, or any other INM protein, is able to associate with chromatin in cells.

Interestingly, *Lmnb1* transcripts have been seen to periodically oscillate in the mouse SCN, liver and kidney[257], and *LMNB1* knockdown correlates with a circadian phase shift resulting in a longer period in human osteosarcoma U2OS cells[257]. Further, lamin A has been shown to bind the CLOCK:BMAL1 coactivators SIRT1 and SIRT6 and lamin A has been implicated in their activation[258,259]. *Lmna* knockout MEFs show a reduced enrichment of SIRT6 at chromatin, raising the possibility that lamin A/C may mediate recruitment of SIRT6 to chromatin[259]. Because SIRT6 is involved in circadian transcription[242], one can speculate that lamin A/C may be indirectly implicated in circadian gene expression patterns.

These studies suggest that the nuclear envelope, and the nuclear lamina in particular, may play a role in regulating circadian transcription. However, they do not shed light on how the lamina may potentially affect rhythms in genome organization

1.5.4   Periodic gene expression and chromatin interactions with the nuclear lamina

The aforementioned issue has been addressed in an investigation of whether interactions of chromatin with the nuclear lamina, and cycles of gene expression and repression, might be regulated in a circadian manner. Using a targeted approach in a human colon cancer cell line

entrained by serum shock, loci of two circadian gene, *VAT1L* and *PARD3*, were shown to be brought to the nuclear lamina in a circadian manner, in concurrence with their transcriptional down-regulation[260]. Mechanistically, this periodic recruitment is mediated by CTCF, a key regulator of 3D chromatin organization[261] and the poly-ADP-ribose (PAR) polymerase PARP1[260]. Once the loci associate with the nuclear lamina, they acquire H3K9me2 marks and become repressed. As the circadian rhythm progresses, the loci are released from the nuclear lamina and gain expression[260] (**Fig. 11**).

This study indicates that periodic interactions of chromatin with the nuclear lamina are involved in regulating circadian gene expression. However, it does not address whether periodic chromatin-lamin interactions constitute a general mechanism of circadian transcription regulation, and whether the circadian clock might drive periodic interactions of chromatin domains such as LADs with the lamina. Therefore, we have examined whether LADs display oscillatory patterns during the circadian cycle in mouse liver (**Paper II**).
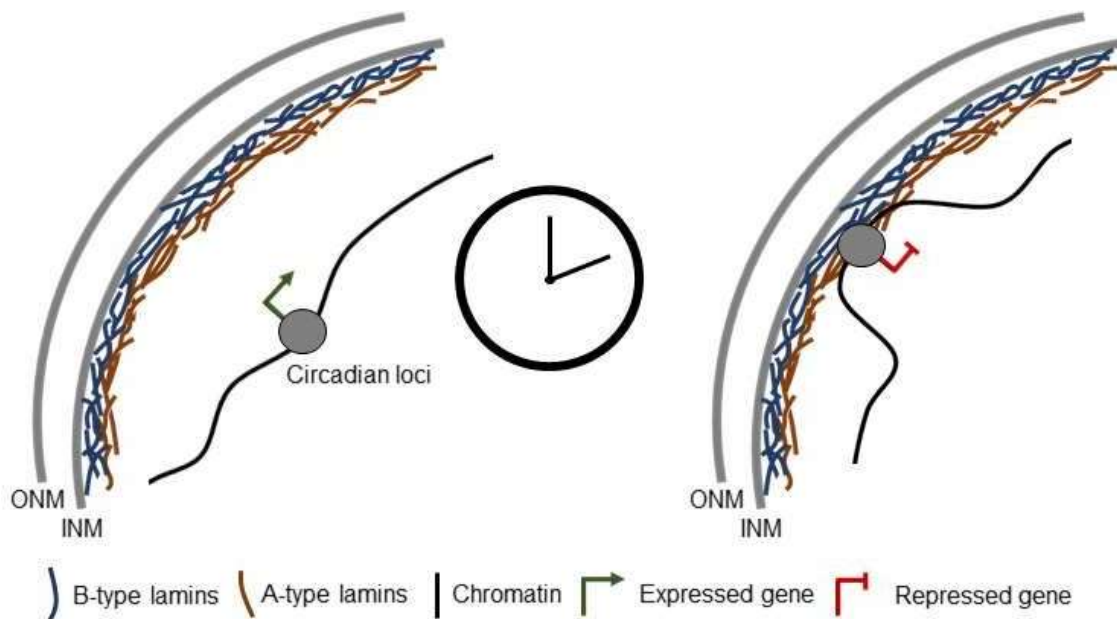
Figure 11. Recruitment of circadian loci to the nuclear lamina. Circadian loci are brought to the nuclear periphery where they associate with the nuclear lamina. At the nuclear lamina, the loci are repressed and as the clock goes on the loci detach from the nuclear lamina and the loci are re-activated.

2. AIMS OF THE STUDY

The nuclear lamina emerges as a dynamic subnuclear compartment affecting the radial topology of the genome. This view is promoted by the complexity of lamin-chromatin interactions and observations that LADs associated with A- and B-type lamins do not strictly overlap. In parallel, a large variation exists in the spatial associations between chromatin domains, which impacts spatial genome organization. Moreover, several lamin-chromatin interactions and intrachromosomal interactions appear to be modulated by external cues, including the circadian rhythm. However, much remains unexplored on the differences between A- *versus* B-type lamins interaction with chromatin, and on whether lamin-chromatin interactions display periodicity which could explain circadian gene expression patterns.

The aims of the present study were therefore to:

- Identify genome-wide interactions between chromatin and A- *versus* B-type lamins in a controlled cell stimulation system (**Paper I**).

- Investigate potential variations of chromatin interaction with A- and B- type lamins in this system (**Paper I**).

- Assess the impact of changes in these interactions on the radial positioning of loci in the nucleus and on associated changes in gene expression (**Paper I**).

- Identify genome wide interactions between chromatin and lamin B1 LADs during the circadian cycle in the mouse liver (**Paper II**).

- Determine whether LADs display circadian patterns of lamin B1 association (**Paper II**)

- Investigate whether any LAD periodicity is linked to periodic gene expression (**Paper II**).

The studies presented in the two publications involve cell and molecular biology approaches (including work using cell lines and mice), high-throughput genomics (RNA-seq and ChIP-seq), bioinformatics analyses and computational 3D genome modeling. The methods used as described in the papers. Collaboration with bioinformaticians in the laboratory was essential to the completion of this work; these are reflected by the authorships.

3. SUMMARY OF PUBLICATIONS

PAPER I

Interplay of lamin A and lamin B LADs on the radial positioning of chromatin

Frida Forsberg, Annaël Brunet, Tharvesh M. Liyakat Ali, and Philippe Collas

Immunosuppressive drugs such as cyclosporin A (CsA) can elicit hepatotoxicity by affecting gene expression. Here, we address the link between CsA and large-scale chromatin organization in HepG2 hepatocarcinoma cells. We show the existence of lamina-associated domains (LADs) interacting with lamin A, lamin B, or both. These 'A-B', 'A-only' and 'B-only' LADs display distinct fates after CsA treatment: A-B LADs remain constitutive or lose A, A-only LADs mainly lose A or switch to B, and B-only LADs remain B-only or acquire A. LAD rearrangement is overall uncoupled from changes in gene expression. Three-dimensional (3D) genome modeling predicts changes in radial positioning of LADs as LADs switch identities, which are corroborated by fluorescence *in situ* hybridization. Our results reveal interplay between A- and B-type lamins on radial locus positioning, suggesting complementary contributions to large-scale genome architecture. The data also unveil a hitherto unsuspected impact of cytotoxic drugs on genome conformation.

PAPER II

Nuclear lamin B1 interactions with chromatin during the circadian cycle are uncoupled from periodic gene expression.

Annaël Brunet*, Frida Forsberg*, Qiong Fan, Thomas Sæther and Philippe Collas.

*shared first authorship

Many mammalian genes exhibit circadian expression patterns concordant with periodic binding of transcription factors, chromatin modifications and chromosomal interactions. Here we investigate whether chromatin periodically associates with nuclear lamins. Entrainment of the circadian clock is accompanied, in mouse liver, by a net gain of lamin B1-chromatin interactions genome-wide, after which the majority of lamina-associated domains (LADs) are conserved during the circadian cycle. By tailoring a bioinformatics pipeline designed to identify periodic gene expression patterns, we also observe hundreds of variable lamin B1-chromatin interactions among which oscillations occur at 64 LADs, affecting one or both LAD extremities or entire LADs. Only a small subset of these oscillations however exhibit highly significant 12, 18, 24 or 30 h periodicity. These periodic LADs display oscillation asynchrony between their 5' and 3' borders, and are uncoupled from periodic gene expression within the LADs or in the vicinity of the LADs. Periodic gene expression is also strikingly unrelated to variations in gene-to-nearest LAD distances detected during the circadian cycle. Accordingly, periodic genes, including central clock-control genes, are located megabases away from LADs throughout circadian time, suggesting a stable residence in a transcriptionally permissive chromatin environment. We conclude that periodic LADs are not a dominant feature of variable lamin B1-chromatin interactions during the circadian cycle in mouse liver. Our results also suggest that periodic hepatic gene expression is overall not regulated by rhythmic chromatin associations with the nuclear lamina.

4. DISCUSSION

This thesis focuses on how external cues influence chromatin association with the nuclear lamina. In **paper I**, we demonstrate that cyclosporin A (CsA) treatment of human hepatocarcinoma HepG2 cells induces dynamic changes in chromatin association with A- and B-type lamins. The interplay we identify between A- and B-type lamins is non-systematically coupled to changes in the radial positioning of loci, with lamin B1 association being a stronger predictor than lamin A/C for locus positioning at the nuclear periphery. In addition, we show in **paper II** that lamin B1-chromatin interactions remain overall stable during the circadian cycle in mouse liver, except for a handful of LADs which display periodic lamin association patterns. However, these periodic LADs are uncoupled from circadian gene expression in the LADs or in the vicinity of the LADs. Altogether, our studies show that external cues can differentially affect chromatin interactions with A- or B-type lamins, highlighting for the first time to our knowledge the intricacy of chromatin-lamina interactions at the nuclear envelope (and possibly in the nuclear interior). Further, changes in these interactions predominantly do not correspond to changes in gene expression, reflecting an apparent uncoupling of two critical aspects of functional nuclear architecture.

4.1 TECHNICAL LIMITATIONS IN DETECTING LAMIN-CHROMATIN ASSOCIATIONS

In order to study lamin association with chromatin, we relied on ChIP using antibodies against lamin B1 and lamin A/C. Studies have shown that the chromatin fragmentation protocol used for lamin ChIP affects the type of LADs which can be detected by subsequent sequencing[122,198]. In our ChIP protocol, we use a high number of sonication rounds to enable the detection of interactions of lamins with heterochromatin. This raises the possibility that we might miss potential euchromatin-lamin interactions in our datasets, as these could be under- represented. However, it is possible that we do detect some euchromatin-lamin interactions in our protocol, but we are unable to distinguish between the two. Previous studies have shown that lamin A/C LADs share common features irrespective of whether they are localized in heterochromatin or euchromatin[122,178]. In contrast, lamin B1 LADs harbor distinct chromatin features in euchromatin compared to heterochromatin[198]. This makes it complicated to interpret the functional implications for some of our results since interactions of lamins with euchromatin and heterochromatin may serve distinct functions. Moreover, when interpreting ChIP data, it is important to consider that lamin-chromatin interactions are identified for a large cell population

(typically 5-10 million cells in our studies). [m6]A tracer and FISH studies have revealed that only ~30% of LADs identified in cell population-based techniques such as DamID, are found at the nuclear periphery in a given cell[36,179]. This argues therefore that LAD-lamin associations detected in our studies are not necessarily present in every single cell in the populations examined in **papers I** and **II**. These interactions may therefore be a lot more variable than what our sequencing results reveal, both after CsA stimulation of HepG2 cells, and during the circadian cycle in mouse liver.

When analyzing our ChIP-seq data, we use the enriched domain detector (EDD) algorithm developed in our laboratory[173]. All bioinformatics tools come with their own advantage and specificities, which need to be taken into account in function of the biological question we are asking. EDD is designed to call broad genomic domains, rather than narrow peaks, which display low yet significant levels of enrichment in a given protein (here, lamins)[173]. Once the domains are called, EDD creates a binary dataset consisting of LAD and inter-LAD regions[173]. This makes it manageable to analyze large sets of genomic data; however, information such as local levels of enrichment are lost. A deeper analysis of lamin A/C ChIP-seq reads have revealed that local areas outside of LADs seems to be enriched in lamin A/C while conversely, local areas within LADs appear to be depleted of lamin enrichment[178]. EDD performs strongly in the calling of LADs and provides a global picture of lamin-chromatin interactions. However, the internal structures of LADs, such as local variations in lamin-chromatin interactions, are not considered: in other words, a LAD may be called even though narrow depletions of lamin interactions occur within them. Thus, EDD might miss local LAD-chromatin interactions that could be of potential interest. An example was recently reported by our laboratory for the local association of lamin A/C with the *MEST/MIR335* locus in human adipose stem cells[134]. Even though the locus is not in a LAD, it binds lamin A/C. Moreover, cells expressing a mutant lamin A/C (lamin A p.R482W) that causes a partial lipodystrophy and a deficiency in adipogenic differentiation, do not show this intereaction[134]. Furthermore, local variations in lamin-chromatin interactions within LADs could potentially explain the apparent heterogeneity of LAD function in transcriptional regulation seen in previous studies[122,173,193].

In future analyses, stepping away from large-scale domain calling algorithms to focus on spatially restricted lamin-chromatin interactions irrespective of LADs may increase our understanding of the significance of these interactions on chromatin architecture and on the regulation of gene expression. Supporting this view, an earlier analysis of lamin A/C interactions with promoter regions using ChIP coupled to a promoter microarray analysis

(ChIP-on-chip) shows that the position of lamin A/C interaction in a ~4 kb promoter region (lamin binding at the TSS or ~2 kb upstream of the TSS) differentially correlates with expression of the corresponding gene[177]. In that study, lamin binding to the TSS is repressive, while binding upstream does not correlate with any gene expression status[177]. In addition, examination of *levels* of enrichment (rather than a binary LAD/inter-LAD approach) may reveal a more layered view of the function of lamin-chromatin interactions in genome organization. However, to be able to analyze and consider levels of lamin enrichment new bioinformatic tools are needed.

4.2   THE EFFECTS OF EXTERNAL CUES ON LAMIN-CHROMATIN INTERACTIONS

Several studies show that LADs exist as both constitutive and variable domains[176,182,183,192]. We now demonstrate that A- and B-type lamins can display similar or distinct patterns of association with chromatin, and that a small subset of lamin B1-chromatin interactions exhibit periodicity detectable after entrainment of the circadian clock.

4.2.1   CsA treatment of HepG2 cells leads to dynamic changes in lamin-chromatin interactions

During adipogenic differentiation, there is a large rearrangement of interactions between A-type lamins and the genome[176], indicating that external cues (in this case an adipocyte differentiation cocktail) can affect global lamin-chromatin interactions (**Fig. 12A**). To examine this more closely in a different model system, we treated the hepatocellular carcinoma cell line HepG2 with CsA (**Paper I**). CsA is an immunosuppressant that binds to cyclophilins to inhibit the phosphatase activity of calcineurin, leading to the inhibition of translocation of transcription factors to the nucleus that are necessary for the activation of T-cells[262]. In addition, CsA inhibits multiple signaling pathways[263,264], which leads to metabolic deregulation and induction of a steatotic-like phenotype in HepG2 cells[265,266].

LADs can stably associate with the nuclear lamina (cLADs) or in contrast display variable lamin associations (vLADs), often in a cell type-dependent manner[176,182,183]. Both A- and B- type lamins can form cLADs and vLADs[176,182,183]. In neural precursor cells and astrocytes, cLADs of lamin A/C and lamin B1 highly overlap whereas vLADs seems to preferentially associate with one type of lamin over the other[183]. However, few studies have explored the interplay between A-and B-type lamins on chromatin interactions and how this could affect genome organization.

In **paper I**, we identify LADs that interact both with lamin A/C and lamin B1 (A-B LADs), LADs that only associate with lamin B1 (B-only LADs) and LADs that only interact with lamin A/C (A-only LADs) (**Fig. 12B**). By classifying LADs into these three categories we have been able to identify behavioral differences between A- and B-type lamin association with chromatin. The majority of A-B LADs remain A-B LADs after CsA treatment (**Fig. 12B**) with a small proportion loosing lamin A/C association. The filamentous networks of A-and B-type lamins occupy both distinct and common regions at the nuclear periphery[105,106]. Therefore, double lamin association (A-B) may occur in regions where the filamentous networks overlap. However, whether this has any specific function is yet to be determined. In addition, after CsA treatment the majority of A-only LADs lose lamin A/C association to either become inter-LAD regions (**Fig. 12B**) or gain lamin B1 association. Furthermore, most B-only LADs remain stable (**Fig. 12B**) with a proportion that either gain A-type lamin association to become A-B LADs, lose lamin B association to become inter-LADs or switch lamin association to become A-only LADs. Thus, we identify in our dataset lamin A/C cLADs; however overall lamin A/C interactions with chromatin seem to be more variable than those of lamin B1. This suggests that A- and B-type lamin association with chromatin might exhibit distinct functions.

Our observation of a lamin A/C-lamin B1 interplay, evidenced by CsA treatment, raises the question of the possible mechanisms CsA may affect for this dynamic relationship to occur. CsA treatment leads to cellular senecense[267] and a recent study has shown large rearrangement of lamin B1-chromatin interactions during oncogene-induced senescence[268,269]. It could therefore be interesting to investigate whether other forms of cellular senescence (such as radiation-induced senescence) correlate with similar dynamics in chromatin-lamin interactions in HepG2 cells as seen for CsA. This would allow us to discriminate if our observation are specifics to senescence or CsA treatment. Another factor that could lead to changes in chromatin-lamin association is intracellular lipid accumulation. During adipose stem cell differentiation, there is an accumulation of lipids[270] . This could be one element in the lamin A/C LAD dynamics seen during adipocyte differentiation[176], that was not explored in this study (**Fig. 12A**). During adipocyte differentiation, lipid accumulation distorts the intercellular environment which is correlated to stiffening of the cell[271]. Speculatively, this may exert physical stress on the cytoskeleton, which through the LINC complex may affect the nuclear lamina and its interactions with the underlying chromatin[116,117]. Alternatively, intracellular lipid storage may provoke a lipotoxic stress signaling to the ER[272]. Since the ER is continuous with the nuclear envelope[79,80], the proteome of the nuclear envelope and/or its signaling functions

may be altered and affect its interactions with lamins or chromatin, potentially resulting in changes in lamin-chromatin interactions. Testing these hypotheses would enhance our understanding of the molecular mechanisms behind the dynamics of lamin-chromatin interactions. For example, treating HepG2 cells with Bisphenol A or Oleic acid (which induce lipid accumulation in HepG2 cells[273]) could be one way to investigate whether lipid accumulation is one of the drivers of the interplay between A- and B-type lamins and chromatin interactions.

Moreover, it would be of high interest to determine if the interplay between A and B type lamins seen in HepG2 cells occurs in primary cells or *in vivo*. In an ESC differentiation context, cLADs and vLADs have been identified by DamID[182]; however only lamin B1 was examined. During embryonic development, A-type lamin expression, in various tissues, is asynchronous and dependent upon cell type, while B-type lamins are ubiquitously expressed[110,111,139]. It is possible that the introduction of the A-type lamin filamentous network during ESC differentiation may lead to a rearrangement of lamin B1 LADs, and in particular lamin B1 vLADs, for example as parts of chromatin are being "handed in" to lamin A/C. It would therefore be compelling to examine the fate of chromatin-lamin B1 interactions upon induction of A-type lamin expression during ESC differentiation or during early embryo development.
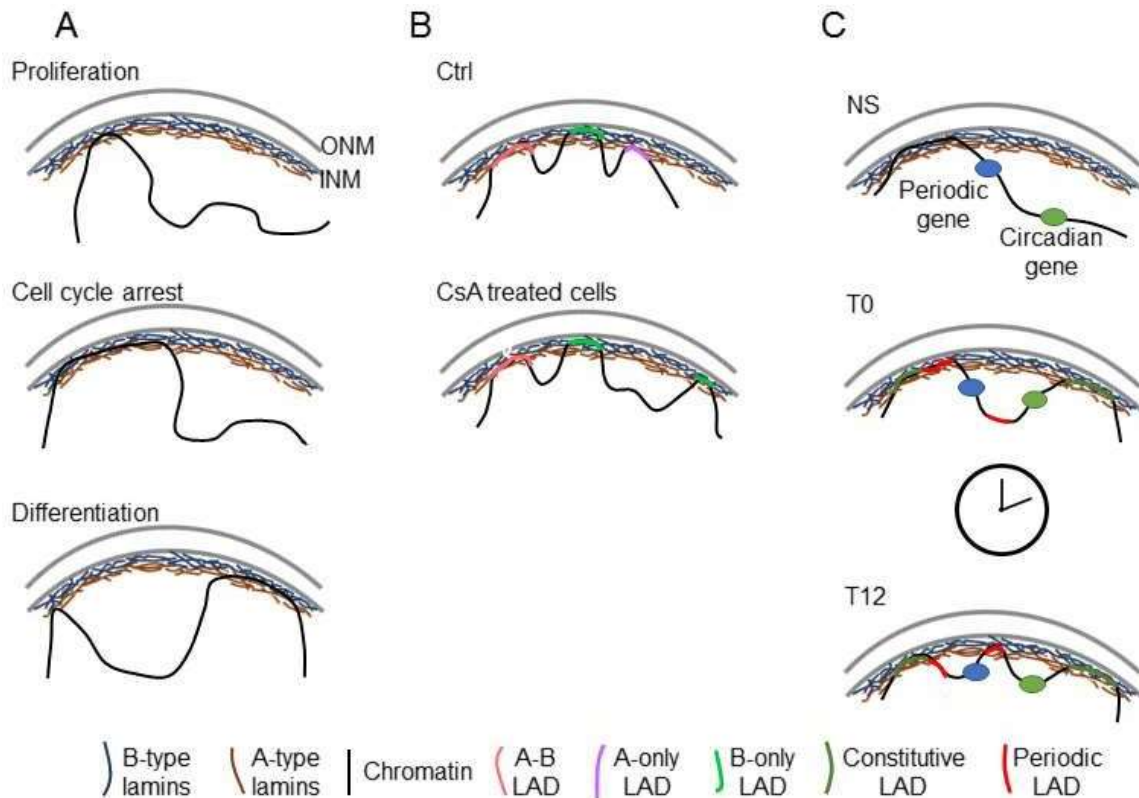
Figure 12. External cues effect LAD association with the nuclear lamina. A. In proliferating adipocyte progenitors, LAD coverage is limited. After cell-cycle arrest, LAD coverage is extended. In undifferentiated cells, lamin A/C LADs contain both repressed and expressed chromatin. Adipogenic differentiation elicits an exchange of lamin A/C LADs. Re-drawn with adaptations from[176]. **B.** CsA treatment of HepG2 cells leads to a dynamic rearrangement of lamin-chromatin interactions. The majority of lamin A/C and lamin B1 (A-B) interactions with chromatin remains stable as do lamin B1 only LADs (B-only). Gain of B-only LAD on chromatin is associated with radial repositioning towards the nuclear periphery. The majority of lamin A/C LADs (A-only) are lost. **C.** Model of LAD patterns after entrainment of the circadian clock. Entrainment of the clock (NS to T0 transition) is accompanied by a net gain of lamin B1 LADs. During the circadian cycle most, LADs are constitutive whereas a small number is periodic. Circadian and periodic genes are often located between LADs and are therefore unlikely to be regulated by periodic associations with nuclear lamins, at least in mouse liver.

4.2.2 Lamin B1-chromatin interactions are overall stable during the circadian cycle

Circadian recruitment of loci to the nuclear lamina has been correlated with transcriptional down-regulation and has been suggested to be one mode of circadian regulation[260] (**Fig. 11**). In **paper II**, we examined changes in lamin B1-chromatin interactions during the circadian cycle to determine whether LAD association with the nuclear lamina occurs in a periodic fashion. To entrain the circadian clock, mice where fasted for 24 h and refeed *ad libitum*[274]. We find that entrainment of the clock leads to a net gain of lamin B1-chromatin interactions, similarly to what has been seen for lamin A/C-chromatin interactions during cell cycle arrest in confluent undifferentiated adipocytes[176] (**Fig. 12A,C**). ChIP-seq on liver tissues or cells is done on a heterogeneous cell population, meaning that lamin-chromatin associations present in the

greatest number of cells will be detected. Therefore, the gain of lamin-chromatin interaction at *zeitgeber* time ZT0 could be due to the "synchronization" of our biological replicates, thereby reducing the heterogeneity in our samples compared to the non-synchronized replicates. Furthermore, analysis of LADs across circadian time reveals that the majority of lamin B1-chromatin interactions do not show a significant periodic pattern; in other words, they are stable, except for a few periodic LADs (**Fig. 12C**). The periodic LADs "oscillate" at one or both LAD borders, or the entire LAD periodically loses lamin association (these are rare occurrences). Moreover, the periodic LADs often display asynchronous 5' and 3' end oscillations in lamin interactions. The asynchronous properties of LAD border extension might simply be due to stochasticity and/or the periodic gene expression of BTB/POZ domain transcription factors found in **paper II**. LAD borders are enriched in binding motifs of BTB/POZ domain proteins[181], some of which target chromatin to the nuclear lamina[185]. Therefore, it is possible that circadian binding at certain BTB/POZ motifs lead to circadian extension of LAD borders.

In the analysis of periodic LADs, the MetaCycle tool calculates a P-value reflecting the assigned periodicity of LAD variations (extension and shortening over time). This P-value is in part dependent on the consistency between biological replicates. This ensures that the periodic LADs that we identify reflect patterns across individuals and are not due to variation between replicates. However, this stringent approach implies that we may enrich for cLADs and potentially miss variable (or in this case, circadian) LADs in addition to those we already find in the population of cells examined.

Zhao et al. have previously shown that the loci of two circadian genes, *VAT1L* and *PARD3*, were brought to the nuclear lamina in a circadian manner in a human colon cancer cell line[260] (**Fig. 11**). In **paper II**, we find that *Vat1l* and *Pard3* are megabases away from the nearest LADs and are not enriched in lamin B1 association. This could be due to species or tissue-specific differences in circadian chromatin organization and/or in gene expression patterns[231,232]. This could also be due to the fact that *Vat1l*/*VAT1L* and *Pard3*/*PARD3* are on different chromosomes in mouse and human: interestingly, the mouse genes are both located on chromosome 8, band qE1 and qE2 respectively (the latter being subtelomeric) whereas the human genes are on two distinct chromosomes (chr16q22.3 and chr10p11.21, respectively). Another important different in our study (paper II) and that of Zhao et al. [260] is that these authors did not examine lamin interactions with LADs (as in domains) but rather, local instances of lamin A/C interactions (as in, punctual interactions at genes). Such local interactions might have been missed during the domain calling of our lamin B1 ChIP-seq data, as discussed in section 4.1.

In **paper II** we only examined lamin B1-chromatin interactions, which raises the possibility that there might be circadian lamin A/C LADs. In **paper I**, we discovered that lamin A/C-LAD interactions are more variable as compared to lamin B1 interactions. Thus, it is possible that a non-negligible number of lamin A/C interactions with chromatin occur in a circadian manner. A ChIP-seq analysis of lamin A/C in mouse liver, which was not part of our study in **paper II**, would be necessary to answer this question. It is also possible that the main regulator of chromatin organization during the circadian cycle is NETs and not the nuclear lamina. The nuclear periphery is a dynamic area where several NETs interact with the lamina and chromatin[89,159,168–170]. In addition, during myogenesis, muscle-specific NETs are responsible for the re-localization of tissue specific-genes to the nuclear lamina for repression[171]. Moreover, the NET MAN1 has been shown to bind to the *BMAL1* promoter *in vitro*[257]. Altogether, this raises the possibility that NETs, rather than or in addition to nuclear lamins, provide anchors for circadian loci at the nuclear periphery.

4.3 CHANGES IN LAD-CHROMATIN INTERACTIONS CORRELATE WITH CHANGES IN CHROMATIN CONFORMATION

The nuclear lamina is a heterochromatin environment[172,177,185,191]. However, not all genes within LADs are inactive[172,177,182] (**Fig. 8**). In **paper I**, the only change in LAD classification correlating with changes in gene expression are genomic regions (A-only LADs or inter-LADs) that gain lamin B1 association after CsA treatment. Moreover, the periodic lamin B1 LADs detected in **paper II** (**Fig. 12C**) are uncoupled from periodic expression of genes within or near the LADs. Altogether, this indicates that regulation of gene expression may not be a predominant function of nuclear lamins.

Changes in LAD-lamina association have been linked to changes in large-scale chromatin conformation, affecting the distance between enhancers and genes as well as TAD-TAD interactions[68,192]. This has been coupled to shorter spatial distance between genes and regulatory elements, as well as altered compartment assignment, with B-compartments becoming A-compartments after release from the nuclear lamina[192] (**Fig. 13**). These findings argue that the nuclear lamina helps maintain global chromatin conformation (at least radially) and could affect chromatin conformation both in the near vicinity and further away from the nuclear lamina than previously thought.
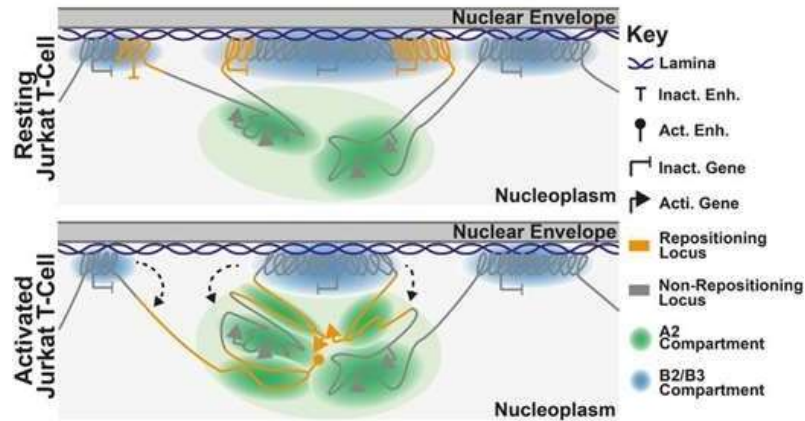
Figure 13. Model of changes in LAD-lamina interactions that lead to change in large scale chromatin interactions. In resting Jurkat T-cells B2/B3 sub-compartments exists as LAD at the nuclear lamina with A2 sub-compartments being distributed towards the nuclear interior. After T-cell activation, activation specific genes and/or enhancers are released from the nuclear periphery where they become transcriptionally active and associate in A2 sub-compartments. Republished from[192] with copyright permission under the creative commons attribution (CC BY) license.

4.3.1 Lamin B1 association is a predictor of peripheral positioning of genomic loci

Our results in **Paper I** suggest that A-LADs and B-LADs may carry out different tasks in genome organization. To check the effect of the different LAD classes on the radial positioning of the genome, we generated 3D models of the genome using Chrom3D[37] and corroborated the predictions from Chrom3D by FISH. We find that lamin B1-chromatin association is a stronger predictor of genome positioning towards the nuclear periphery (**Fig. 12B**). Moreover, loss of lamin B1 correlates with locus repositioning towards the nuclear center, even if the locus gains lamin A/C association. In addition, we identify LADs interacting with both lamin A/C and lamin B1 which were positioned towards the nuclear periphery. However, this may be due to lamin B1 rather than lamin A/C. This raises the possibility that the periodic gain and loss of lamin B1 we see in **paper II** affects the radial positioning of LADs. During the circadian cycle, the gene-to-nearest LAD distance decreases with the shortage distance occurring at T12. This is not correlated to changes in gene expression but is rather due to a gain in the number of LADs. How this change in linear distance between genes and LADs affect the overall spatial organization of chromatin during the circadian cycle could be explored through Chrom3D modeling and FISH experiments.

In **Paper I** we show that CsA treatment of HepG2 cells induces pre-lamin A accumulation. Thus we hypothesized that a change in radial positioning could be due to the pre-lamin A accumulation. To investigate this, we overexpressed FLAG-tagged lamin A WT and lamin A

44

L647R mutant (which lacks the ZMPSTE24 cleavage site and is therefore unable to fully mature into lamin A[275]) in HepG2 cells. Overexpression of the lamin A L647R mutant did not correlate with a change in radial positioning in the loci affected by CsA treatment. This suggests that CsA influence on chromatin organization is not due to accumulation of pre-lamin A *per se*.

It is possible that an intrinsic feature that differs between A-and B-type lamins may explain why we detect differences in the influence of lamin A/C or B1 on radial positioning of loci. B- type lamins are permanently C-terminal farnesylated and incorporated in the INM[100,105,147,150], whereas A-type lamins lose their farnesyl group and are released from the nuclear membrane upon maturation[100,152,156]. Therefore, it is tempting to speculate that the stably incorporated lamin B1 at the nuclear membrane explains why lamin B1 association better predicts locus localization towards the nuclear periphery than A-type lamins. However, there is a pool of B-type lamins in the nuclear interior, often in association with nuclear foci such as sites of DNA replication[142] or nucleoli[141]. Moreover, A-type lamins exist both at the nuclear lamina and the nucleoplasm[100,121,122] and A-type lamins in the nuclear interior depend on interactions with LAP2α[121,122]. In addition, euchromatin A-LADs associate with LAP2α and knockdown of LAP2α results in a decrease of A-type lamins in the nucleoplasm and a redistribution of A-LADs to heterochromatin[122]. This suggests that A-LADs might exist and interact with A-type lamins in the nucleoplasm, which could be one of the reasons why we do not see a change in radial positioning of loci when they gain A-type lamin association after CsA treatment.

Histone PTMs and chromatin state have been tied to the stability of association between lamins and chromatin, with LADs being enriched in H3K9me2 and H3K9me3 independently of the type of lamins it interacts with[172,177]. Moreover, how often a LAD contacts the lamina correlates with H3K9me3 and low gene expression in these LADs[179]. In addition, vLADs have a lower contact frequency with the nuclear lamina[174,179]. Therefore, the determination of chromatin marks in our LAD classes **in paper I** could shed further light on the contact frequency of LADs and on how the chromatin environment is affected be these dynamic lamin-chromatin associations. Do we see lower H3K9me3 enrichment in the more dynamic LADs than in the more stable ones? In addition, in *C. elegans* recruitment of loci to the nuclear periphery is driven by step-wise mono-, di- and trimethylation of H3K9[189] (**Fig. 14**). A time study following histone H3K9 methylation after CsA treatment (or during the circadian cycle) could shed light on whether a similar process occurs in mammals. Furthermore, the repositioning of LADs to the nuclear periphery after CsA treatment could be due to several factors. cKROX, HDAC3 and tissue-specific NETs have been suggested to tether chromatin to the lamina[171,185,186]. It would

be interesting to investigate whether loci that are repositioned to the nuclear periphery are bound by any repositioning factors after CsA treatment.
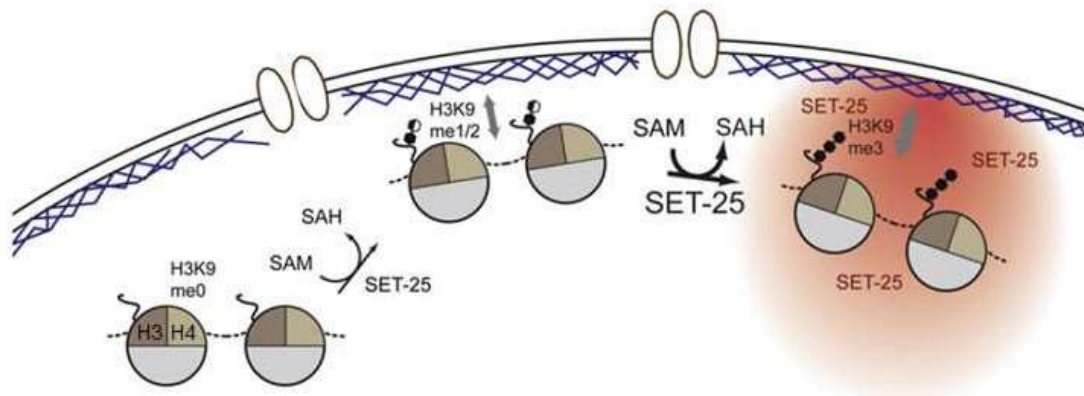
Figure 14. Step-wise gain of H3K9 methylation during peripheral repositioning in *C. elegans*. H3K9 is methylated in a stepwise manner. H3K9me1/me2 (methylated by SET-25 and MET-2) initiates reversible chromatin targeting to the nuclear lamina (grey arrows) whereas H3K9me3 (methylated by SET-25) is needed for complete silencing and attachment. H3K9me3 is necessary for SET-25 to accumulate in nuclear foci (red). Reprinted from[189] with permission from Elsevier.

4.3.2 Where does interplay between nuclear lamins and chromatin occur?

In recent years, multiple studies have shown that LADs do not only occupy the nuclear lamina but are also present in the nucleoplasm[36,174,179,184]. However, there is little direct evidence of LADs interacting with lamins in the nuclear interior. Knockout of *Lmna* in MEFs leads to faster telomere diffusion in the nuclear center[126,195,196]. In addition, down-regulation of lamin B1 correlates with diffusion of chromosome territories[144]. Altogether, these studies suggest that lamins are important for chromatin organization in the nuclear center, but they do not shed light on possible LAD- lamin interactions in the nuclear interior. The current techniques used for LAD detection, such as DamID and ChIP-seq, do not reveal the position of LADs in the nuclear space[172,173]. In contrast, the m^{6A} tracer approach enables for detection of LAD positioning in the nuclear space[174]. However, the technique enables the detection of any DNA sequence that has been, at some point, in contact with the lamin, even though this physical interaction is no longer present at the time of observation[174], making it particularly challenging to determine if LADs in fact interact with lamins in the nuclear interior.

5. CONCLUSION AND FUTURE PERSPECTIVES

This thesis has investigated how different external cues can affect lamin-chromatin interactions in two different model systems – an *in vitro* human hepatocarcinoma cell line stimulated with CsA, and mouse liver *in vivo* during the circadian cycle. Furthermore, we explored differences between A- and B-type lamins in their association with chromatin. Our findings demonstrate that the majority of B-type lamin associations remain impervious to external cues, both after CsA treatment and during the circadian cycle. In contrast, A-type lamin-chromatin interactions are highly susceptible to CsA treatment; however, whether this also holds true for the circadian rhythm remains to be determined. In addition, we find that a gain of lamin B1-chromatin association is the main predictor (over lamin A/C) for positioning loci towards the nuclear periphery.

Further work exploring differences in LAD-lamin interactions in other cell types and model systems will elucidate if the differences in the stability of interactions between A- and B-type lamin can be applied as a general rule. Speculatively, if A-type lamins are more variable in their association, genomic regions that would require only transient interactions with the nuclear lamina might favor A- type lamins over B-type lamins. While B-type lamins may predominantly play a structural role in maintaining global nuclear architecture and the radial distribution of chromatin in the nucleus, A-type lamins may play a more regulatory role on genome function, influencing gene expression, chromatin dynamics and local genome conformation. It would be informative to investigate the dynamics of lamin A/C binding to chromatin in close time-scale studies or in single-cell experiments, e.g. using DamID[174,179], which would reveal LAD heterogeneity between cells in a population as a readout for the dynamics of interactions.

In order to start to understand the observed differences between A- and B-type lamins in our study, it will be important to clarify interaction between lamins and euchromatin *versus* heterochromatin. Does heterochromatin interact more stably with the lamina as compared to euchromatin? If so, do the more "stable" B-type lamins interact to a greater extent with heterochromatin? In addition, whether lamins can interact with chromatin in the nuclear interior, which is suggested from lamin interactions with euchromatic domains and the LAP2 dependency of lamin A/C interaction with euchromatin[122], and to what extent this is seen for A- and B-type lamins, need to be examined. At the moment, the field has assumed that all lamin-chromatin interactions occur at the nuclear periphery. If lamins can interact with chromatin in the nuclear interior, it is possible that A- and B-type lamins interact with chromatin in the interior

to different extents. Since euchromatin is enriched mainly in the nuclear interior and heterochromatin at the nuclear periphery, it is possible that potential interior lamin- chromatin interactions will be enriched in euchromatin.

It is becoming clearer that lamin-chromatin interactions are more complex than previously understood: interactions can be peripheral or occur in the nuclear interior, involve hetero- or euchromatin, involve large domains or punctual sites, can be constitutive or variable, encompass distinct genomic regions between A- and B-type lamins, and display distinct dynamics. New approaches and tools for bioinformatics analysis (for example, analyzing lamin enrichment *levels* rather than as on/off interactions) in combination with live cell imaging studies are necessary to understand the full spectrum of roles that the nuclear lamina play in organizing chromatin.

6. REFERENCES

1. Griffiths, A. J. F. *et al. An Introduction to Genetic Analysis*.

2. Lander, E. S. *et al.* Initial sequencing and analysis of the human genome. *Nature* **409**, 860–921 (2001).

3. Costantini, M., Clay, O., Auletta, F. & Bernardi, G. An isochore map of human chromosomes. *Genome Res.* **16**, 536–541 (2006).

4. Caron, H. *et al.* The human transcriptome map: clustering of highly expressed genes in chromosomal domains. *Science* **291**, 1289–1292 (2001).

5. Lercher, M. J., Urrutia, A. O. & Hurst, L. D. Clustering of housekeeping genes provides a unified model of gene order in the human genome. *Nat. Genet.* **31**, 180–183 (2002).

6. Kornberg, R. D. Chromatin structure: a repeating unit of histones and DNA. *Science* **184**, 868–871 (1974).

7. Luger, K., Mäder, A. W., Richmond, R. K., Sargent, D. F. & Richmond, T. J. Crystal structure of the nucleosome core particle at 2.8 A resolution. *Nature* **389**, 251–260 (1997).

8. Ray, G. & Longworth, M. S. Epigenetics, DNA Organization, and Inflammatory Bowel Disease. *Inflamm. Bowel Dis.* **25**, 235–247 (2019).

9. Thoma, F., Koller, T. & Klug, A. Involvement of histone H1 in the organization of the nucleosome and of the salt-dependent superstructures of chromatin. *J. Cell Biol.* **83**, 403–427 (1979).

10. Widom, J. & Klug, A. Structure of the 300A chromatin filament: X-ray diffraction from oriented samples. *Cell* **43**, 207–213 (1985).

11. Bannister, A. J. & Kouzarides, T. Regulation of chromatin by histone modifications. *Cell Res.* **21**, 381–395 (2011).

12. Kouzarides, T. Chromatin modifications and their function. *Cell* **128**, 693–705 (2007).

13. Ram, O. *et al.* Combinatorial patterning of chromatin regulators uncovered by genome-wide location analysis in human cells. *Cell* **147**, 1628–1639 (2011).

14. Ernst, J. *et al.* Mapping and analysis of chromatin state dynamics in nine human cell types. *Nature* **473**, 43–49 (2011).

15. Zegerman, P., Canas, B., Pappin, D. & Kouzarides, T. Histone H3 lysine 4 methylation disrupts binding of nucleosome remodeling and deacetylase (NuRD) repressor complex. *J. Biol. Chem.* **277**, 11621–11624 (2002).

16. Zeng, L. *et al.* Mechanism and regulation of acetylated histone binding by the tandem PHD finger of DPF3b. *Nature* **466**, 258–262 (2010).

17. Rea, S. *et al.* Regulation of chromatin structure by site-specific histone H3 methyltransferases. *Nature* **406**, 593–599 (2000).

18. Kundaje, A. *et al.* Integrative analysis of 111 reference human epigenomes. *Nature* **518**, 317–330 (2015).

19. Consortium, T. E. P. The ENCODE (ENCyclopedia Of DNA Elements) Project. *Science* **306**, 636–640 (2004).

20. Ravasi, T. *et al.* An Atlas of Combinatorial Transcriptional Regulation in Mouse and Man. *Cell* **140**, 744–752 (2010).

21. Boyle, A. P. *et al.* High-Resolution Mapping and Characterization of Open Chromatin across the Genome. *Cell* **132**, 311–322 (2008).

22. Schwaiger, M. *et al.* Chromatin state marks cell-type- and gender-specific replication of the Drosophila genome. *Genes Dev.* **23**, 589–601 (2009).

23. Fedorova, E. & Zink, D. Nuclear architecture and gene regulation. *Biochim. Biophys. Acta* **1783**, 2174–2184 (2008).

24. Creyghton, M. P. *et al.* Histone H3K27ac separates active from poised enhancers and predicts developmental state. *Proc. Natl. Acad. Sci. U. S. A.* **107**, 21931–21936 (2010).

25. Schneider, R. *et al.* Histone H3 lysine 4 methylation patterns in higher eukaryotic genes. *Nat. Cell Biol.* **6**, 73–77 (2004).

26. Barski, A. *et al.* High-Resolution Profiling of Histone Methylations in the Human Genome. *Cell* **129**, 823–837 (2007).

27. Bernstein, B. E. *et al.* A bivalent chromatin structure marks key developmental genes in embryonic stem cells. *Cell* **125**, 315–326 (2006).

28. Chi, A. S. & Bernstein, B. E. Chromatin and the pluripotent ground state. *Science* **323**, 220–221 (2009).

29. Trojer, P. & Reinberg, D. Facultative heterochromatin: is there a distinctive molecular signature? *Mol. Cell* **28**, 1–13 (2007).

30. Geng, T., Zhang, D. & Jiang, W. Concise Review: Epigenetic Regulation of Transition among Different Pluripotent States. *Stem Cells Dayt. Ohio* (2019).

31. Li, F. *et al.* Bivalent Histone Modifications and Development. *Curr. Stem Cell Res. Ther.* **13**, 83–90 (2018).

32. Lupiáñez, D. G., Spielmann, M. & Mundlos, S. Breaking TADs: How Alterations of Chromatin Domains Result in Disease. *Trends Genet. TIG* **32**, 225–237 (2016).

33. Bolzer, A. *et al.* Three-dimensional maps of all chromosomes in human male fibroblast nuclei and prometaphase rosettes. *PLoS Biol.* **3**, e157 (2005).

34. Bintu, B. *et al.* Super-resolution chromatin tracing reveals domains and cooperative interactions in single cells. *Science* **362**, (2018).

35. Boettiger, A. N. *et al.* Super-resolution imaging reveals distinct chromatin folding for different epigenetic states. *Nature* **529**, 418–422 (2016).

36. Paulsen, J. *et al.* Chrom3D: three-dimensional genome modeling from Hi-C and nuclear lamin-genome contacts. *Genome Biol.* **18**, 21 (2017).

37. Paulsen, J., Liyakat Ali, T. M. & Collas, P. Computational 3D genome modeling using Chrom3D. *Nat. Protoc.* **13**, 1137–1152 (2018).

38. Dixon, J. R. *et al.* Topological domains in mammalian genomes identified by analysis of chromatin interactions. *Nature* **485**, 376–380 (2012).

39. Nora, E. P. *et al.* Spatial partitioning of the regulatory landscape of the X-inactivation centre. *Nature* **485**, 381–385 (2012).

40. Beagrie, R. A. *et al.* Complex multi-enhancer contacts captured by genome architecture mapping. *Nature* **543**, 519–524 (2017).

41. Szabo, Q. *et al.* TADs are 3D structural units of higher-order chromosome organization in Drosophila. *Sci. Adv.* **4**, eaar8082 (2018).

42. Dixon, J. R. *et al.* Chromatin architecture reorganization during stem cell differentiation. *Nature* **518**, 331–336 (2015).

43. Kragesteen, B. K. *et al.* Dynamic 3D chromatin architecture contributes to enhancer specificity and limb morphogenesis. *Nat. Genet.* **50**, 1463–1473 (2018).

44. Cremer, T. & Cremer, M. Chromosome territories. *Cold Spring Harb. Perspect. Biol.* **2**, a003889 (2010).

45. Saitoh, N. *et al.* Proteomic analysis of interchromatin granule clusters. *Mol. Biol. Cell* **15**, 3876–3890 (2004).

46. Zhong, S., Salomoni, P. & Pandolfi, P. P. The transcriptional role of PML and the nuclear body. *Nat. Cell Biol.* **2**, E85-90 (2000).

47. Boisvert, F.-M., van Koningsbruggen, S., Navascués, J. & Lamond, A. I. The multifunctional nucleolus. *Nat. Rev. Mol. Cell Biol.* **8**, 574–585 (2007).

48. Delbarre, E. *et al.* PML protein organizes heterochromatin domains where it regulates histone H3.3 deposition by ATRX/DAXX. *Genome Res.* **27**, 913–921 (2017).

49. Morimoto, M. & Boerkoel, C. F. The Role of Nuclear Bodies in Gene Expression and Disease. *Biology* **2**, 976–1033 (2013).

50. Pontvianne, F. *et al.* Identification of Nucleolus-Associated Chromatin Domains Reveals a Role for the Nucleolus in 3D Organization of the A. thaliana Genome. *Cell Rep.* **16**, 1574–1587 (2016).

51. Németh, A. *et al.* Initial genomics of the human nucleolus. *PLoS Genet.* **6**, e1000889 (2010).

52. Two contrasting classes of nucleolus-associated domains in mouse fibroblast heterochromatin. *Genome Res.* **29**, 1235-1249 (2019).

53. Strom, A. R. *et al.* Phase separation drives heterochromatin domain formation. *Nature* **547**, 241–245 (2017).

54. Shin, Y. *et al.* Liquid Nuclear Condensates Mechanically Sense and Restructure the Genome. *Cell* **175**, 1481-1491.e13 (2018).

55. Sabari, B. R. *et al.* Coactivator condensation at super-enhancers links phase separation and gene control. *Science* **361**, (2018).

56. Tatavosian, R. *et al.* Nuclear condensates of the Polycomb protein chromobox 2 (CBX2) assemble through phase separation. *J. Biol. Chem.* **294**, 1451–1463 (2019).

57. Parada, L. & Misteli, T. Chromosome positioning in the interphase nucleus. *Trends Cell Biol.* **12**, 425–432 (2002).

58. Bickmore, W. A. The Spatial Organization of the Human Genome. *Annu. Rev. Genomics Hum. Genet.* **14**, 67–84 (2013).

59. Zimmer, C. & Fabre, E. Principles of chromosomal organization: lessons from yeast. *J. Cell Biol.* **192**, 723–733 (2011).

60. Bickmore, W. A. & van Steensel, B. Genome architecture: domain organization of interphase chromosomes. *Cell* **152**, 1270–1284 (2013).

61. Lieberman-Aiden, E. *et al.* Comprehensive mapping of long-range interactions reveals folding principles of the human genome. *Science* **326**, 289–293 (2009).

62. Nagano, T. *et al.* Cell-cycle dynamics of chromosomal organization at single-cell resolution. *Nature* **547**, 61–67 (2017).

63. Finn, E. H. *et al.* Extensive Heterogeneity and Intrinsic Variation in Spatial Genome Organization. *Cell* **176**, 1502-1515.e10 (2019).

64. Dixon, J. R., Gorkin, D. U. & Ren, B. Chromatin Domains: The Unit of Chromosome Organization. *Mol. Cell* **62**, 668–680 (2016).

65. Rao, S. S. P. *et al.* A 3D map of the human genome at kilobase resolution reveals principles of chromatin looping. *Cell* **159**, 1665–1680 (2014).

66. Van Bortle, K. *et al.* Insulator function and topological domain border strength scale with architectural protein occupancy. *Genome Biol.* **15**, R82 (2014).

67. Forsberg, F., Brunet, A., Ali, T. M. L. & Collas, P. Interplay of lamin A and lamin B LADs on the radial positioning of chromatin. *Nucleus* **10**, 7–20 (2019).

68. Paulsen, J. *et al.* Long-range interactions between topologically associating domains shape the four-dimensional genome during differentiation. *Nat. Genet.* **51**, 835–843 (2019).

69. Stadhouders, R. *et al.* Transcription factors orchestrate dynamic interplay between genome topology and gene regulation during cell reprogramming. *Nat. Genet.* **50**, 238–249 (2018).

70. Niskanen, H. *et al.* Endothelial cell differentiation is encompassed by changes in long range interactions between inactive chromatin regions. *Nucleic Acids Res.* **46**, 1724–1740 (2018).

71. Bonev, B. *et al.* Multiscale 3D Genome Rewiring during Mouse Neural Development. *Cell* **171**, 557-572.e24 (2017).

72. Olivares-Chauvet, P. *et al.* Capturing pairwise and multi-way chromosomal conformations using chromosomal walks. *Nature* **540**, 296–300 (2016).

73. Fraser, J. *et al.* Hierarchical folding and reorganization of chromosomes are linked to transcriptional changes in cellular differentiation. *Mol. Syst. Biol.* **11**, 852 (2015).

74. Quinodoz, S. A. *et al.* Higher-Order Inter-chromosomal Hubs Shape 3D Genome Organization in the Nucleus. *Cell* **174**, 744-757.e24 (2018).

75. Doynova, M. D., Markworth, J. F., Cameron-Smith, D., Vickers, M. H. & O'Sullivan, J. M. Linkages between changes in the 3D organization of the genome and transcription during myotube differentiation in vitro. *Skelet. Muscle* **7**, 5 (2017).

76. Szabo, Q., Bantignies, F. & Cavalli, G. Principles of genome folding into topologically associating domains. *Sci. Adv.* **5**, eaaw1668 (2019).

77. Grossman, E., Medalia, O. & Zwerger, M. Functional architecture of the nuclear pore complex. *Annu. Rev. Biophys.* **41**, 557–584 (2012).

78. Wente, S. R. & Rout, M. P. The Nuclear Pore Complex and Nuclear Transport. *Cold Spring Harb. Perspect. Biol.* **2**, (2010).

79. Schirmer, E. C. & Gerace, L. The nuclear membrane proteome: extending the envelope. *Trends Biochem. Sci.* **30**, 551–558 (2005).

80. Stewart, C. L., Roux, K. J. & Burke, B. Blurring the boundary: the nuclear envelope extends its reach. *Science* **318**, 1408–1412 (2007).

81. Terry, L. J., Shows, E. B. & Wente, S. R. Crossing the nuclear envelope: hierarchical regulation of nucleocytoplasmic transport. *Science* **318**, 1412–1416 (2007).

82. D'Angelo, M. A. & Hetzer, M. W. The role of the nuclear envelope in cellular organization. *Cell. Mol. Life Sci. CMLS* **63**, 316–332 (2006).

83. Crisp, M. *et al.* Coupling of the nucleus and cytoplasm: role of the LINC complex. *J. Cell Biol.* **172**, 41–53 (2006).

84. Sosa, B. A., Rothballer, A., Kutay, U. & Schwartz, T. U. LINC complexes form by binding of three KASH peptides to domain interfaces of trimeric SUN proteins. *Cell* **149**, 1035–1047 (2012).

85. Lombardi, M. L. *et al.* The interaction between nesprins and sun proteins at the nuclear envelope is critical for force transmission between the nucleus and cytoskeleton. *J. Biol. Chem.* **286**, 26743–26753 (2011).

86. Schirmer, E. C., Florens, L., Guan, T., Yates, J. R. & Gerace, L. Nuclear Membrane Proteins with Potential Disease Links Found by Subtractive Proteomics. *Science* **301**, 1380–1382 (2003).

87. Wilkie, G. S. *et al.* Several Novel Nuclear Envelope Transmembrane Proteins Identified in Skeletal Muscle Have Cytoskeletal Associations. *Mol. Cell. Proteomics* **10**, M110.003129 (2011).

88. Korfali, N. *et al.* The Leukocyte Nuclear Envelope Proteome Varies with Cell Activation and Contains Novel Transmembrane Proteins That Affect Genome Architecture. *Mol. Cell. Proteomics* **9**, 2571–2585 (2010).

89. Malik, P. *et al.* Cell-specific and lamin-dependent targeting of novel transmembrane proteins in the nuclear envelope. *Cell. Mol. Life Sci.* **67**, 1353–1369 (2010).

90. Holmer, L. & Worman, H. J. Inner nuclear membrane proteins: functions and targeting. *Cell. Mol. Life Sci. CMLS* **58**, 1741–1747 (2001).

91. Nili, E. *et al.* Nuclear membrane protein LAP2beta mediates transcriptional repression alone and together with its binding partner GCL (germ-cell-less). *J. Cell Sci.* **114**, 3297–3307 (2001).

92. Martins, S., Eikvar, S., Furukawa, K. & Collas, P. HA95 and LAP2β mediate a novel chromatin–nuclear envelope interaction implicated in initiation of DNA replication. *J. Cell Biol.* **160**, 177–188 (2003).

93. Mislow, J. M. K. *et al.* Nesprin-1alpha self-associates and binds directly to emerin and lamin A in vitro. *FEBS Lett.* **525**, 135–140 (2002).

94. Wheeler, M. A. *et al.* Distinct functional domains in nesprin-1alpha and nesprin-2beta bind directly to emerin and both interactions are disrupted in X-linked Emery-Dreifuss muscular dystrophy. *Exp. Cell Res.* **313**, 2845–2857 (2007).

95. Zhang, Q. *et al.* Nesprin-2 is a multi-isomeric protein that binds lamin and emerin at the nuclear envelope and forms a subcellular network in skeletal muscle. *J. Cell Sci.* **118**, 673–687 (2005).

96. Lammerding, J. *et al.* Abnormal nuclear shape and impaired mechanotransduction in emerin-deficient cells. *J. Cell Biol.* **170**, 781–791 (2005).

97. Markiewicz, E. *et al.* The inner nuclear membrane protein emerin regulates beta-catenin activity by restricting its accumulation in the nucleus. *EMBO J.* **25**, 3275–3285 (2006).

98. Pan, D. *et al.* The integral inner nuclear membrane protein MAN1 physically interacts with the R-Smad proteins to repress signaling by the transforming growth factor-{beta} superfamily of cytokines. *J. Biol. Chem.* **280**, 15992–16001 (2005).

99. Lin, F., Morrison, J. M., Wu, W. & Worman, H. J. MAN1, an integral protein of the inner nuclear membrane, binds Smad2 and Smad3 and antagonizes transforming growth factor-beta signaling. *Hum. Mol. Genet.* **14**, 437–445 (2005).

100. Burke, B. & Stewart, C. L. The nuclear lamins: flexibility in function. *Nat. Rev. Mol. Cell Biol.* **14**, 13–24 (2013).

101. Dobrzynska, A., Gonzalo, S., Shanahan, C. & Askjaer, P. The nuclear lamina in health and disease. *Nucleus* **7**, 233–248 (2016).

102. Dhe-Paganon, S., Werner, E. D., Chi, Y.-I. & Shoelson, S. E. Structure of the Globular Tail of Nuclear Lamin. *J. Biol. Chem.* **277**, 17381–17384 (2002).

103. Loewinger, L. & McKeon, F. Mutations in the nuclear lamin proteins resulting in their aberrant assembly in the cytoplasm. *EMBO J.* **7**, 2301–2309 (1988).

104. Gruenbaum, Y. & Medalia, O. Lamins: the structure and protein complexes. *Curr. Opin. Cell Biol.* **32**, 7–12 (2015).

105. Turgay, Y. *et al.* The molecular architecture of lamins in somatic cells. *Nature* **543**, 261–264 (2017).

106. Shimi, T. *et al.* The A- and B-type nuclear lamin networks: microdomains involved in chromatin organization and transcription. *Genes Dev.* **22**, 3409–3421 (2008).

107. Fisher, D. Z., Chaudhary, N. & Blobel, G. cDNA sequencing of nuclear lamins A and C reveals primary and secondary structural homology to intermediate filament proteins. *Proc. Natl. Acad. Sci.* **83**, 6450–6454 (1986).

108. Kolb, T., Maass, K., Hergt, M., Aebi, U. & Herrmann, H. Lamin A and lamin C form homodimers and coexist in higher complex forms both in the nucleoplasmic fraction and in the lamina of cultured human cells. *Nucl. Austin Tex* **2**, 425–433 (2011).

109. Eckersley-Maslin, M. A., Bergmann, J. H., Lazar, Z. & Spector, D. L. Lamin A/C is expressed in pluripotent mouse embryonic stem cells. *Nucl. Austin Tex* **4**, 53–60 (2013).

110. Röber, R. A., Weber, K. & Osborn, M. Differential timing of nuclear lamin A/C expression in the various organs of the mouse embryo and the young animal: a developmental study. *Dev. Camb. Engl.* **105**, 365–378 (1989).

111. Röber, R. A., Sauter, H., Weber, K. & Osborn, M. Cells of the cellular immune and hemopoietic system of the mouse lack lamins A/C: distinction versus other somatic cells. *J. Cell Sci.* **95 (Pt 4)**, 587–598 (1990).

112. Vargas, J. D., Hatch, E. M., Anderson, D. J. & Hetzer, M. W. Transient nuclear envelope rupturing during interphase in human cancer cells. *Nucleus* **3**, 88–100 (2012).

113. Sullivan, T. *et al.* Loss of a-Type Lamin Expression Compromises Nuclear Envelope Integrity Leading to Muscular Dystrophy. *J. Cell Biol.* **147**, 913–920 (1999).

114. Libotte, T. *et al.* Lamin A/C–dependent Localization of Nesprin-2, a Giant Scaffolder at the Nuclear Envelope. *Mol. Biol. Cell* **16**, 3411–3424 (2005).

115. Harborth, J., Elbashir, S. M., Bechert, K., Tuschl, T. & Weber, K. Identification of essential genes in cultured mammalian cells using small interfering RNAs. *J. Cell Sci.* **114**, 4557–4565 (2001).

116. Lammerding, J. *et al.* Lamin A/C deficiency causes defective nuclear mechanics and mechanotransduction. *J. Clin. Invest.* **113**, 370–378 (2004).

117. Haque, F. *et al.* SUN1 interacts with nuclear lamin A and cytoplasmic nesprins to provide a physical connection between the nuclear lamina and the cytoskeleton. *Mol. Cell. Biol.* **26**, 3738–3751 (2006).

118. Rowat, A. C. *et al.* Nuclear Envelope Composition Determines the Ability of Neutrophil-type Cells to Passage through Micron-scale Constrictions. *J. Biol. Chem.* **288**, 8610–8618 (2013).

119. Swift, J. *et al.* Nuclear lamin-A scales with tissue stiffness and enhances matrix-directed differentiation. *Science* **341**, 1240104 (2013).

120. Le, H. Q. *et al.* Mechanical regulation of transcription controls Polycomb-mediated gene silencing during lineage commitment. *Nat. Cell Biol.* **18**, 864–875 (2016).

121. Dechat, T. *et al.* Lamina-associated polypeptide 2alpha binds intranuclear A-type lamins. *J. Cell Sci.* **113 Pt 19**, 3473–3484 (2000).

122. Gesson, K. *et al.* A-type lamins bind both hetero- and euchromatin, the latter being regulated by lamina-associated polypeptide 2 alpha. *Genome Res.* (2016).

123. Kochin, V. *et al.* Interphase phosphorylation of lamin A. *J. Cell Sci.* **127**, 2683–2696 (2014).

124. Broers, J. L. *et al.* Dynamics of the nuclear lamina as monitored by GFP-tagged A-type lamins. *J. Cell Sci.* **112 (Pt 20)**, 3463–3475 (1999).

125. Gilchrist, S. *et al.* Altered protein dynamics of disease-associated lamin A mutants. *BMC Cell Biol.* **5**, 46 (2004).

126. Bronshtein, I. *et al.* Loss of lamin A function increases chromatin dynamics in the nuclear interior. *Nat. Commun.* **6**, 8044 (2015).

127. Naetar, N., Ferraioli, S. & Foisner, R. Lamins in the nuclear interior - life outside the lamina. *J. Cell Sci.* **130**, 2087–2096 (2017).

128. Naetar, N. *et al.* Loss of nucleoplasmic LAP2alpha-lamin A complexes causes erythroid and epidermal progenitor hyperproliferation. *Nat. Cell Biol.* **10**, 1341–1348 (2008).

129. Pekovic, V. *et al.* Nucleoplasmic LAP2alpha-lamin A complexes arerequired to maintain a proliferative state in human fibroblasts. *J. Cell Biol.* **176**, 163–172 (2007).

130. Cesarini, E. *et al.* Lamin A/C sustains PcG protein architecture, maintaining transcriptional repression at target genes. *J. Cell Biol.* **211**, 533–551 (2015).

131. Marullo, F. *et al.* Nucleoplasmic Lamin A/C and Polycomb group of proteins: An evolutionarily conserved interplay. *Nucl. Austin Tex* **7**, 103–111 (2016).

132. Viré, E. *et al.* The Polycomb group protein EZH2 directly controls DNA methylation. *Nature* **439**, 871–874 (2006).

133. Briand, N. *et al.* The lipodystrophic hotspot lamin A p.R482W mutation deregulates the mesodermal inducer T/Brachyury and early vascular differentiation gene networks. *Hum. Mol. Genet.* **27**, 1447–1459 (2018).

134. Oldenburg, A. *et al.* A lipodystrophy-causing lamin A mutant alters conformation and epigenetic regulation of the anti-adipogenic MIR335 locus. *J. Cell Biol.* **216**, 2731–2743 (2017).

135. Cesarini, E. *et al.* Lamin A/C sustains PcG protein architecture, maintaining transcriptional repression at target genes. *J. Cell Biol.* **211**, 533–551 (2015).

136. Peter, M. *et al.* Cloning and sequencing of cDNA clones encoding chicken lamins A and B1 and comparison of the primary structures of vertebrate A- and B-type lamins. *J. Mol. Biol.* **208**, 393–404 (1989).

137. Vorburger, K., Lehner, C. F., Kitten, G. T., Eppenberger, H. M. & Nigg, E. A. A second higher vertebrate B-type lamin: cDNA sequence determination and in vitro processing of chicken lamin B2. *J. Mol. Biol.* **208**, 405–415 (1989).

138. Lin, F. & Worman, H. J. Structural organization of the human gene (LMNB1) encoding nuclear lamin B1. *Genomics* **27**, 230–236 (1995).

139. Stewart, C. & Burke, B. Teratocarcinoma stem cells and early mouse embryos contain only a single major lamin polypeptide closely resembling lamin B. *Cell* **51**, 383–392 (1987).

140. Vergnes, L., Péterfy, M., Bergo, M. O., Young, S. G. & Reue, K. Lamin B1 is required for mouse development and nuclear integrity. *Proc. Natl. Acad. Sci.* **101**, 10428–10433 (2004).

141. Sen Gupta, A. & Sengupta, K. Lamin B2 Modulates Nucleolar Morphology, Dynamics, and Function. *Mol. Cell. Biol.* **37**, (2017).

142. Moir, R. D., Montag-Lowy, M. & Goldman, R. D. Dynamic properties of nuclear lamins: lamin B is associated with sites of DNA replication. *J. Cell Biol.* **125**, 1201–1212 (1994).

143. Shumaker, D. K. *et al.* The highly conserved nuclear lamin Ig-fold binds to PCNA: its role in DNA replication. *J. Cell Biol.* **181**, 269–280 (2008).

144. Camps, J. *et al.* Loss of lamin B1 results in prolongation of S phase and decondensation of chromosome territories. *FASEB J. Off. Publ. Fed. Am. Soc. Exp. Biol.* **28**, 3423–3434 (2014).

145. Shimi, T. *et al.* The role of nuclear lamin B1 in cell proliferation and senescence. *Genes Dev.* **25**, 2579–2593 (2011).

146. Freund, A., Laberge, R.-M., Demaria, M. & Campisi, J. Lamin B1 loss is a senescence-associated biomarker. *Mol. Biol. Cell* **23**, 2066–2075 (2012).

147. Kitten, G. T. & Nigg, E. A. The CaaX motif is required for isoprenylation, carboxyl methylation, and nuclear membrane association of lamin B2. *J. Cell Biol.* **113**, 13–23 (1991).

148. Beck, L. A., Hosick, T. J. & Sinensky, M. Isoprenylation is required for the processing of the lamin A precursor. *J. Cell Biol.* **110**, 1489–1499 (1990).

149. Holtz, D., Tanaka, R. A., Hartwig, J. & McKeon, F. The CaaX motif of lamin A functions in conjunction with the nuclear localization signal to target assembly to the nuclear envelope. *Cell* **59**, 969–977 (1989).

150. Adam, S. A., Butin-Israeli, V., Cleland, M. M., Shimi, T. & Goldman, R. D. Disruption of lamin B1 and lamin B2 processing and localization by farnesyltransferase inhibitors. *Nucleus* **4**, 142–150 (2013).

151. Maske, C. P. *et al.* A carboxyl-terminal interaction of lamin B1 is dependent on the CAAX endoprotease Rce1 and carboxymethylation. *J. Cell Biol.* **162**, 1223–1232 (2003).

152. Barrowman, J., Hamblet, C., Kane, M. S. & Michaelis, S. Requirements for efficient proteolytic cleavage of prelamin A by ZMPSTE24. *PloS One* **7**, e32120 (2012).

153. Corrigan, D. P. *et al.* Prelamin A endoproteolytic processing in vitro by recombinant Zmpste24. *Biochem. J.* **387**, 129–138 (2005).

154. Bergo, M. O. *et al.* Isoprenylcysteine carboxyl methyltransferase deficiency in mice. *J. Biol. Chem.* **276**, 5841–5845 (2001).

155. Lau, H. Y. *et al.* An improved isoprenylcysteine carboxylmethyltransferase inhibitor induces cancer cell death and attenuates tumor growth in vivo. *Cancer Biol. Ther.* **15**, 1280–1291 (2014).

156. Weber, K., Plessmann, U. & Traub, P. Maturation of nuclear lamin A involves a specific carboxy-terminal trimming, which removes the polyisoprenylation site from the precursor; implications for the structure of the nuclear lamina. *FEBS Lett.* **257**, 411–414 (1989).

157. Young, S. G., Fong, L. G. & Michaelis, S. Prelamin A, Zmpste24, misshapen cell nuclei, and progeria--new evidence suggesting that protein farnesylation could be important for disease pathogenesis. *J. Lipid Res.* **46**, 2531–2558 (2005).

158. Eriksson, M. *et al.* Recurrent de novo point mutations in lamin A cause Hutchinson-Gilford progeria syndrome. *Nature* **423**, 293–298 (2003).

159. Solovei, I. *et al.* LBR and lamin A/C sequentially tether peripheral heterochromatin and inversely regulate differentiation. *Cell* **152**, 584–598 (2013).

160. Thanisch, K. *et al.* Nuclear envelope localization of LEMD2 is developmentally dynamic and lamin A/C dependent yet insufficient for heterochromatin tethering. *Differ. Res. Biol. Divers.* **94**, 58–70 (2017).

161. Ye, Q., Callebaut, I., Pezhman, A., Courvalin, J. C. & Worman, H. J. Domain-specific interactions of human HP1-type chromodomain proteins and inner nuclear membrane protein LBR. *J. Biol. Chem.* **272**, 14983–14989 (1997).

162. Bannister, A. J. *et al.* Selective recognition of methylated lysine 9 on histone H3 by the HP1 chromo domain. *Nature* **410**, 120–124 (2001).

163. Lee, K. K. *et al.* Distinct functional domains in emerin bind lamin A and DNA-bridging protein BAF. *J. Cell Sci.* **114**, 4567–4573 (2001).

164. Shumaker, D. K., Lee, K. K., Tanhehco, Y. C., Craigie, R. & Wilson, K. L. LAP2 binds to BAF.DNA complexes: requirement for the LEM domain and modulation by variable regions. *EMBO J.* **20**, 1754–1764 (2001).

165. Lin, F. *et al.* MAN1, an inner nuclear membrane protein that shares the LEM domain with lamina-associated polypeptide 2 and emerin. *J. Biol. Chem.* **275**, 4840–4847 (2000).

166. Somech, R. *et al.* The nuclear-envelope protein and transcriptional repressor LAP2beta interacts with HDAC3 at the nuclear periphery, and induces histone H4 deacetylation. *J. Cell Sci.* **118**, 4017–4025 (2005).

167. Milon, B. C. *et al.* Role of histone deacetylases in gene regulation at nuclear lamina. *PloS One* **7**, e49692 (2012).

168. Worman, H. J., Yuan, J., Blobel, G. & Georgatos, S. D. A lamin B receptor in the nuclear envelope. *Proc. Natl. Acad. Sci. U. S. A.* **85**, 8531–8534 (1988).

169. Furukawa, K. & Kondo, T. Identification of the lamina-associated-polypeptide-2-binding domain of B-type lamin. *Eur. J. Biochem.* **251**, 729–733 (1998).

170. Clements, L., Manilal, S., Love, D. R. & Morris, G. E. Direct interaction between emerin and lamin A. *Biochem. Biophys. Res. Commun.* **267**, 709–714 (2000).

171. Robson, M. I. *et al.* Tissue-Specific Gene Repositioning by Muscle Nuclear Membrane Proteins Enhances Repression of Critical Developmental Genes during Myogenesis. *Mol. Cell* **62**, 834–847 (2016).

172. Guelen, L. *et al.* Domain organization of human chromosomes revealed by mapping of nuclear lamina interactions. *Nature* **453**, 948–951 (2008).

173. Lund, E., Oldenburg, A. R. & Collas, P. Enriched domain detector: a program for detection of wide genomic enrichment domains robust against local variations. *Nucleic Acids Res.* **42**, e92 (2014).

174. Kind, J. *et al.* Single-cell dynamics of genome-nuclear lamina interactions. *Cell* **153**, 178–192 (2013).

175. Vogel, M. J., Peric-Hupkes, D. & van Steensel, B. Detection of *in vivo* protein–DNA interactions using DamID in mammalian cells. *Nat. Protoc.* **2**, 1467–1478 (2007).

176. Rønningen, T. *et al.* Prepatterning of differentiation-driven nuclear lamin A/C-associated chromatin domains by GlcNAcylated histone H2B. *Genome Res.* **25**, 1825–1835 (2015).

177. Lund, E. *et al.* Lamin A/C-promoter interactions specify chromatin state-dependent transcription outcomes. *Genome Res.* **23**, 1580–1589 (2013).

178. Lund, E. G., Duband-Goulet, I., Oldenburg, A., Buendia, B. & Collas, P. Distinct features of lamin A-interacting chromatin domains mapped by ChIP-sequencing from sonicated or micrococcal nuclease-digested chromatin. *Nucl. Austin Tex* **6**, 30–39 (2015).

179. Kind, J. *et al.* Genome-wide maps of nuclear lamina interactions in single human cells. *Cell* **163**, 134–147 (2015).

180. Zheng, X. *et al.* Lamins Organize the Global Three-Dimensional Genome from the Nuclear Periphery. *Mol. Cell* **71**, 802-815.e7 (2018).

181. Harr, J. C. *et al.* Directed targeting of chromatin to the nuclear lamina is mediated by chromatin state and A-type lamins. *J. Cell Biol.* **208**, 33–52 (2015).

182. Peric-Hupkes, D. *et al.* Molecular maps of the reorganization of genome-nuclear lamina interactions during differentiation. *Mol. Cell* **38**, 603–613 (2010).

183. Meuleman, W. *et al.* Constitutive nuclear lamina-genome interactions are highly conserved and associated with A/T-rich sequence. *Genome Res.* **23**, 270–280 (2013).

184. van Koningsbruggen, S. *et al.* High-resolution whole-genome sequencing reveals that specific chromatin domains from most human chromosomes associate with nucleoli. *Mol. Biol. Cell* **21**, 3735–3748 (2010).

185. Zullo, J. M. *et al.* DNA sequence-dependent compartmentalization and silencing of chromatin at the nuclear lamina. *Cell* **149**, 1474–1487 (2012).

186. Poleshko, A. *et al.* Genome-Nuclear Lamina Interactions Regulate Cardiac Stem Cell Lineage Restriction. *Cell* **171**, 573-587.e14 (2017).

187. Bian, Q., Khanna, N., Alvikas, J. & Belmont, A. S. β-Globin cis-elements determine differential nuclear targeting through epigenetic modifications. *J. Cell Biol.* **203**, 767–783 (2013).

188. Chen, X. *et al.* The visualization of large organized chromatin domains enriched in the H3K9me2 mark within a single chromosome in a single cell. *Epigenetics* **9**, 1439–1445 (2014).

189. Towbin, B. D. *et al.* Step-wise methylation of histone H3K9 positions heterochromatin at the nuclear periphery. *Cell* **150**, 934–947 (2012).

190. Shachar, S., Voss, T. C., Pegoraro, G., Sciascia, N. & Misteli, T. Identification of Gene Positioning Factors Using High-Throughput Imaging Mapping. *Cell* **162**, 911–923 (2015).

191. Reddy, K. L., Zullo, J. M., Bertolino, E. & Singh, H. Transcriptional repression mediated by repositioning of genes to the nuclear lamina. *Nature* **452**, 243–247 (2008).

192. Robson, M. I. *et al.* Constrained release of lamina-associated enhancers and genes from the nuclear envelope during T-cell activation facilitates their association in chromosome compartments. *Genome Res.* **27**, 1126–1138 (2017).

193. Leemans, C. *et al.* Promoter-Intrinsic and Local Chromatin Features Determine Gene Repression in LADs. *Cell* **177**, 852-864.e14 (2019).

194. Marshall, W. F. *et al.* Interphase chromosomes undergo constrained diffusional motion in living cells. *Curr. Biol.* **7**, 930–939 (1997).

195. Bronshtein, I. *et al.* Exploring chromatin organization mechanisms through its dynamic properties. *Nucleus* **7**, 27–33 (2016).

196. Vivante, A., Brozgol, E., Bronshtein, I., Levi, V. & Garini, Y. Chromatin dynamics governed by a set of nuclear structural proteins. *Genes. Chromosomes Cancer* **58**, 437–451 (2019).

197. Solovei, I. *et al.* Nuclear architecture of rod photoreceptor cells adapts to vision in mammalian evolution. *Cell* **137**, 356–368 (2009).

198. Pascual-Reguant, L. *et al.* Lamin B1 mapping reveals the existence of dynamic and functional euchromatin lamin B1 domains. *Nat. Commun.* **9**, 3420 (2018).

199. Worman, H. J. & Bonne, G. 'Laminopathies': a wide spectrum of human diseases. *Exp. Cell Res.* **313**, 2121–2133 (2007).

200. De Sandre-Giovannoli, A. *et al.* Lamin a truncation in Hutchinson-Gilford progeria. *Science* **300**, 2055 (2003).

201. Goldman, R. D. *et al.* Accumulation of mutant lamin A causes progressive changes in nuclear architecture in Hutchinson-Gilford progeria syndrome. *Proc. Natl. Acad. Sci. U. S. A.* **101**, 8963–8968 (2004).

202. Shumaker, D. K. *et al.* Mutant nuclear lamin A leads to progressive alterations of epigenetic control in premature aging. *Proc. Natl. Acad. Sci. U. S. A.* **103**, 8703–8708 (2006).

203. McCord, R. P. *et al.* Correlated alterations in genome organization, histone methylation, and DNA-lamin A/C interactions in Hutchinson-Gilford progeria syndrome. *Genome Res.* **23**, 260–269 (2013).

204. Toth, J. I. *et al.* Blocking protein farnesyltransferase improves nuclear shape in fibroblasts from humans with progeroid syndromes. *Proc. Natl. Acad. Sci. U. S. A.* **102**, 12873–12878 (2005).

205. Vigouroux, C. *et al.* Nuclear envelope disorganization in fibroblasts from lipodystrophic patients with heterozygous R482Q/W mutations in the lamin A/C gene. *J. Cell Sci.* **114**, 4459–4468 (2001).

206. Beisaw, A. *et al.* BRACHYURY directs histone acetylation to target loci during mesoderm development. *EMBO Rep.* **19**, 118–134 (2018).

207. Mohawk, J. A., Green, C. B. & Takahashi, J. S. Central and peripheral circadian clocks in mammals. *Annu. Rev. Neurosci.* **35**, 445–462 (2012).

208. Panda, S. Circadian physiology of metabolism. *Science* **354**, 1008–1015 (2016).

209. Lowrey, P. L. & Takahashi, J. S. Mammalian circadian biology: elucidating genome-wide levels of temporal organization. *Annu. Rev. Genomics Hum. Genet.* **5**, 407–441 (2004).

210. Cheng, M. Y. *et al.* Prokineticin 2 transmits the behavioural circadian rhythm of the suprachiasmatic nucleus. *Nature* **417**, 405 (2002).

211. Kramer, A. *et al.* Regulation of Daily Locomotor Activity and Sleep by Hypothalamic EGF Receptor Signaling. *Science* **294**, 2511–2515 (2001).

212. Allen, G., Rappe, J., Earnest, D. J. & Cassone, V. M. Oscillating on Borrowed Time: Diffusible Signals from Immortalized Suprachiasmatic Nucleus Cells Regulate Circadian Rhythmicity in Cultured Fibroblasts. *J. Neurosci.* **21**, 7937–7943 (2001).

213. Moore, R. Y. & Eichler, V. B. Loss of a circadian adrenal corticosterone rhythm following suprachiasmatic lesions in the rat. *Brain Res.* **42**, 201–206 (1972).

214. Stephan, F. K. & Zucker, I. Circadian Rhythms in Drinking Behavior and Locomotor Activity of Rats Are Eliminated by Hypothalamic Lesions. *Proc. Natl. Acad. Sci. U. S. A.* **69**, 1583–1586 (1972).

215. Schwartz, W. J. & Gainer, H. Suprachiasmatic nucleus: use of 14C-labeled deoxyglucose uptake as a functional marker. *Science* **197**, 1089–1091 (1977).

216. Rudic, R. D. *et al.* BMAL1 and CLOCK, Two Essential Components of the Circadian Clock, Are Involved in Glucose Homeostasis. *PLOS Biol.* **2**, e377 (2004).

217. Dupuis, J. *et al.* New genetic loci implicated in fasting glucose homeostasis and their impact on type 2 diabetes risk. *Nat. Genet.* **42**, 105–116 (2010).

218. Karlsson, B., Knutsson, A. & Lindahl, B. Is there an association between shift work and having a metabolic syndrome? Results from a population based study of 27 485 people. *Occup. Environ. Med.* **58**, 747–752 (2001).

219. Gekakis, N. *et al.* Role of the CLOCK protein in the mammalian circadian mechanism. *Science* **280**, 1564–1569 (1998).

220. Hogenesch, J. B., Gu, Y. Z., Jain, S. & Bradfield, C. A. The basic-helix-loop-helix-PAS orphan MOP3 forms transcriptionally active complexes with circadian and hypoxia factors. *Proc. Natl. Acad. Sci. U. S. A.* **95**, 5474–5479 (1998).

221. Lee, C., Etchegaray, J. P., Cagampang, F. R., Loudon, A. S. & Reppert, S. M. Posttranslational mechanisms regulate the mammalian circadian clock. *Cell* **107**, 855–867 (2001).

222. Jin, X. *et al.* A molecular mechanism regulating rhythmic output from the suprachiasmatic circadian clock. *Cell* **96**, 57–68 (1999).

223. Kume, K. *et al.* mCRY1 and mCRY2 are essential components of the negative limb of the circadian clock feedback loop. *Cell* **98**, 193–205 (1999).

224. Yu, W., Nomura, M. & Ikeda, M. Interactivating feedback loops within the mammalian clock: BMAL1 is negatively autoregulated and upregulated by CRY1, CRY2, and PER2. *Biochem. Biophys. Res. Commun.* **290**, 933–941 (2002).

225. Sato, T. K. *et al.* A functional genomics strategy reveals Rora as a component of the mammalian circadian clock. *Neuron* **43**, 527–537 (2004).

226. Preitner, N. *et al.* The orphan nuclear receptor REV-ERBalpha controls circadian transcription within the positive limb of the mammalian circadian oscillator. *Cell* **110**, 251–260 (2002).

227. Balsalobre, A., Damiola, F. & Schibler, U. A serum shock induces circadian gene expression in mammalian tissue culture cells. *Cell* **93**, 929–937 (1998).

228. Nagoshi, E. *et al.* Circadian gene expression in individual fibroblasts: cell-autonomous and self-sustained oscillators pass time to daughter cells. *Cell* **119**, 693–705 (2004).

229. Welsh, D. K., Yoo, S.-H., Liu, A. C., Takahashi, J. S. & Kay, S. A. Bioluminescence imaging of individual fibroblasts reveals persistent, independently phased circadian rhythms of clock gene expression. *Curr. Biol. CB* **14**, 2289–2295 (2004).

230. Yoo, S.-H. *et al.* PERIOD2::LUCIFERASE real-time reporting of circadian dynamics reveals persistent circadian oscillations in mouse peripheral tissues. *Proc. Natl. Acad. Sci. U. S. A.* **101**, 5339–5346 (2004).

231. Zhang, R., Lahens, N. F., Ballance, H. I., Hughes, M. E. & Hogenesch, J. B. A circadian gene expression atlas in mammals: implications for biology and medicine. *Proc. Natl. Acad. Sci. U. S. A.* **111**, 16219–16224 (2014).

232. Storch, K.-F. *et al.* Extensive and divergent circadian gene expression in liver and heart. *Nature* **417**, 78–83 (2002).

233. Reick, M., Garcia, J. A., Dudley, C. & McKnight, S. L. NPAS2: an analog of clock operative in the mammalian forebrain. *Science* **293**, 506–509 (2001).

234. Koike, N. *et al.* Transcriptional architecture and chromatin landscape of the core circadian clock in mammals. *Science* **338**, 349–354 (2012).

235. Takahashi, J. S. Transcriptional architecture of the mammalian circadian clock. *Nat. Rev. Genet.* **18**, 164–179 (2017).

236. Etchegaray, J.-P., Lee, C., Wade, P. A. & Reppert, S. M. Rhythmic histone acetylation underlies transcription in the mammalian circadian clock. *Nature* **421**, 177–182 (2003).

237. Hosoda, H. *et al.* CBP/p300 is a cell type-specific modulator of CLOCK/BMAL1-mediated transcription. *Mol. Brain* **2**, 34 (2009).

238. Curtis, A. M. *et al.* Histone acetyltransferase-dependent chromatin remodeling and the vascular clock. *J. Biol. Chem.* **279**, 7091–7097 (2004).

239. Katada, S. & Sassone-Corsi, P. The histone methyltransferase MLL1 permits the oscillation of circadian gene expression. *Nat. Struct. Mol. Biol.* **17**, 1414–1421 (2010).

240. Valekunja, U. K. *et al.* Histone methyltransferase MLL3 contributes to genome-scale circadian transcription. *Proc. Natl. Acad. Sci. U. S. A.* **110**, 1554–1559 (2013).

241. Doi, M., Hirayama, J. & Sassone-Corsi, P. Circadian regulator CLOCK is a histone acetyltransferase. *Cell* **125**, 497–508 (2006).

242. Masri, S. *et al.* Partitioning circadian transcription by SIRT6 leads to segregated control of cellular metabolism. *Cell* **158**, 659–672 (2014).

243. Nakahata, Y. *et al.* The NAD+-dependent deacetylase SIRT1 modulates CLOCK-mediated chromatin remodeling and circadian control. *Cell* **134**, 329–340 (2008).

244. Nakahata, Y., Sahar, S., Astarita, G., Kaluzova, M. & Sassone-Corsi, P. Circadian control of the NAD+ salvage pathway by CLOCK-SIRT1. *Science* **324**, 654–657 (2009).

245. DiTacchio, L. *et al.* Histone lysine demethylase JARID1a activates CLOCK-BMAL1 and influences the circadian clock. *Science* **333**, 1881–1885 (2011).

246. Nam, H. J. *et al.* Phosphorylation of LSD1 by PKCα Is Crucial for Circadian Rhythmicity and Phase Resetting. *Mol. Cell* **53**, 791–805 (2014).

247. Le Martelot, G. *et al.* Genome-wide RNA polymerase II profiles and RNA accumulation reveal kinetics of transcription and associated epigenetic changes during diurnal cycles. *PLoS Biol.* **10**, e1001442 (2012).

248. Duong, H. A., Robles, M. S., Knutti, D. & Weitz, C. J. A molecular mechanism for circadian clock negative feedback. *Science* **332**, 1436–1439 (2011).

249. Duong, H. A. & Weitz, C. J. Temporal orchestration of repressive chromatin modifiers by circadian clock Period complexes. *Nat. Struct. Mol. Biol.* **21**, 126–132 (2014).

250. Feng, D. *et al.* A circadian rhythm orchestrated by histone deacetylase 3 controls hepatic lipid metabolism. *Science* **331**, 1315–1319 (2011).

251. Zhang, Y. *et al.* Discrete functions of nuclear receptor Rev-erbα couple metabolism to the clock. *Science* **348**, 1488–1492 (2015).

252. Fang, B. *et al.* Circadian enhancers coordinate multiple phases of rhythmic gene transcription in vivo. *Cell* **159**, 1140–1152 (2014).

253. Kim, Y. H. *et al.* Rev-erbα dynamicallymodulates chromatin looping to control circadian gene transcription. *Science* **359**, 1274–1277 (2018).

254. Beytebiere, J. R. *et al.* Tissue-specific BMAL1 cistromes reveal that rhythmic transcription is associated with rhythmic enhancer-enhancer interactions. *Genes Dev.* **33**, 294–309 (2019).

255. Yeung, J. *et al.* Transcription factor activity rhythms and tissue-specific chromatin interactions explain circadian gene expression across organs. *Genome Res.* **28**, 182–191 (2018).

256. Aguilar-Arnal, L. *et al.* Cycles in spatial and temporal chromosomal organization driven by the circadian clock. *Nat. Struct. Mol. Biol.* **20**, 1206–1213 (2013).

257. Lin, S.-T. *et al.* Nuclear envelope protein MAN1 regulates clock through BMAL1. *eLife* **3**, e02981 (2014).

258. Liu, B. *et al.* Resveratrol rescues SIRT1-dependent adult stem cell decline and alleviates progeroid features in laminopathy-based progeria. *Cell Metab.* **16**, 738–750 (2012).

259. Ghosh, S., Liu, B., Wang, Y., Hao, Q. & Zhou, Z. Lamin A Is an Endogenous SIRT6 Activator and Promotes SIRT6-Mediated DNA Repair. *Cell Rep.* **13**, 1396–1406 (2015).

260. Zhao, H. *et al.* PARP1- and CTCF-Mediated Interactions between Active and Repressed Chromatin at the Lamina Promote Oscillating Transcription. *Mol. Cell* **59**, 984–997 (2015).

261. Ong, C.-T. & Corces, V. G. CTCF: an architectural protein bridging genome topology and function. *Nat. Rev. Genet.* **15**, 234–246 (2014).

262. Matsuda, S. & Koyasu, S. Mechanisms of action of cyclosporine. *Immunopharmacology* **47**, 119–125 (2000).

263. Qi, R., Wang, D., Xing, L. & Wu, Z. Cyclosporin A inhibits mitochondrial biogenesis in Hep G2 cells. *Biochem. Biophys. Res. Commun.* **496**, 941–946 (2018).

264. Benet, M. *et al.* Repression of the Nuclear Receptor Small Heterodimer Partner by Steatotic Drugs and in Advanced Nonalcoholic Fatty Liver Disease. *Mol. Pharmacol.* **87**, 582–594 (2015).

265. Bäckman, L., Appelkvist, E. L., Sundberg, A., Teclebrhan, H. & Brunk, U. Modulation of metabolism in HepG2 cells upon treatment with cyclosporin A and Nva2-cyclosporin. *Exp. Mol. Pathol.* **54**, 242–254 (1991).

266. Lausada, N., de Gómez Dumm, I. N. T., Raimondi, J. C. & de Alaniz, M. J. T. Effect of Cyclosporine and Sirolimus on Fatty Acid Desaturase Activities in Cultured HEPG2 Cells. *Transplant. Proc.* **41**, 1865–1870 (2009).

267. Koppelstaetter, C. *et al.* Effect of cyclosporine, tacrolimus and sirolimus on cellular senescence in renal epithelial cells. *Toxicol. Vitro Int. J. Publ. Assoc. BIBRA* **48**, 86–92 (2018).

268. Lenain, C. *et al.* Massive reshaping of genome-nuclear lamina interactions during oncogene-induced senescence. *Genome Res.* **27**, 1634–1644 (2017).

269. Shah, P. P. *et al.* Lamin B1 depletion in senescent cells triggers large-scale changes in gene expression and the chromatin landscape. *Genes Dev.* **27**, 1787–1799 (2013).

270. Ghaben, A. L. & Scherer, P. E. Adipogenesis and metabolic health. *Nat. Rev. Mol. Cell Biol.* **20**, 242–258 (2019).

271. Shoham, N. *et al.* Adipocyte stiffness increases with accumulation of lipid droplets. *Biophys. J.* **106**, 1421–1431 (2014).

272. Hapala, I., Marza, E. & Ferreira, T. Is fat so bad? Modulation of endoplasmic reticulum stress by lipid droplet formation. *Biol. Cell* **103**, 271–285 (2011).

273. Müller, F. A. & Sturla, S. J. Human in vitro models of nonalcoholic fatty liver disease. *Curr. Opin. Toxicol.* **16**, 9–16 (2019).

274. Tahara, Y., Otsuka, M., Fuse, Y., Hirao, A. & Shibata, S. Refeeding after fasting elicits insulin-dependent regulation of Per2 and Rev-erbα with shifts in the liver clock. *J. Biol. Rhythms* **26**, 230–240 (2011).

275. Wang, Y. *et al.* A mutation abolishing the ZMPSTE24 cleavage site in prelamin A causes a progeroid disorder. *J. Cell Sci.* **129**, 1975–1980 (2016).

I

Interplay of lamin A and lamin B LADs on the radial positioning of chromatin

Frida Forsberg, Annaël Brunet, Tharvesh M. Liyakat Ali & Philippe Collas

Taylor & Francis
Taylor & Francis Group

RESEARCH ARTICLE

∂ OPEN ACCESS ⊙ Check for updates

Interplay of lamin A and lamin B LADs on the radial positioning of chromatin

Frida Forsberg[a], Annaël Brunet[a], Tharvesh M. Liyakat Ali[a], and Philippe Collas[a,b]

[a]Department of Molecular Medicine, Institute of Basic Medical Sciences, Faculty of Medicine, University of Oslo, Oslo, Norway; [b]Norwegian Center for Stem Cell Research, Department of Immunology and Transfusion Medicine, Oslo University Hospital, Oslo, Norway

ABSTRACT

Immunosuppressive drugs such as cyclosporin A (CsA) can elicit hepatotoxicity by affecting gene expression. Here, we address the link between CsA and large-scale chromatin organization in HepG2 hepatocarcinoma cells. We show the existence of lamina-associated domains (LADs) interacting with lamin A, lamin B, or both. These 'A-B', 'A-only' and 'B-only' LADs display distinct fates after CsA treatment: A-B LADs remain constitutive or lose A, A-only LADs mainly lose A or switch to B, and B-only LADs remain B-only or acquire A. LAD rearrangement is overall uncoupled from changes in gene expression. Three-dimensional (3D) genome modeling predicts changes in radial positioning of LADs as LADs switch identities, which are corroborated by fluorescence *in situ* hybridization. Our results reveal interplay between A- and B-type lamins on radial locus positioning, suggesting complementary contributions to large-scale genome architecture. The data also unveil a hitherto unsuspected impact of cytotoxic drugs on genome conformation.

Abbreviations: ChIP-seq: chromatin immunoprecipitation sequencing; CsA: cyclosporin A; FISH: fluorescence *in situ* hybridization; ICMT: isoprenylcysteine methyltransferase; LAD: lamina-associated domain; TAD: topologically-associated domain

Introduction

Drug-induced hepatotoxicity, a common cause of clinical trial failure, has led to the use of cellular models such as HepG2 hepatocarcinoma cells for drug testing [1,2]. At micromolar concentrations, the steatotic drug cyclosporin A (CsA) inhibits several signaling pathways in HepG2 cells [3], resulting in metabolic alterations [1,3,4]. Interestingly, CsA can also act by modulating the binding of transcription factors to chromatin [3], suggesting an impact on genome organization.

The mammalian genome is organized into compartments of active and inactive chromatin [5] and within these, regions of high-frequency chromosomal interactions termed topologically associated domains (TADs) [6,7]. The genome is also radially organized, with lamina-associated domains (LADs) anchoring chromatin to the nuclear lamina, at the nuclear periphery [8], a meshwork of lamins A/C (from here on, 'lamin A') and B [9]. As such, lamin-chromatin interactions play an important role in the radial (center – periphery) positioning of loci in

the nucleus [10]. LADs are typically 0.1–10 megabases (Mb), gene-poor, enriched in heterochromatin and display low gene activity [8,11]. While lamins A and B are localized at the nuclear lamina, a nucleoplasmic pool of lamin A also interacts with euchromatic regions [12–16]. Intriguingly, a minor fraction of lamin B1 has also been found in the nuclear interior also in association with euchromatin [17]. These observations suggest that alterations in lamin-genome interactions may impact genome organization at the nuclear periphery and in the nuclear interior.

Lamin-chromatin interactions can be altered during differentiation [14,15,18–20], indicating that some of these interactions are dynamic. Moreover, lamins A and B can form LADs that overlap but can also be distinct [12,13], suggesting redundant but also complementary roles of A- and B-type lamins in the modulation of radial genome conformation [21,22].

In light of these observations, to address the relationship between CsA exposure and genome

CONTACT Annaël Brunet ✉ annaelle.brunet@medisin.uio.no; Philippe Collas ✉ philippe.collas@medisin.uio.no ⊟ Department of Molecular Medicine, Institute of Basic Medical Sciences, Faculty of Medicine, University of Oslo, Oslo, Norway

ⓘ Supplemental data for this article can be accessed here.

organization, we examined here the effect of CsA on the association of chromatin with nuclear lamina. We report an impact of CsA on the dynamics of interactions of lamins A and B with the genome. Such interactions can be gained, lost or interchanged in a manner uncoupled from gene expression changes. They also correlate with distinct patterns of radial repositioning of loci predicted from 3D genome models and confirmed by fluorescence *in situ* hybridization (FISH). The data suggest an A- and B-type lamin interplay in radial genome conformation and reveal unsuspected effects of cyto-toxic compounds such as CsA on nuclear organization.

Results

CsA elicits pre-lamin A accumulation

Before investigating changes in genome organization that might be elicited by CsA, we determined whether CsA altered levels of nuclear lamins. We used 10 μM CsA, a concentration in the range of doses used in hepatotoxicity assays [4,23]. This dose is sub-cytotoxic over the 72 h period considered here, avoiding necrotic or apoptotic drawbacks [3]. Western blot analysis shows that exposure of HepG2 cells to CsA did not alter levels of lamins A/C and B1; however CsA elicited consistent and sig-nificant pre-lamin A accumulation (P = 6 × 10^{-5}], paired t-tests relative to controls; Figure 1(a,b)). This was verified using another lamin A/C antibody (Santa-Cruz sc7292x) and an antibody against pre-lamin A (Santa-Cruz sc6214) (Figure 1(c,d)). Immunofluorescence labeling confirmed the upregu-lation and localization of pre-lamin A at the nuclear periphery (Figure 1(e)). We also generated RNA-sequencing (RNA-seq) data for control and CsA-treated cells, and show that CsA did not alter *LMNA* or *LMNB1* transcript levels (Figure 1(f); Supplementary Table S1).

Importantly, CsA does not affect protein or tran-script levels of ZMPSTE24 (Figure 1(a,f)), the protease involved in lamin A maturation [9], suggesting that processes other than altered ZMPSTE24 levels inter-fere with lamin A maturation upon CsA exposure. This finding is consistent with the fact that ablation of ZMPSTE24 in mice results in complete inhibition of pre-lamin A maturation [24]. Our findings, rather, are reminiscent of partial pre-lamin A processing

observed after depletion or inhibition of isoprenylcys-teine carboxymethylation [24]. We cannot at present exclude that this pre-lamin A accumulation results from a senescence phenotype or cellular stress elicited by CsA [1,2,23,25]. Accumulation of pre-lamin A at the nuclear envelope however suggests that interac-tions of chromatin with the nuclear lamina could be altered.

Lamin A association with lamin B LADs

We thus determined whether LADs were remodeled in CsA-treated cells. We mapped lamin B LADs (from here on called 'B-LADs') and lamin A LADs ('A-LADs') by chromatin immunoprecipitation-sequencing (ChIP-seq) of lamin B1 and lamin A/C, respectively. Of note, the anti-lamin A/C ChIP anti-body (Santa-Cruz sc7292x) immunoprecipitated not only lamin A/C but also pre-lamin A (Figure 1(g)), ruling out a distinction between chromatin binding to pre-lamin A and matured lamin A/C. We respectively identify in control and CsA-treated cells 244 and 178 A-LADs, and 239 and 278 B-LADs, each ranging from ~0.5 to ~15 megabases (Mb) (Figure 2(a,b); Supplementary Table S2). While size and genome coverage of B-LADs are not altered by CsA, number and size of A-LADs are lower, resulting in a 50% reduction in A-LAD coverage (Figure 2(b); Supplementary Table S2). This reduced association of chromatin with lamin A is likely not due to less efficient lamin A/C ChIP in CsA-treated cells because Western blot analysis reveals similar amounts of immunoprecipitated lamins A and C in these cells and in controls (Figure 1(g)). Alterations observed in our LAD analyses suggest marked changes in the distribution of A- and B-LADs.

We therefore examined the overlap of A- and B-LADs in control and CsA-treated cells by com-puting Jaccard indices (Ji) of their genome cover-age (Figure 2(c)). We find a low overlap between A-LADs and B-LADs in control cells (Ji 0.29), reflecting distinct A- and B-LAD subpopulations. Moreover, whereas B-LADs are well conserved in CsA-treated cells (Ji 0.64), A-LADs show little overlap (Ji 0.24), reflecting a redistribution of these LADs (in addition to the loss reported above). Interestingly however, A-LADs after CsA treatment coincide with B-LADs in control cells (Ji
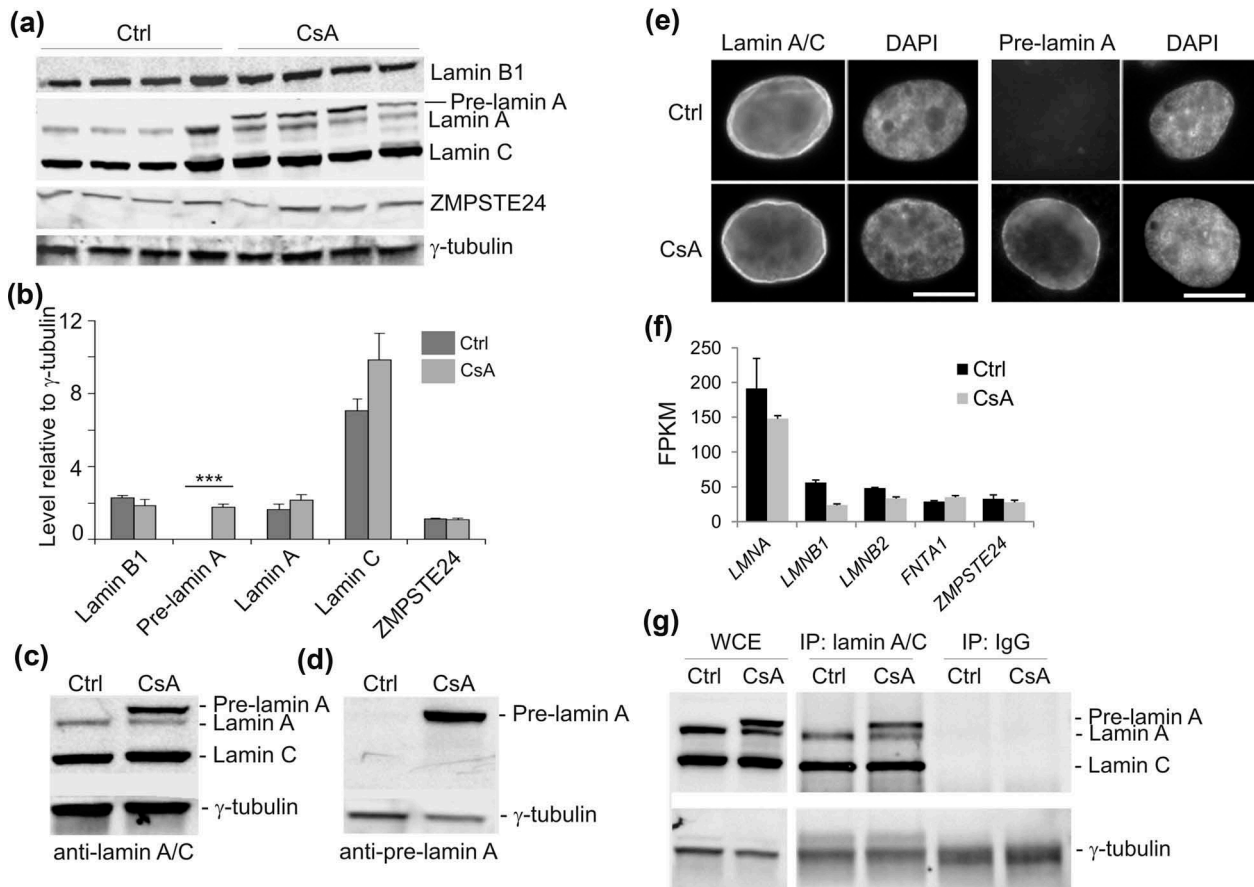
Figure 1. Cyclosporin A elicits pre-lamin A accumulation in HepG2 cells. (a) Western blot analysis of nuclear lamins and ZMPSTE24 in control (Ctrl) and HepG2 cells treated with 10 µM CsA for 72 h. γ-tubulin was used as loading control; data from 4 experiments. Anti-lamin A/C antibody used was a characterized rabbit antibody [44]. (b) Quantification of the blot shown in (a), relative to γ-tubulin; mean ± SD; ***P = 6.0×10^{-5}, paired t-tests relative to Ctrl. (c) Western blot of lamin A/C using the Santa-Cruz sc7292x anti-lamin A/C antibody used for ChIP. (d) Confirmation of pre-lamin A induction using a pre-lamin A antibody (Santa-Cruz sc6214). (e) Immunofluorescence labeling of lamin A/C (sc7292x) and pre-lamin A (sc6214 antibody). DNA was stained with DAPI. Bars, 10 µm. (f) Expression of lamin genes and *ZMPSTE24* in control and CsA-treated cells (mean ± SD FPKM from duplicate RNA-seq data). *FNTA1* was used as unaltered expression control. (g) Western blot of lamin A/C in whole cell extract (WCE) and after immunoprecipitation (IP) of lamin A/C (sc7292x) or IP with an irrelevant IgG, from control and CsA-treated cells under ChIP conditions. Detection was with the rabbit anti-lamin A/C antibody.

0.46; Figure 2(a,c)), indicating a significant overlap of *de novo* A-LADs with pre-existing B-LADs.

Distinct behaviors of lamin A and B association with chromatin

To further investigate the relationship between A-LADs and B-LADs, we divided these into LAD classes associated with lamin A only, lamin B only and both lamins A and B ('A-only', 'B-only' and 'A-B' LADs) and analyzed the properties of these LADs in control and CsA-treated cells (Supplementary Table

S3). We find that (i) genome coverage by B-only LADs slightly increases (Figure 2(d)) due to an increase in LAD number (Supplementary Figure S1(a)); however, overlap of these B-only LADs is low (Ji 0.218; Figure 2 (e)), indicating a genomic redistribution after CsA treatment. (ii) In contrast, A-only LADs show reduced coverage resulting from lower numbers and size (Figure 2(d); Supplementary Figure S1(a)), and no overlap with LADs in controls (Ji 0.017; Figure 2(e)). (iii) A-B LADs are the most conserved, although variation in their position also occurs (Figure 2(d,e); Supplementary Figure S1(a)). We infer from
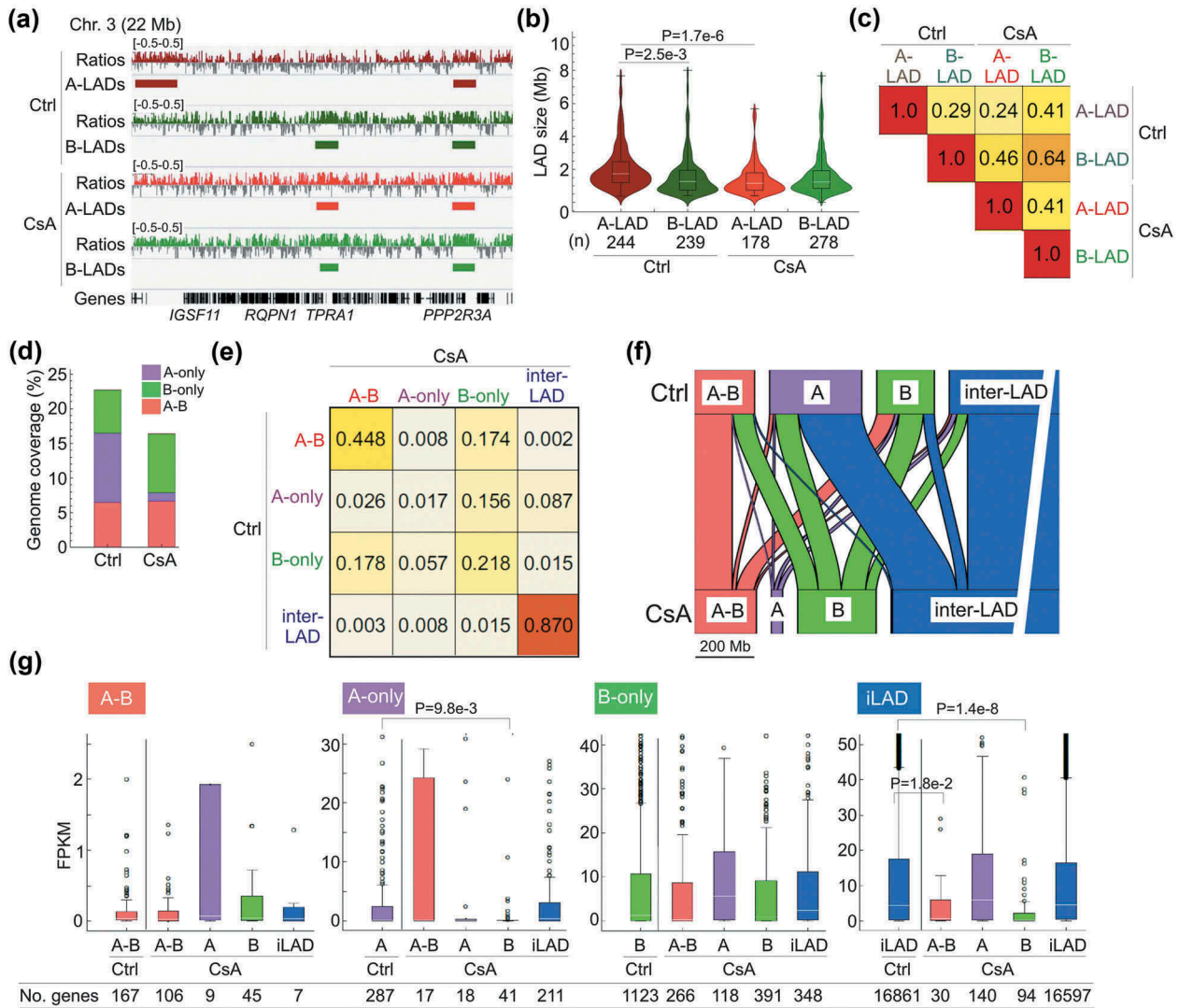
Figure 2. Differential patterns of lamin A and B association with the genome. (a) Browser view of lamin A/C and B1 ChIP-seq profiles of log_2(ChIP/input) ratios and of mapped A- and B-LADs. (b) LAD size distribution (n, number of LADs; P-value: 2-way ANOVA followed by Tukey's HSD posthoc test). (c) Jaccard indices of genome coverage by A- and B-LADs in control and CsA-treated cells. A ratio of 1 indicates a perfect overlap. (d) Relative genome coverage of A-B, A-only and B-only LADs. (e) Jaccard indices of overlap of all LAD classes in control and CsA-treated cells. (f) Alluvial representation of the outcome of A-B LADs, A-only LADs, B-only LADs and inter-LADs in CsA-treated cells. Width of boxes reflects proportions of each LAD class in the genome; width of lines reflects proportions of LAD classes turning into another. (g) Gene expression levels in each LAD class in control cells (Ctrl) and in their derivative sub-classes after CsA treatment (CsA). FPKMs are from RNA-seq data. Significant P-values (< 0.01; unpaired t-tests) and numbers of genes in each LAD class are shown.

these data a redistribution of A-only and B-only LADs after CsA treatment, while A-B LADs are the most conserved.

We further examined the fate of these LADs using an alluvial graph representation of the extent to which A-only, B-only and A-B LADs remained unaltered or turned into another LAD class with CsA. Figure 2(f) shows that (i) A-B LADs mostly remain 'A-B' while a smaller fraction loses lamin A to become B-only. (ii) Strikingly, most A-only LADs lose lamin A and become inter-LADs while

the remaining switch to B-only or become A-B. (iii) B-only LADs mainly remain B-only, while ~30% turn into A-B, demonstrating the *de novo* acquisition of lamin A on B LADs inferred from Jaccard indices (Figure 2(e,f); Supplementary Table S4). (iv) *De novo* A-only and B-only LADs appear in inter-LAD regions, albeit in minor proportions (Figure 2(f)). These results argue that association of lamin A with the genome is more dynamic than that of lamin B in this experimental system. They also highlight a rearrangement of

lamin-genome interactions through lamin loss, lamin exchange or acquisition of lamin A on regions interacting with lamin B.

Gene expression changes associated with LAD dynamics

We next determined whether LAD dynamics was associated with changes in gene expression. Genes in A-B, A-only and B-only LADs are not significantly differently expressed after CsA treatment (Supplementary Figure S1(b), P > 0.01, unpaired t-tests) although trends are detectable. We thus asked whether genes in each LAD class in control cells showed altered expression as a function of LAD class fate after CsA treatment. Due to the low number of genes in LAD classes of CsA-treated cells, many LAD class changes were not associated with significant expression changes (Figure 2(g)). However, genes in A-only LADs switching to B-only were downregulated (P = 9.8×10^{-3}; unpaired t-tests; Figure 2(g), 'A-only'). Acquisition of A-B or B-only LADs from inter-LADs was also accompanied by downregulation of gene expression (P = 0.018 and 1.4×10^{-8} respectively, unpaired t-tests; Figure 2(g), 'iLAD'). Thus, a gain of lamin B interaction, including a switch from lamin A to B, correlates with expression downregulation in these LADs. In contrast, gain or loss of lamin A, or loss of lamin B, is uncoupled from gene expression changes (Figure 2(g)). We conclude that in line with earlier findings [26], LAD dynamics is overall unlikely to be driven by transcriptional changes.

Prediction of radial repositioning of loci by CsA

To assess whether a gain or loss of LAD or a change in LAD identity would coincide with changes in the radial positioning of these domains, we generated 3-dimensional (3D) models of the HepG2 genome and analyzed properties of the models. We used Chrom3D, a 3D genome modeling platform that integrates TAD-TAD interactions from Hi-C data, and genome interactions with the nuclear periphery from lamin ChIP-seq data [27,28]. Our input data were Hi-C data for HepG2 (ENCODE, NCBI GEO accession GSE105381, sample GSM2825569) and lamin B1 ChIP-seq data for control and CsA-treated cells. We

generated 800 Chrom3D models for each condition, mapped A-B, A-only and B-only LADs onto the models and computed their normalized distances to the nuclear center to estimate their radial position. The structures recapitulate chromosome territories within which LADs can be highlighted (Figure 3(a,b)). Analysis of the models shows that A-B, A-only and B-only LADs are as expected more peripheral than inter-LADs, and between LAD classes, A-only LADs are more centrally placed than A-B or B-only LADs (P < 2.2×10^{-16}, unpaired t-tests; Figure 3(c)).

We next estimated the radial repositioning of each LAD class according to their fate in CsA-treated cells (Figure 3(d)). Loss of lamin association altogether correlates with repositioning of loci towards the nuclear center (Figure 3(d), comparison pair 4, 8, 12; P < 2.2×10^{-16}). Moreover, retention of a LAD class does not result in significant repositioning. Significantly however, loss of lamin B from an A-B LAD (pair 2) or a switch from a B-only to an A-only LAD (pair 10) correlates with repositioning towards the center (P < 2.2×10^{-16}). In contrast, gain of lamin B resulting from an A-only to B-only switch (pair 7), a *de novo* gain of A-B (pair 13) or a *de novo* gain of B-only (pair 15), correlates with repositioning towards the periphery (P < 2.2×10^{-16}). Lastly, gain of lamin A does not correlate with significant repositioning (pair 9, 14); however the impact of lamin A loss on radial placement depends on whether lamin B is bound in the region (pair 3, 4, 7, 8; P < 2.2×10^{-16}). Analysis of 3D genome models therefore predicts a dominant impact of lamin B over lamin A on radial positioning of the genome.

FISH analysis validates predictions on locus repositioning from 3D models

To independently validate Chrom3D model predictions on locus repositioning, we designed FISH probes to loci found in specific LAD classes in the ChIP-seq data (Supplementary Table S5). We also positioned in Chrom3D models the loci targeted by each FISH probe and measured their distance from the nucleus center (Figure 4(a,b); Supplementary Figure S2(a,b)). FISH analysis shows that maintenance of an inter-LAD does not alter radial positioning (Figure 4(a)), consistent with modeling predictions of FISH probe
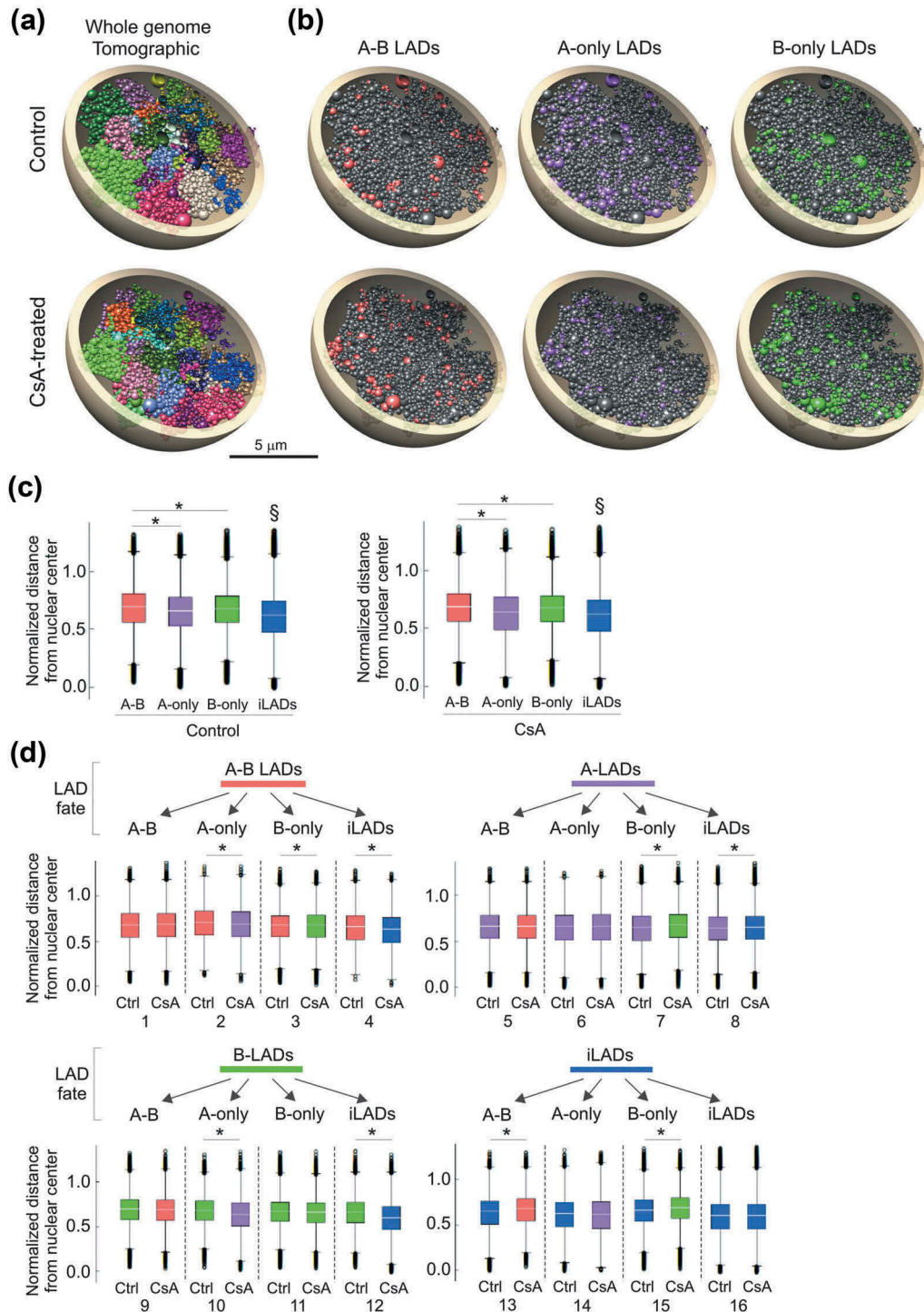
Figure 3. Structural 3D genome modeling reveals changes in radial LAD positioning related to LAD fate. (a) Chrom3D models of the HepG2 genome built from Hi-C and lamin B1 ChIP-seq data used as positional constraints for TADs and LADs. Tomographic views show individual chromosomes (differentially colored) modeled as beads on a string, each bead representing a TAD identified in the Hi-C data. One example structure out of 800 generated for control and CsA-treated cells is shown. (b) Tomographic views of the structures shown in (a) showing A-B, A-only and B-only LADs in control and CsA-treated cells. Beads (TADs) may harbor more than one LAD class due to their size. (c) Normalized LAD distance from the nuclear center across 800 3D structures of control and CsA-treated cells, for each LAD class and for all remaining TADs (inter-LADs). $^{§}P < 2.2 \times 10^{-16}$ compared to each LAD class; unpaired t-tests; $^{*}P < 2.2 \times 10^{-16}$; unpaired t-tests. These distances were calculated as absolute distances divided by the radius of the modeled nucleus (5 μm). (d) Normalized LAD distance from nuclear center for each LAD class and all remaining TADs (iLADs); $^{*}P < 2.2 \times 10^{-16}$, unpaired t-tests. LAD fate diagram (top) reflects the transition from one LAD class to another (see Figure 2F). Compared sample pairs (see main text) are numbered at the bottom.
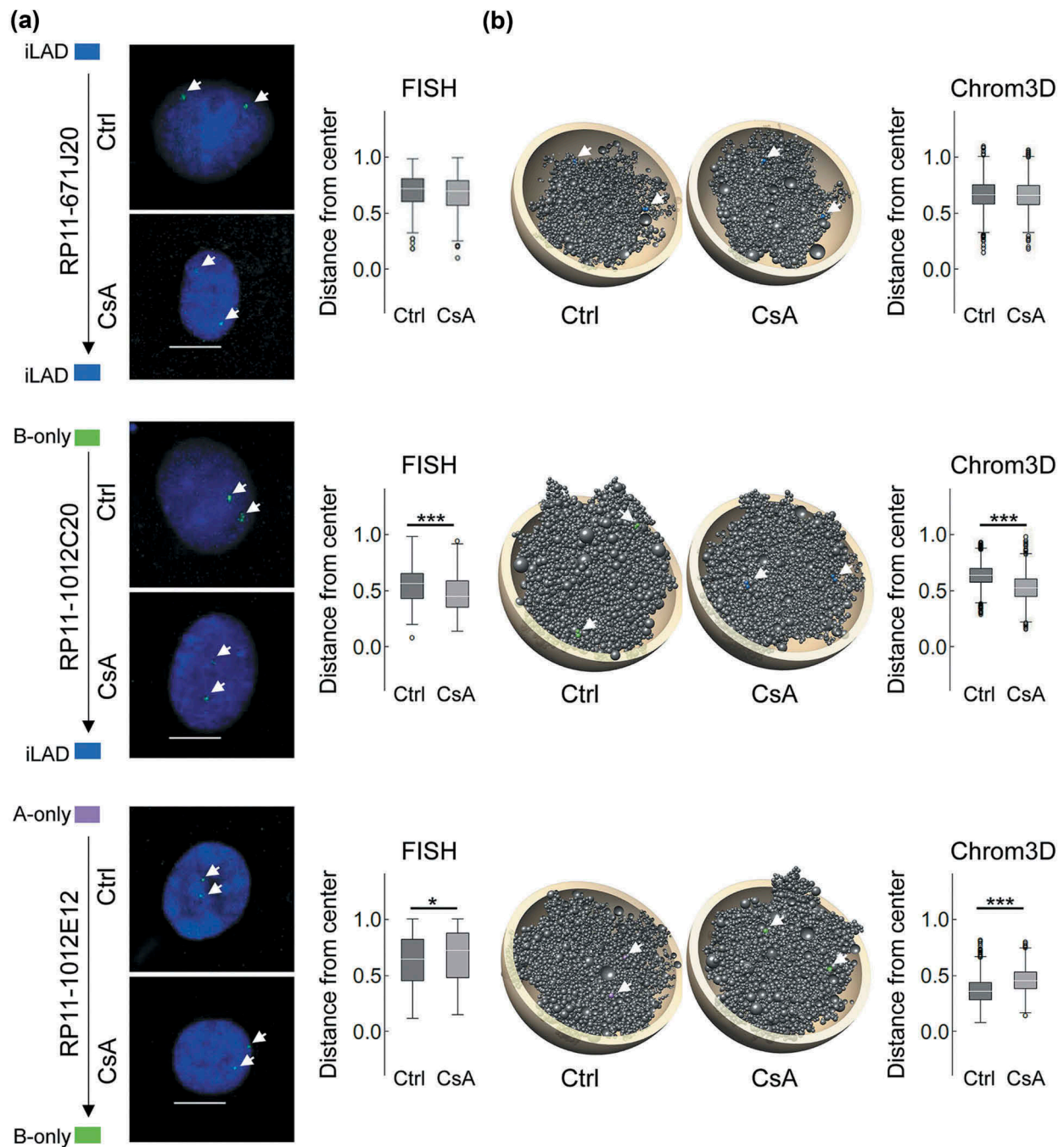
Figure 4. Chrom3D and FISH analysis of radial repositioning of loci after CsA treatment. (a) FISH analysis of locus positioning (arrows) in indicated LADs in control and CsA-treated cells. Representative FISH images are shown, with normalized probe distance from the nuclear center (0 = center; 1 = periphery defined as the border of DAPI staining; n = 100 nuclei analyzed per probe per condition; bars, 10 μm), (b) Chrom3D models showing FISH probe positions (arrows), and normalized probe distance from the nuclear center measured in 800 models. Probe number is shown. P-values: FISH: *P = 0.006, ***P = 1.4×10^{-5}; unpaired t-tests; Chrom3D: ***P < 2.2×10^{-16}, unpaired t-tests. See also Supplementary Figure S2.

position (Figure 4(b)) and with genome-wide 3D models (see Figure 3(d), pair 16). Similarly, we observe no repositioning after formation of A-B LADs from A- or B-only LADs, or after loss of an A-only LAD (Supplementary Figure S2). However, loss of a B-only LAD reveals locus-dependent repositioning towards the nuclear center (Figure 4; Supplementary Figure S2). Lastly, a switch from an A-only to B-only LAD correlates with peripheral locus repositioning (P = 0.006, t-tests; Figure 4(a)), again validating model predictions (Figure 4(b); P < 2.2×10^{-16}, t-tests) (Supplementary Figure S2). Thus, FISH data

validate predictions from the 3D models and confirm that lamin B association influences the radial distribution of loci more prominently than lamin A.

Pre-lamin A accumulation following CsA exposure (see Figure 1(a)) could influence locus positioning independently of CsA treatment *per se*. To address this, we expressed a Flag-tag wild-type (wt) pre-lamin A construct. Since, as we have shown earlier, wt pre-lamin A is fully processed into mature lamin A[27], we also expressed a lamin A mutant (L647R) exclusively localized at the nuclear periphery as unprocessed pre- lamin A[27] by retention of its pre-lamin A farnesyl group [29]. We then determined by immuno-FISH using anti-Flag antibodies the radial positioning of loci localized in an inter-LAD, in a B-only LAD losing B, and in an A-only LAD switching to B (see Figure 4(a)).

The data strikingly reveal no significant repositioning of the three loci in lamin A L647R vs. wt cells (Supplementary Figure S3). Thus, overexpression of pre-lamin A (as lamin A L647R) does not recapitulate locus repositioning detected in CsA-treated cells (which show some pre-lamin A expression). This suggests that relocalization observed after CsA treatment is a CsA-linked phenotype and not a pre-lamin A expression phenotype *per se*. Repositioning is probably independent of pre-lamin A interaction with chromatin; it is however likely dependent on lamin B, as discussed above.

Discussion

We report a marked effect of CsA on the association of chromatin with A- and/or B-type lamins. We notably reveal distinct patterns of lamin A and B interaction with chromatin, resulting in variable LAD identities and correlated with a radial repositioning of loci concordant with predictions from 3D genome models. An account of redistribution of lamin A and B (A-B) LADs, A-only and B-only LADs between two cellular states provides biochemical evidence for previous microscopy-based observations of distinct lamin A and B micro-domains [30]. Our results suggest a greater dynamics of lamin A association with chromatin than lamin B, but a dominant influence of lamin B on radial repositioning of loci elicited by a perturbation in cellular state.

Studies of drug hepatotoxicity have revealed an accumulation of pre-lamin A in HepG2 cells exposed to an inhibitor of isoprenylcysteine carboxylmethyltransferases (ICMTs) [31]. Pre-lamin A accumulation in cells treated with CsA is reminiscent of ICMT inhibition or depletion in that a pool of mature lamina is also detected [24]. Thus, proteolytic cleavage of pre-lamin A leading to mature lamin A is partially impaired [9]. ZPMSTE24, the protease implicated in lamin A maturation [9], is not affected by CsA; this is again in line with the detection of mature lamin A after CsA treatment. CsA is not a reported ICMT inhibitor, but could conceivably directly or indirectly affect ICMT activity.

A key question in understanding spatial genome architecture is whether changes in lamin-chromatin interactions reported here occur at the nuclear periphery or in the nuclear interior. Pre-lamin A is detected at the nuclear envelope but could also be nucleoplasmic (if not farnesylated [9]), suggesting that alterations in lamin-chromatin interactions may occur both at the peripheral nuclear lamina and in the nuclear interior. Accordingly, 3D genome modeling and FISH analyses indicate that most changes in LADs and in radial position do not systematically occur *at* the nuclear periphery at the single-cell level. In addition, lamin B-chromatin interactions detected by ChIP from millions of cells do not imply peripheral association of loci in all cells. Our results extend previous findings [27,32,33] and may be explained by dynamic lamin interactions with chromatin [34]. They also support the view that lamin B (in addition to lamin A[12] [13,15,18,35,36],) may interact with chromatin in the nuclear interior, such as gene-poor perinucleolar heterochromatin [37] or euchromatic regions [17].

Lamins A and B are important regulators of spatial genome organization [21,22,38], and our findings suggest a complementary influence of both lamin types. Lamin association with the genome appears to be more dynamic in regions associated with lamin A than with lamin B, consistent with a view of dynamic A-LADs during adipogenic differentiation [14]. In both experimental systems, lamin B LADs are relatively invariant, while a subset of these also gains lamin A. Nevertheless, the most stable lamin-genome association observed in our data is with A-B LADs. Yet the data suggest that a key contributor to A-B LAD stability is lamin B, which appears to be more stably associated with chromatin than lamin

A. Moreover, as our lamin A ChIP precipitates both lamin A and pre-lamin A, we do not at present know whether pre-lamin A accumulation elicited by CsA contributes to LAD dynamics.

Global loss of lamin A results in increased chromatin mobility in the nuclear interior [21]. A loss of A-only LADs in our study may be perceived as a 'local' lamin A loss yet bear similar but spatially restricted implications. Thus one may anticipate local gains in chromatin mobility in regions losing lamin A, which is predicted from our modeling data. We therefore raise the hypothesis that not only a global loss of lamin A[21] but also a more local depletion promotes a restricted conformation change manifested by increased chromatin mobility. It will be relevant to investigate the impact of a local loss of LAD on the biophysical properties of chromatin in the vicinity.

Notwithstanding, repositioning of A-LADs upon loss of lamin A depends on whether lamin B is in the neighborhood. When a lamin B LAD appears *de novo*, we predict and observe locus repositioning towards the periphery. In contrast, in the local absence of lamin B, A-LAD loss correlates with repositioning towards the center. This suggests that lamin B is an important factor in the directional radial organization of chromatin. The surrounding LAD neighborhood could also influence LAD behavior: LAD repositioning may not only depend on the LAD class *per se*, but also on LADs in the vicinity. For instance, absence of repositioning of a B-only LAD towards the nuclear center after losing lamin B, as seen by FISH, could be due to an A-B LAD in the vicinity. Thus, radial genome positioning may be influenced by a combination of both local and medium-range contributions of the linearly nearest region. This idea extends our previous observations that a lamin A neighborhood affects expression of genes in that neighborhood even though they are not bound by lamin A[18].

These findings raise the question of which factors may regulate the radial positioning of chromatin. Nuclear envelope proteins [38], histone deacetylases [39,40] and histone methyltransferases [41] are central in the radial placement and anchoring of heterochromatin. A FISH-based screen of factors involved in radial placement of a set of genes further shows that locus position is under influence of multiple pathways involving nuclear envelope proteins, centromeric proteins, chromatin remodelers and DNA replication and repair factors [42]. However, as seen in our data, radial repositioning is overall uncoupled from gene activity [42] and thus not driven by transcriptional changes. Nonetheless, radial placement can vary between cell types [42] and may be regulated by cell type-dependent mechanisms. These processes are deregulated under cellular states or disease conditions affecting lamin-chromatin interactions, such as senescence [26] or laminopathies [27,35,36,43], and influenced by structural and numerical chromosomal anomalies, as in cancer cells [42].

It is becoming increasingly clear that patterns and mechanisms of nuclear lamin association with the genome are more complex and dynamic than previously understood. Functional and live-cell imaging studies are needed in order to fully understand the mechanisms by which lamins contribute to organizing the 3D conformation of chromatin in the nucleus.

Materials and methods

Cell culture

HepG2 cells were cultured in DMEM/F12 (Life Technologies) with 10% fetal calf serum and 1% penicillin-streptomycin. Cells were also cultured with 10 μM CsA (Novartis; diluted 1:1000 from a 10 mM stock in cell media) for 72 h before harvest.

Plasmids and transfections

HepG2 cells were transiently transfected with pCMV-Flag-preLA-WT (lamin A wt) and pCMV-Flag-preLA-L647R (pre-lamin A L647R) plasmids [27] using Lipofectamine 2000 (ThermoFisher). Lamin A expression was assessed by immunostaining using anti-Flag antibodies. Cells were analyzed by immuno-FISH after 48 h using anti-Flag antibodies and indicated FISH probes.

Immunoblotting

Proteins were separated by 10% SDS-PAGE, transferred onto an Immobilon-FL membrane (Millipore) and membranes blocked with Odyssey blocking buffer (LI-COR). Membranes were incubated in Odyssey blocking buffer with antibodies against lamin A/C (1:2000, sc7292x, Santa Cruz Biotechnology; or

a rabbit anti-lamin A/C antibody [44]; 1:1000), pre-lamin A (1:200, sc6214, Santa Cruz Biotechnology), lamin B1 (1:1000, sc6216, Santa Cruz Biotechnology), ZMPSTE24 (1:1000, AP2415a, Abgent) or γ-tubulin (1:10,000, T5326, Sigma-Aldrich). Proteins were detected with IRDye-800- or IRD IRDye-680-coupled secondary antibodies.

Immunofluorescence

Cells cultured on coverslips were fixed with 3% par-aformaldehyde and permeabilized for 10 min in PBS/0.1% Triton X-100. Cells were blocked with 2% BSA in PBS/0.1% Tween (PBST-BSA) for 30 min and incubated with primary antibodies in PBST-BSA overnight at 4°C. Cells were incubated with secondary antibodies in PBST-BSA for 45 min and washed in PBST-BSA before mounting with DAPI (1:1000, D-9942, Sigma-Aldrich). Antibodies used were mouse anti-lamin A/C (1:1000, sc7292x, Santa Cruz Biotechnology), goat anti-pre-lamin A (1:100, sc6214, Santa Cruz Biotechnology), anti-mouse Alexa Fluor® 594 and anti-goat Alexa Fluor® 488 (both 1:1000, Jackson ImmunoResearch).

FISH

FISH was done as described [27]. Cells were incubated in 0.25% KCl/0.5% tri-sodium citrate for 10 min, fixed in ice-cold 3:1 methanol:acetic acid and dropped on slides. BAC FISH probe DNA (BacPac Resource Center) was labeled using Biotin-16-dUTP (Roche). 200–300 ng labeled probe per slide was mixed with 8 μg Cot-1 DNA and 30 μg salmon sperm DNA (Invitrogen) and precipitated. DNA was dissolved in 11 μl hybridization mix (50% deionized formamide, 2x SSC, 1% Tween 20, 10% dextran sulphate) at 42°C for 20 min and pre-annealed for 1 h at 37°C. Slides were RNase-treated and washed twice in 2x SSC, dehydrated in ethanol and air-dried. Slides were dena-tured for 1 min 20 sec in 70% deionized formamide/2x SSC (pH 7.5) at 70°C, dehydrated in ice-cold 70%, 90% and 100% ethanol and air-dried. Probes were denatured for 5 min at 70°C and pre-annealed for 15 min at 37°C. 10 μl of probe was applied onto coverslips which were then mounted on a slide. Slides were hybridized overnight at 37°C. Slides were washed 4x in 2x SSC at 45°C and 4x in 0.1x SSC at 60°C. Slides were blocked in 5% skim milk and incubated

at 37°C with Avidin-Alexa Fluor 488 (Invitrogen; 1.7 μg/ml). Slides were washed in 4x SSC/0.1% Tween 20 and incubated with Biotinylated Anti-Avidin D (goat; 1.0 μg/ml; Vector) for 45 min at 37°C. Slides were washed and incubated with Avidin-Alexa Fluor 488 as above and mounted with DAPI in Dako Fluorescent Mounting Medium.

Based on ChIP-seq profiles, FISH probes were designed for regions changing LAD class after CsA (Supplementary Table S5). Since HepG2 cells harbor copy number variations, probes were designed outside these areas. 100 FISH images (200 alleles) were analyzed using FISHfinder [45] to calculate the distance to the nuclear periphery determined by the edge of DAPI staining. Distance to the periphery was normalized to the radius of the nucleus. T-tests were used to determine the significance of distance differences between control and CsA-treated cells.

Immuno-FISH

Immuno-FISH was done as described [46]. Trans fected cells grown on slides were fixed with 3% paraformaldehyde for 15 min, washed 3 × 5 min in PBS, blocked, and permeabilized in PBS with 0.01% Tween-20, 2% BSA, and 0.1% Triton X-100 for 30 min. Cells were incubated for 2 h with anti-Flag antibodies (1:1000, F1804, Sigma-Aldrich) and for 45 min with mouse anti-FLAG and rabbit anti-mouse Alexa 594 antibodies (1:1000, Jackson ImmunoResearch). Slides were washed 3 × 5 min in PBS with 0.01% Tween-20 and 2% BSA between and after incubations. Immunostaining was fixed with 3% PFA for 15 min. Slides were washed 3× in PBS, 2 × 2 min in 2× SSC and 3 min in 2× SSC at 80°C. Slides were denatured for 20 min in 80°C in 70% deionized formamide (Ambion) in 2× SSC (pH 7.5). FISH probes were labeled and ensuing FISH procedure was done as described above.

ChIP-sequencing

ChIP was done as described [14]. Cells (5×10^6 cells per ChIP) were cross-linked with 1% formaldehyde and lysed in RIPA buffer (140 mM NaCl, 10 mM Tris-HCl, pH 8.0, 1 mM EDTA, 0.5 mM EGTA, 1% Triton X-100, 1% SDS, 0.1% sodium deoxycholate, 1 mM PMSF, protease inhibitors). To generate

200–500 bp DNA fragments, cells were sonicated 4 × 10 min in a Bioruptor (Diagenode). After sedimentation, the supernatant was diluted 10x in RIPA and incubated with anti-lamin A/C (10 µg, sc7292x, Santa Cruz Biotechnology) or lamin B1 (10 µg, ab16048, Abcam) antibodies coupled to Dynabeads Protein G (Invitrogen). ChIP samples were washed 3x in ice-cold-RIPA. Samples were incubated for 6 h at 68°C in elution buffer (50 mM NaCl, 20 mM Tris-HCl, pH 7.5, 5 mM EDTA, 1% SDS) and 40 ng proteinase K for crosslink reversal and DNA elution. DNA was extracted and libraries prepared and sequenced on an Illumina HiSeq2500.

ChIP-seq data processing

ENCODE ChIP input data for HepG2 cells were downloaded from NCBI GEO accession No. GSE29611. Lamin A and B ChIP-seq reads and input reads were mapped to hg19 using Bowtie v2.25.0 [47] with default parameters after removing duplicate reads using Picard's MarkDuplicates. To avoid normalization bias, we ensured that each pair of aligned input and ChIP read files had the same read depth by down-sampling reads for each chromosome individually. Mapped reads were used to call LADs using Enriched Domain Detector (EDD) [11] with the following alteration. To account for technical variation that might occur in LAD calling, we first ran EDD 10 times on each lamin ChIP-seq dataset in auto-estimation mode for GapPenalty (GP) and BinSize (BS). Average GP standard deviation from the 10 runs was < 1 unit, while BS did not vary. GP variations elicited minimal alterations in LAD calls, allowing estimation of technical variability. Median length of these variable subdomains was 0.39 Mb for all LADs, i.e. < 2% of total LAD coverage, and 10–20 times smaller than median A- and B-LAD sizes. We concluded that intrinsic EDD variability did not significantly impact LAD calling. Average GP and BS values were then used to manually set GP and BS before a final EDD run with each dataset. Parameters were, for control/CsA conditions, respectively: lamin A, BS 16/17 kilobase (kb), GP 4.1/3.9; lamin B, BS 16/16, GP 5.4/5.9. Intersects between LADs and genes were computed using BEDTools v2.21.0 [48] and BEDOPS v2.4.27 [49]. Scripts were written in Perl [50] or R [51] and ggplot2 in R was used for plots. Browser files were generated by calculating ratios of ChIP over input for each 1 kb bin with input normalized to the ratio of total ChIP reads over total input reads.

3D genome modeling using chrom3D

Hi-C data processing

Hi-C data of HepG2 cells were downloaded from ENCODE (GEO accession No. GSM2825569) [52] and processed using HiC-Pro [53] with default settings to generate Hi-C contact matrices. The pipeline creates intra- and inter-chromosomal contact matrices at various bin sizes. We chose a 50-kb bin size intra-chromosomal contact matrices and 1-Mb bin size inter-chromosomal contact matrices for analyses. 50-kb contact matrices were used to call TADs using Armatus v2.3 [54].

3D models

We applied Chrom3D to generate 3D genome models from Hi-C and lamin B1 ChIP-seq data [27,28]. We generated 800 models each for control and CsA-treated cells, using Hi-C data for HepG2 cells [52] and the lamin B1 LADs mapped in this study for control and CsA-treated cells. In the simulations, chromosomes are modeled as beads on a string, each bead representing a TAD, and of size proportional to the linear size of the TAD. For each model we computed the Euclidean distance between beads and the nucleus center. We then extracted all beads (and their Euclidean distances) harboring lamin A or lamin B LADs and classified these LADs as A-only, B-only and A-B LADs (or beads) for statistical analyses (see below) and illustrations. In the models, distances between a bead and the nuclear center were normalized by dividing the Euclidian distance by the radius of the modeled nucleus (5 µm).

RNA-seq and gene expression analysis

Total RNA was isolated from two CsA exposure experiments using the RNeasy Mini Kit (Qiagen). Libraries were sequenced on an Illumina HiSeq2500. RNA-seq reads were processed with Tuxedo [55]. TopHat v2.10 was used to align reads with no mismatch against the hg19 reference genome with default settings, applying the Bowtie2 preset option 'b2-very

sensitive' [56,57]. Transcript abundance was estimated using cufflinks v2.2.1, and differential gene expression determined using cuffdiff v2.2.1 [55]. Genes with absolute FPKM change < 0.05 between control and CsA conditions were considered stably expressed. A gene was ascribed to a LAD class if its transcription start site overlapped with the LAD.

Statistical analyses

FPKM levels from RNA-seq data were compared using unpaired t-tests. For LAD size comparisons, a 2-way ANOVA was first applied to determine the global significance of CsA treatment vs. control. A Tukey honest significant difference (HSD) test was then applied to determine the significance of any difference between LAD classes. Comparisons of normalized LAD distances to the nuclear center in Chrom3D models and in FISH analyses were done using unpaired t-tests.

Data access

Our ChIP-seq and RNA-seq data are available under GEO accession No. GSE119631. ChIP input data are available under GEO accession No. GSE29611. Hi-C data for HepG2 cells [52] are available under GEO accession No. GSM2825569.

Disclosure statement

No potential conflict of interest was reported by the authors.

References

[1] Backman L, Appelkvist EL, Sundberg A, et al. Modulation of metabolism in HepG2 cells upon treatment with cyclosporin A and Nva2-cyclosporin. Exp Mol Pathol. 1991;54:242–254.

[2] Lopez-Riera, M., Conde, I., Tolosa, L. et al. New microRNA biomarkers for drug-induced steatosis and their potential to predict the contribution of drugs to non-alcoholic fatty liver disease. Front Pharmacol. 2017;8:3.

[3] Benet, M., Guzmán, C., Pisonero-Vaquero, S. et al. Repression of the nuclear receptor small heterodimer partner by steatotic drugs and in advanced nonalcoholic fatty liver disease. Mol Pharmacol. 2015;87:582–594.

[4] Lausada N, de Gomez Dumm IN, Raimondi JC, et al. Effect of cyclosporine and sirolimus on fatty acid desaturase activities in cultured HEPG2 cells. Transplant Proc. 2009;41:1865–1870.

[5] Lieberman-Aiden, E., Van Berkum, N. L., Williams, L. et al. Comprehensive mapping of long-range interactions reveals folding principles of the human genome. Science. 2009;326:289–293.

[6] Dixon JR, Selvaraj S, Yue F, et al. Topological domains in mammalian genomes identified by analysis of chromatin interactions. Nature. 2012;485:376–380.

[7] Nora EP, Lajoie BR, Schulz EG, et al. Spatial partitioning of the regulatory landscape of the X-inactivation centre. Nature. 2012;485:381–385.

[8] Guelen L, Pagie L, Brasset E, et al. Domain organization of human chromosomes revealed by mapping of nuclear lamina interactions. Nature. 2008;453:948–951.

[9] Burke B, Stewart CL. The nuclear lamins: flexibility in function. Nat Rev Mol Cell Biol. 2013;14:13–24.

[10] Reddy KL, Zullo JM, Bertolino E, et al. Transcriptional repression mediated by repositioning of genes to the nuclear lamina. Nature. 2008;452:243–247.

[11] Lund EG, Oldenburg AR, Collas P. Enriched domain detector: a program for detection of wide genomic enrichment domains robust against local variations. Nucleic Acids Res. 2014;42:e92.

[12] Gesson K, Rescheneder P, Skoruppa MP, et al. A-type lamins bind both hetero- and euchromatin, the latter being regulated by lamina-associated polypeptide 2 alpha. Genome Res. 2016;26:462–473.

[13] Lund EG, Duband-Goulet I, Oldenburg A, et al. Distinct features of lamin A-interacting chromatin domains mapped by ChIP-sequencing from sonicated or micrococcal nuclease-digested chromatin. Nucleus. 2015;6:30–38.

[14] Rønningen T, Shah A, Oldenburg AR, et al. Prepatterning of differentiation-driven nuclear lamin A/C-associated chromatin domains by GlcNAcylated histone H2B. Genome Res. 2015;25:1825–1835.

[15] Cesarini E, Mozzetta C, Marullo F, et al. Lamin A/C sustains PcG protein architecture, maintaining transcriptional repression at target genes. J Cell Biol. 2015;211:533–551.

[16] Marullo F, Cesarini E, Antonelli L, et al. Nucleoplasmic Lamin A/C and Polycomb group of proteins: an evolutionarily conserved interplay. Nucleus. 2016;7:103–111.

[17] Pascual-Reguant L, Blanco E, Galan S, et al. Lamin B1 mapping reveals the existence of dynamic and functional euchromatin lamin B1 domains. Nat Commun. 2018;9:3420.

[18] Lund E, Oldenburg AR, Delbarre E, et al. Lamin A/C-promoter interactions specify chromatin state-dependent transcription outcomes. Genome Res. 2013;23:1580–1589.

[19] Peric-Hupkes D, Meuleman W, Pagie L, et al. Molecular maps of the reorganization of genome-nuclear lamina interactions during differentiation. Mol Cell. 2010;38:603–613.

[20] Robson MI, de Las Heras JI, Czapiewski R, et al. Constrained release of lamina-associated enhancers and genes from the nuclear envelope during T-cell activation facilitates their association in chromosome compartments. Genome Res. 2017;27:1126–1138.

[21] Bronshtein I, Kepten E, Kanter I, et al. Loss of lamin A function increases chromatin dynamics in the nuclear interior. Nat Commun. 2015;6:8044.

[22] Camps J, Wangsa D, Falke M, et al. Loss of lamin B1 results in prolongation of S phase and decondensation of chromosome territories. FASEB J. 2014;28:3423–3434.

[23] Jennings P, Koppelstaetter C, Aydin S, et al. Cyclosporine A induces senescence in renal tubular epithelial cells. Am J Physiol Renal Physiol. 2007;293:F831–F838.

[24] Barrowman J, Hamblet C, Kane MS, et al. Requirements for efficient proteolytic cleavage of pre-lamin A by ZMPSTE24. PLoS One. 2012;7:e32120.

[25] Koppelstaetter C, Kern G, Leierer G, et al. Effect of cyclosporine, tacrolimus and sirolimus on cellular senescence in renal epithelial cells. Toxicol In Vitro. 2018;48:86–92.

[26] Lenain C, de Graaf CA, Pagie L, et al. Massive reshaping of genome-nuclear lamina interactions during oncogene-induced senescence. Genome Res. 2017;27:1634–1644.

[27] Paulsen J, Sekelja M, Oldenburg AR, et al. Chrom3D: three-dimensional genome modeling from Hi-C and nuclear lamin-genome contacts. Genome Biol. 2017;18:21.

[28] Paulsen J, Liyakat Ali TM, Collas P. Computational 3D genome modeling using Chrom3D. Nat Protoc. 2018;13:1137–1152.

[29] Wang Y, Lichter-Konecki U, Anyane-Yeboa K, et al. A mutation abolishing the ZMPSTE24 cleavage site in prelamin A causes a progeroid disorder. J Cell Sci. 2016;129:1975–1980.

[30] Shimi T, Pfleghaar K, Kojima S-I, et al. The A- and B-type nuclear lamin networks: microdomains involved in chromatin organization and transcription. Genes Dev. 2008;22:3409–3421.

[31] Lau HY, Ramanujulu PM, Guo D, et al. An improved isoprenylcysteine carboxylmethyltransferase inhibitor induces cancer cell death and attenuates tumor growth in vivo. Cancer Biol Ther. 2014;15:1280–1291.

[32] Kind J, Pagie L, de Vries SS, et al. Genome-wide maps of nuclear lamina interactions in single human cells. Cell. 2015;163:134–147.

[33] Kind J, Pagie L, Ortabozkoyun H, et al. Single-cell dynamics of genome-nuclear lamina interactions. Cell. 2013;153:178–192.

[34] Akhtar W, de Jong J, Pindyurin AV, et al. Chromatin position effects assayed by thousands of reporters integrated in parallel. Cell. 2013;154:914–927.

[35] Briand N, Guénantin A-C, Jeziorowska D, et al. The lipodystrophic hotspot lamin A p.R482W mutation deregulates the mesodermal inducer T/Brachyury and early vascular differentiation gene networks. Hum Mol Genet. 2018;27:1447–1459.

[36] Oldenburg A, Briand N, Sørensen AL, et al. A lipodystrophy-causing lamin A mutant alters conformation and epigenetic regulation of the anti-adipogenic MIR335 locus. J Cell Biol. 2017;216:2731–2743.

[37] van Koningsbruggen S, Gierlinski M, Schofield P, et al. High-resolution whole-genome sequencing reveals that specific chromatin domains from most human chromosomes associate with nucleoli. Mol Biol Cell. 2010;21:3735–3748.

[38] Solovei I, Wang AS, Thanisch K, et al. LBR and lamin A/C sequentially tether peripheral heterochromatin and inversely regulate differentiation. Cell. 2013;152:584–598.

[39] Milon BC, Cheng H, Tselebrovsky MV, et al. Role of histone deacetylases in gene regulation at nuclear lamina. PLoS One. 2012;7:e49692.

[40] Poleshko A, Shah PP, Gupta M, et al. Genome-nuclear lamina interactions regulate cardiac stem cell lineage restriction. Cell. 2017;171:573–587.

[41] Towbin BD, González-Aguilera C, Sack R, et al. Stepwise methylation of histone H3K9 positions heterochromatin at the nuclear periphery. Cell. 2012;150:934–947.

[42] Shachar S, Voss TC, Pegoraro G, et al. Identification of gene positioning factors using high-throughput imaging mapping. Cell. 2015;162:911–923.

[43] Perovanovic J, Breen M, Choyke P, et al. Laminopathies disrupt epigenomic developmental programs and cell fate. Sci Transl Med. 2016;8:335ra58.

[44] Duband-Goulet I, Woerner S, Gasparini S, et al. Subcellular localization of SREBP1 depends on its interaction with the C-terminal region of wild-type and disease related A-type lamins. Exp Cell Res. 2011;317:2800–2813.

[45] Shirley JW, Ty S, Takebayashi S, et al. a high-throughput tool for analyzing FISH images. Bioinformatics. 2011;27:933–938.

[46] Delbarre E, Ivanauskiene K, Spirkoski J, et al. PML protein organizes heterochromatin domains where it regulates histone H3.3 deposition by ATRX/DAXX. Genome Res. 2017;27:913–921.

[47] Langmead B, Trapnell C, Pop M, et al. Ultrafast and memory-efficient alignment of short DNA sequences to the human genome. Genome Biol. 2009;10:R25.

[48] Quinlan AR, Hall IM. BEDTools: a flexible suite of utilities for comparing genomic features. Bioinformatics. 2010;26:841–842.

[49] Neph S, Kuehn MS, Reynolds AP, et al. BEDOPS: high-performance genomic feature operations. Bioinformatics. 2012;28:1919–1920.

[50] Stajich JE, Block D, Boulez K, et al. The Bioperl toolkit: perl modules for the life sciences. Genome Res. 2002;12:1611–1618.

[51] Team RCR. A language and environment for statistical computing. Vienna, Austria:R Foundation for Statistical Computing; 2015. Available from: https://www.R-project.org.

[52] Consortium EP. An integrated encyclopedia of DNA elements in the human genome. Nature. 2012;489:57–74.

[53] Servant N, Skaletsky H, Koutseva N, et al. HiC-Pro: an optimized and flexible pipeline for Hi-C data processing. Genome Biol. 2015;16:259.

[54] Filippova D, Patro R, Duggal G, et al. Identification of alternative topological domains in chromatin. Algorithms Mol Biol. 2014;9:14.

[55] Trapnell C, Williams BA, Pertea G, et al. Transcript assembly and quantification by RNA-Seq reveals unannotated transcripts and isoform switching during cell differentiation. Nat Biotechnol. 2010;28:511–515.

[56] Kim D, Pertea G, Trapnell C, et al. TopHat2: accurate alignment of transcriptomes in the presence of insertions, deletions and gene fusions. Genome Biol. 2013;14:R36.

[57] Langmead B, Salzberg SL. Fast gapped-read alignment with Bowtie 2. Nat Methods. 2012;9:357–359.

Supplementary information

Supplementary Figures
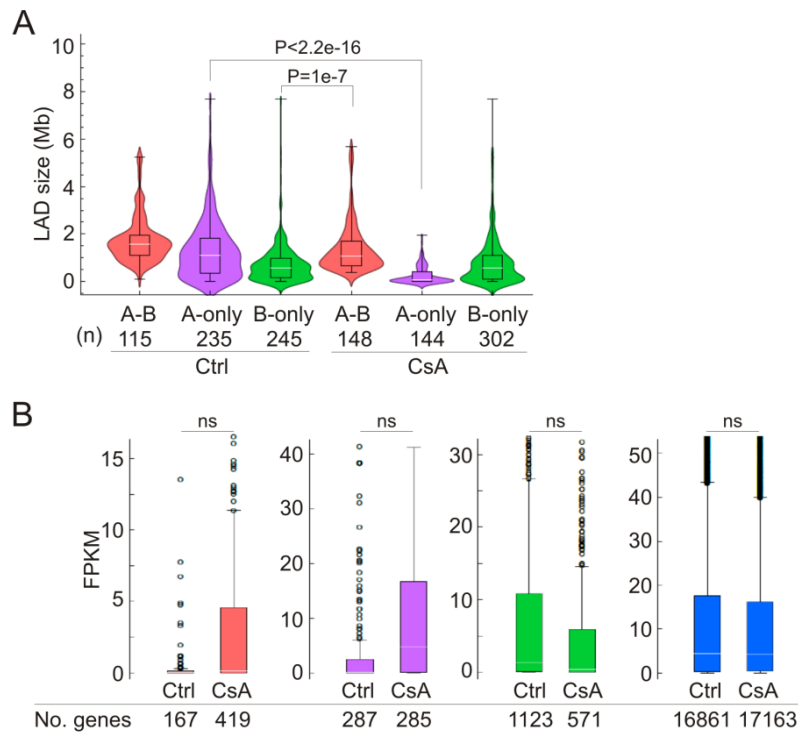
Figure S1. Characterization of LADs in control and CsA-treated HepG2 cells. (A) LAD size distribution, P-values shown only for significant differences (Tukey test after 2-way ANOVA.). (B) Gene expression level in each LAD class. No significant differences are detected (ns) at the $P < 0.01$ level (unpaired t-tests). FPKM values are from duplicate RNA-seq data.

Forsberg et al.
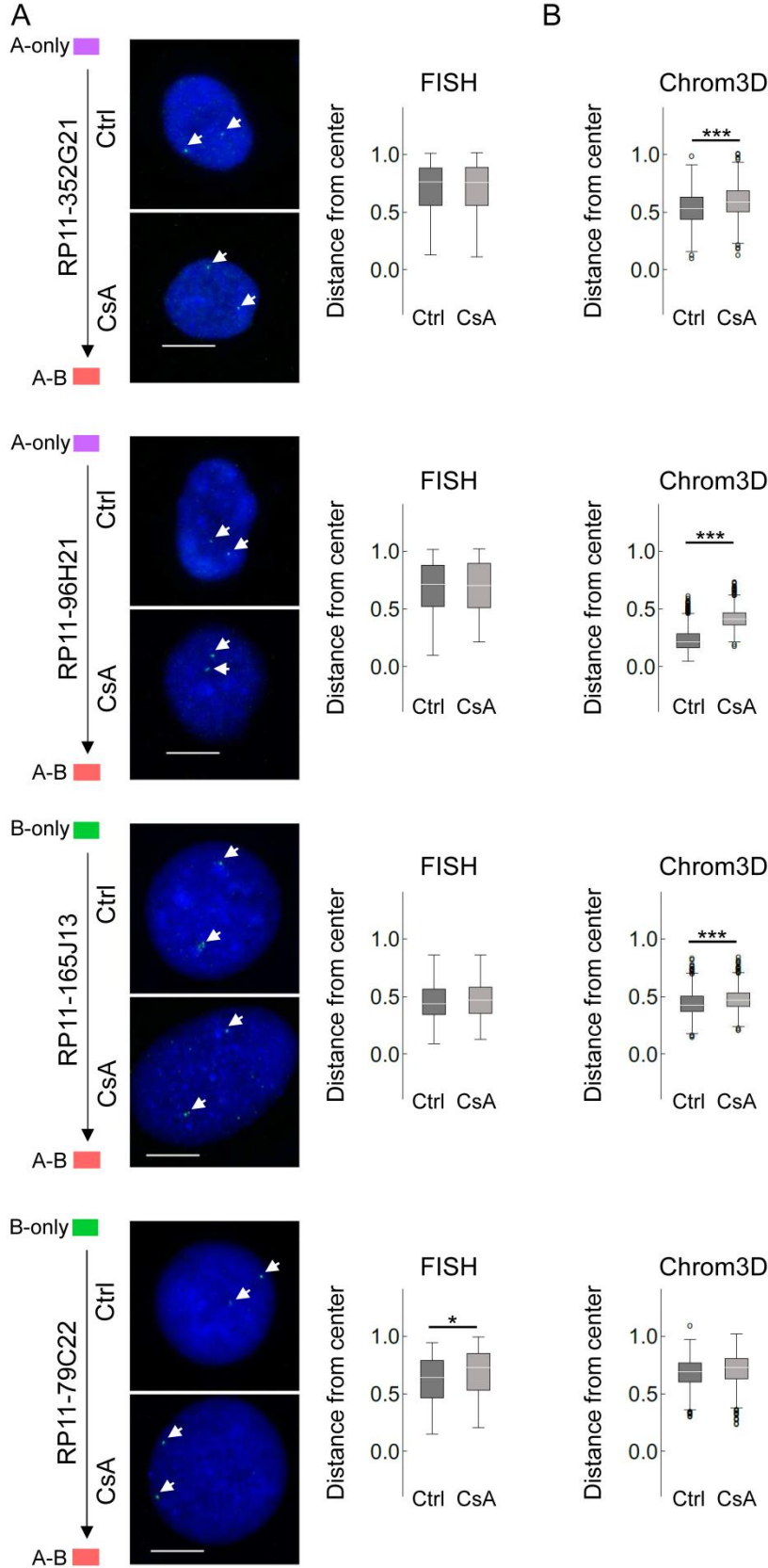
Figure S2. (part 1; legend on next page).
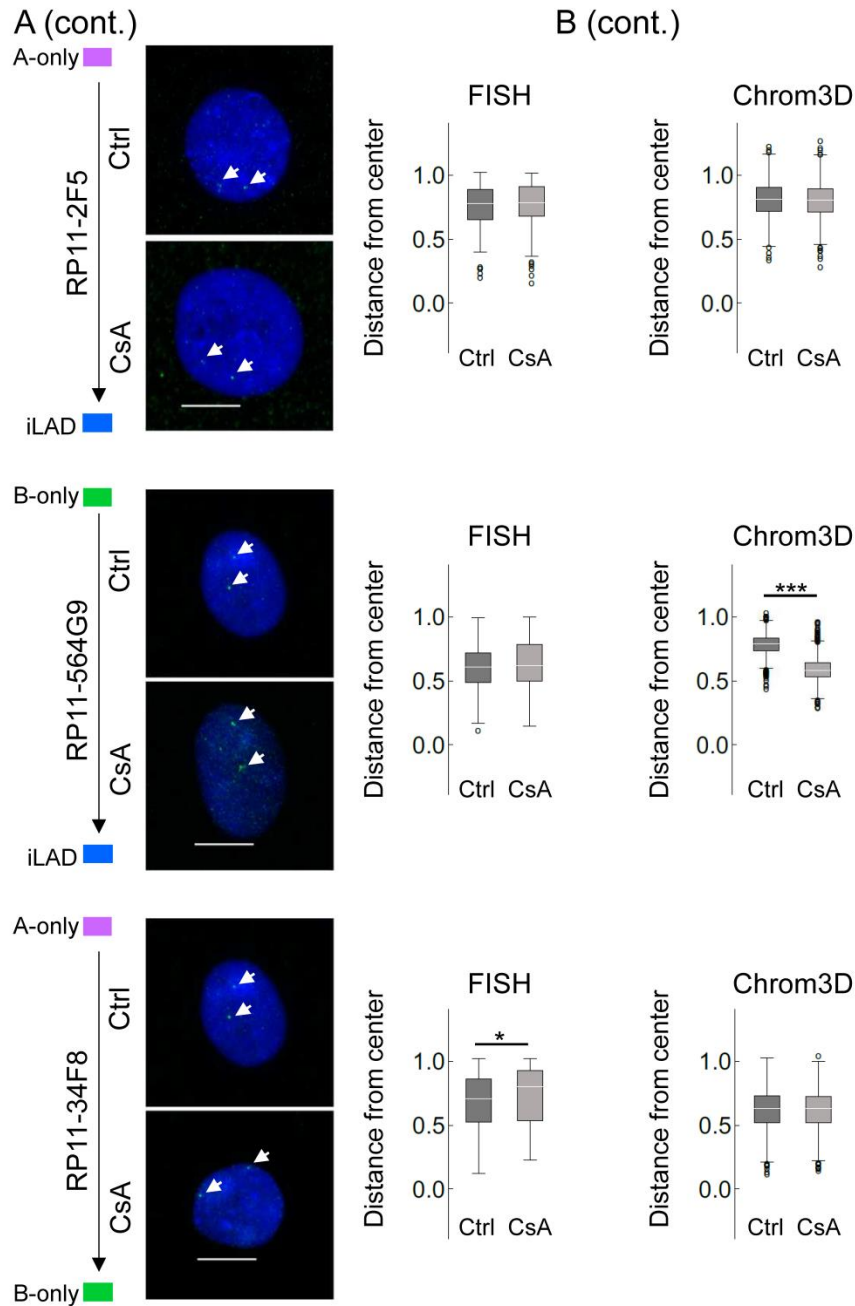
Figure S2. Chrom3D and FISH analysis of radial repositioning of loci after CsA treatment. (A) FISH analysis of locus positioning (arrows) in indicated LAD class in control and CsA-treated cells. Representative FISH images are shown, with normalized probe distance from the nucleus center (0 = center; 1 = periphery defined as the border of DAPI staining); n = 200 FISH signals analyzed per probe per condition; bars, 10 μm. (B) Normalized FISH probe distance from the nucleus center measured in 800 Chrom3D models. Probe number is shown. FISH: *P = 0.006, unpaired t-tests; Chrom3D: ***P < 2.2x10^{-16}, unpaired t-tests.
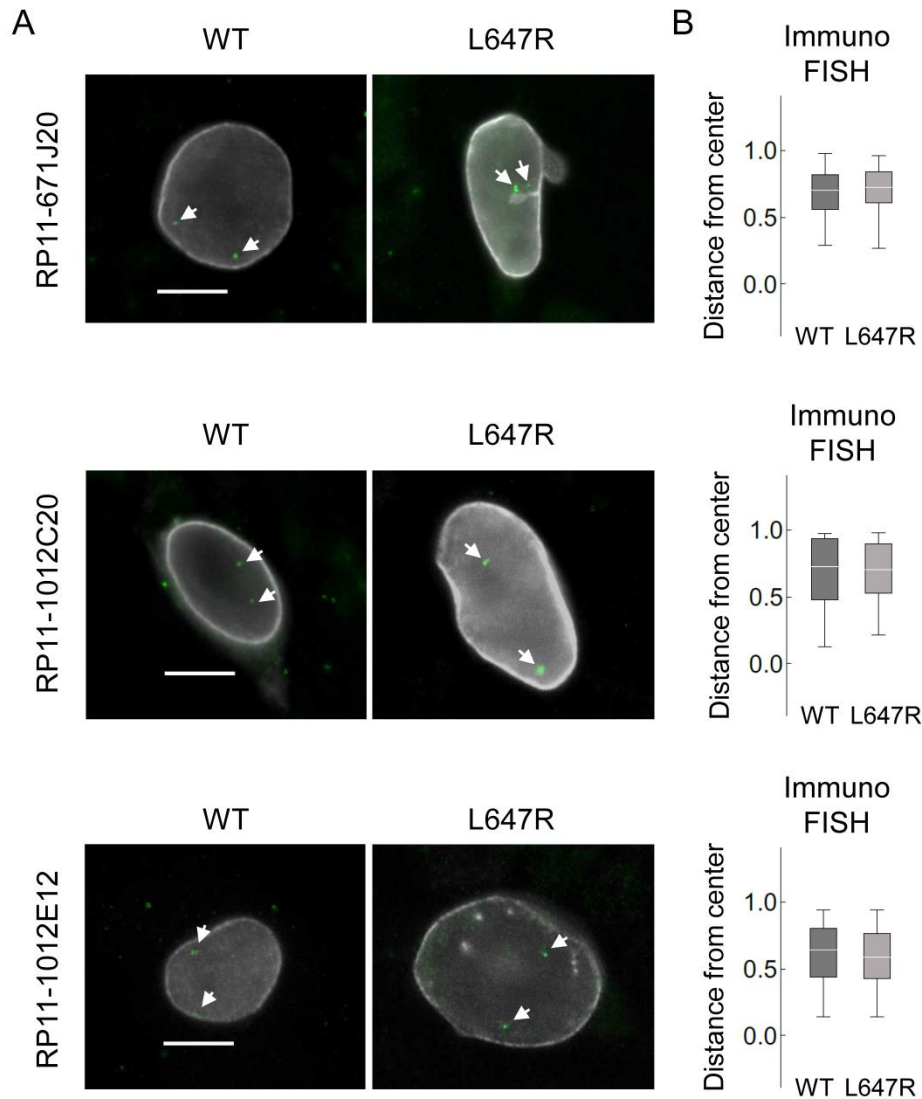
Figure S3. Expression of pre-lamin A wild type or pre-lamin A (L647R) in HepG2 cells does not radially relocalize loci. (A) Immuno-FISH images of positioning of indicated loci (detected by FISH probes; arrows) in HepG2 cells expressing either Flag-tagged wild-type lamin A (WT) or a Flag-tagged lamin A L647R mutant. Lamin A proteins were detected using anti-Flag antibodies. Probe number is shown; bars, 10 μm. (B) Quantification of relative distances of FISH signals from the nucleus center (0 = center; 1 = periphery defined by the border of Flag-lamin A staining at the nucleus edge); n = ~100 nuclei per sample. Distances are not significantly different between the two cell types (P > 0.05; unpaired t-tests.).

Forsberg et al.

Supplementary Tables

Table S1. Gene expression level (FPKM) and LAD class in control and CsA-treated cells. (Excel)

Table S2. Lamin A and lamin B LAD characteristics in control and CsA-treated cells.

Table S3. Characteristics of LAD classes and inter-LADs in control and CsA-treated cells.

Table S4. Characteristics of LAD class transitions.

Table S5. FISH probe information.

Table S2. Lamin A and lamin B LAD characteristics in control and CsA-treated cells.

	LAD class	No. LADs	Genome coverage (% mappable)	Coverage (Mb)	No. genes	Genes / Mb	Median (Mb)
Ctrl	A	244	17.8	510.05	1673	3.28	1.73
	B	239	13.7	392.53	2614	6.66	1.28
CsA	A	178	8.6	245.55	1535	6.25	1.16
	B	278	16.5	470.77	2484	5.28	1.25

Table S3. Characteristics of LAD classes and inter-LADs in control and CsA-treated cells.

	LAD class	No. LADs	Genome coverage (%)	Coverage (Mb)	No. genes	Genes / Mb	Median (Mb)
Ctrl	A-B	115	7.1	202.03	659	3.26	1.56
	A-only	235	10.8	308.02	1045	3.39	1.11
	B-only	245	6.7	190.5	2033	10.67	0.59
	Inter-LAD	642	75.5	2160.76	25633	11.86	1.24
CsA	A-B	148	7.3	208.32	1118	5.37	1.08
	A-only	144	1.3	37.23	427	11.47	0.07
	B-only	302	9.2	262.46	1435	5.47	0.58
	Inter-LAD	574	82.2	2353.31	26390	11.21	1.21

Table S4. Characteristics of LAD class transitions.

LAD class (Ctrl)	LAD class (CsA)	No. LADs	Genome coverage (%)	Genome coverage (Mb)	No. genes	Genes / Mb	Median (Mb)
A-B	A-B	80	4.4	127.03	430	3.38	1.59
	A-only	13	0.1	1.97	19	9.65	0.15
	B-only	79	2.4	68.78	192	2.79	0.87
	Inter-LAD	21	0.1	4.24	18	4.24	0.20
A-only	A-B	36	0.4	12.85	104	8.09	0.19
	A-only	32	0.2	5.64	40	7.09	0.06
	B-only	97	2.7	76.79	199	2.59	0.50
	Inter-LAD	206	7.4	212.74	702	3.30	0.70
B-only	A-B	106	2.1	60.35	524	8.68	0.49
	A-only	50	0.4	12.37	163	13.18	0.06
	B-only	166	2.8	81.22	819	10.08	0.18
	Inter-LAD	129	1.3	36.56	527	14.42	0.11
Inter-LAD	A-B	41	0.3	8.08	60	10.7	0.07
	A-only	92	0.6	17.25	205	13.8	0.10
	B-only	142	1.2	35.66	225	4.4	0.11
	Inter-LAD	676	73.4	2099.77	25143	9.7	1.15

Table S5. FISH probe information.

Probe ID	Clone ID	Change LAD class	Chr.	Start pos.	End pos.	No. genes
p1	RP11-2F5	A switch to Inter-LAD	Chr.2	185216500	185377594	*7*
p2	RP11-671J20	Inter-LAD	Chr.3	9722941	9900724	*51*
p3	RP11-1012C20	B switch to Inter-LAD	Chr.1	2301890	2502158	*95*
p4	RP11-564G9	B switch to Inter-LAD	Chr.5	176865042	177055093	*66*
P5	RP11-79C22	A gain on B	Chr.10	7304838	7461350	*28*
P6	RP11-165J13	A gain on B	Chr.17	77197376	77328294	
P7	RP11-102E12	A switch to B	Chr.18	4467862	4624130	*24*
P8	RP11-34F8	A switch to B	Chr.11	40922548	41092384	*2*
P9	RP11-96H21	B gain on A	Chr.21	31932883	32103229	*61*
P10	RP11-352G21	B gain on A	Chr.9	8000830	8162993	*6*

II

Nuclear Lamin B1 Interactions With Chromatin During the Circadian Cycle Are Uncoupled From Periodic Gene Expression

Annaël Brunet[1†], Frida Forsberg[1†], Qiong Fan[1], Thomas Sæther[1] and Philippe Collas[1,2]*

[1] Department of Molecular Medicine, Institute of Basic Medical Sciences, Faculty of Medicine, University of Oslo, Oslo, Norway, [2] Department of Immunology and Transfusion Medicine, Oslo University Hospital, Oslo, Norway

Many mammalian genes exhibit circadian expression patterns concordant with periodic binding of transcription factors, chromatin modifications, and chromosomal interactions. Here we investigate whether chromatin periodically associates with nuclear lamins. Entrainment of the circadian clock is accompanied, in mouse liver, by a net gain of lamin B1–chromatin interactions genome-wide, after which the majority of lamina-associated domains (LADs) are conserved during the circadian cycle. By tailoring a bioinformatics pipeline designed to identify periodic gene expression patterns, we also observe hundreds of variable lamin B1–chromatin interactions among which oscillations occur at 64 LADs, affecting one or both LAD extremities or entire LADs. Only a small subset of these oscillations however exhibit highly significant 12, 18, 24, or 30 h periodicity. These periodic LADs display oscillation asynchrony between their 5′ and 3′ borders, and are uncoupled from periodic gene expression within or in the vicinity of these LADs. Periodic gene expression is also unrelated to variations in gene-to-nearest LAD distances detected during the circadian cycle. Accordingly, periodic genes, including central clock-control genes, are located megabases away from LADs throughout circadian time, suggesting stable residence in a transcriptionally permissive chromatin environment. We conclude that periodic LADs are not a dominant feature of variable lamin B1–chromatin interactions during the circadian cycle in mouse liver. Our results also suggest that periodic hepatic gene expression is not regulated by rhythmic chromatin associations with the nuclear lamina.

Keywords: circadian rhythm, lamin B, lamina-associated domain, oscillation, period

INTRODUCTION

Thousands of mammalian genes exhibit autonomous oscillatory patterns of expression concordant with the circadian (24 h) rhythm (Hastings et al., 2018). The circadian rhythm is governed by central and peripheral clocks, respectively in the nervous system and in individual organs including adipose tissue, lungs and liver, controlled by transcriptional and translational negative feedback loops (Takahashi, 2017). The core clock is regulated by the CLOCK and BMAL1 transcription factors

(TFs) which drive expression of clock-controlled genes including *Per*, *Cry*, *Nr1d1/Nr1d2* (encoding REV-ERB alpha/beta proteins, respectively), and *Ror* genes (encoding ROR alpha/beta/gamma), by binding to E-boxes in their promoters. The PER-CRY repressor complex inhibits activity of CLOCK–BMAL1, lowering transcription of *Per* and *Cry* and generating a negative feedback loop. RORs and REV-ERBs act as activators and repressors, respectively, of *Arntl* (also called *Bmal1*) and other clock genes, driving their rhythmic transcription. Stability of PER and CRY proteins is regulated by post-translational modifications leading to their time-dependent degradation, enabling a new cycle of CLOCK–BMAL1-driven gene expression.

Circadian binding of TFs and chromatin modifiers to promoters and enhancers generates rhythmic chromatin modifications and remodeling (Koike et al., 2012; Masri et al., 2014; Zhang et al., 2015; Kim et al., 2018). In mouse liver, histone H3 lysine 4 trimethylation (H3K4me3) levels oscillate at promoters of circadian genes (Vollmers et al., 2012; Aguilar-Arnal et al., 2015), while rhythmic H3K4me1 and H3K27 acetylation (H3K27ac) levels define oscillating enhancers (Koike et al., 2012; Vollmers et al., 2012; Fang et al., 2014; Takahashi, 2017). Recruitment to chromatin of the sirtuin SIRT1, a histone deacetylase (HDAC) involved in circadian control of metabolism (Nakahata et al., 2008; Masri et al., 2014), is under influence of oscillatory levels of metabolites (Aguilar-Arnal et al., 2015) and provides a molecular link between metabolism, chromatin and circadian rhythms. Periodic recruitment of HDAC3 to chromatin also regulates circadian rhythms (Feng et al., 2011). These oscillatory cistromes and chromatin modifications raise the possibility that other chromatin-linked processes also show rhythmic patterns. Indeed, periodic promoter–enhancer interactions regulate and connect circadian liver gene expression networks (Aguilar-Arnal et al., 2013; Xu et al., 2016; Kim et al., 2018; Mermet et al., 2018). Thus, circadian-dependent changes in chromatin topology contribute to shaping the nuclear landscape (Yeung and Naef, 2018).

Dynamic interactions of chromatin with the nuclear lamina, a meshwork of A-type lamins [lamins A and C (LMNA and LMNC)], products of the *Lmna* gene, and B-type lamins [lamins B1 and B2 (LMNB1 and LMNB2)], encoded by the *Lmnb1* and *Lmnb2* genes respectively, at the nuclear periphery (Burke and Stewart, 2013) also constitute one mechanism of regulation of gene expression (van Steensel and Belmont, 2017). Interestingly, A- and B-type lamins are not only found at the nuclear periphery, where the nuclear lamina is located, but also in the nucleoplasm where interactions with chromatin have been reported to also occur (Naetar et al., 2017; Pascual-Reguant et al., 2018). Regions of chromatin interacting with lamins, so-called lamina-associated domains (LADs), are typically heterochromatic and relatively well conserved between cell types (Peric-Hupkes et al., 2010). However, other LADs are variable and altered during differentiation (Peric-Hupkes et al., 2010; Rønningen et al., 2015; Poleshko et al., 2017; Paulsen et al., 2019). It remains however unclear to what extent variable LADs arise and disappear as a consequence of regulatory mechanisms or through random interactions of chromatin with nuclear lamins. Whether individual loci or broader domains such as LADs display oscillatory

interactions with nuclear lamins has also to our knowledge not been addressed.

Scarce evidence links the nuclear envelope to circadian gene expression. HDAC3, a component of the clock negative feedback loop (Shi et al., 2016) and a regulator of lamina-associated genes (Demmerle et al., 2013), interacts with the inner nuclear membrane proteins TMPO/lamina-associated polypeptide 2β (Somech et al., 2005) and emerin (Demmerle et al., 2013). The clock regulators SIRT1 and SIRT6 deacetylases interact with LMNA (Liu et al., 2012; Ghosh et al., 2015) at the nuclear lamina, where they modulate histone acetylation and gene expression. *In vitro*, BMAL1 expression seems to be modulated by MAN1, another protein of the inner nuclear membrane, through MAN1 binding to the *ARNTL* (also called *BMAL1*) promoter (Lin et al., 2014). Lastly, in a human colon cancer cell line, a handful of circadian genes have been shown to rhythmically interact with the nuclear lamina, regulating their transcription (Zhao et al., 2015). These observations suggest that nuclear lamins may contribute to the regulation of circadian gene expression. However, whether chromatin exhibits genome-scale periodic associations with the lamina has not been examined.

Here, we determined whether chromatin exhibits periodic interactions with LMNB1 after entrainment of the circadian clock in mouse liver. We opted to examine this feature of genome organization in the liver because it is highly responsive to entrainment of the circadian clock at the metabolic level and as such is the most studied organ in investigations of circadian control of transcriptional regulation (Takahashi, 2017) and spatial chromatin conformation (Aguilar-Arnal et al., 2013; Kim et al., 2018). We show that periodic lamin B1–chromatin interactions are not a dominant feature of LADs during the circadian cycle and are uncoupled from periodic gene expression. Our data strongly suggest that periodic gene expression is not under direct regulation of rhythmic association of chromatin with the nuclear lamina.

MATERIALS AND METHODS

Mice
Wild-type C57Bl/6 male mice (Jackson Laboratories) were housed in 12 h light/12 h dark cycles with lights on at 6 am and lights off at 6 pm. Mice were kept off chow for 24 h, refed *ad libitum* at circadian time CT0 (6 am) and sacrificed at CT6, 12, 18, 24, and 30 h (n = 7 mice per CT). Non-synchronized (NS) mice (n = 7) were sacrificed at 12:00 noon on the day prior to food restriction. Livers were collected from all mice, partitioned and snap-frozen in liquid nitrogen. Procedures were approved by the University of Oslo and Norwegian Regulatory Authorities (approval No. 8565).

RNA-Sequencing and Gene Expression Analysis
Total RNA was isolated from livers of five mice at each CT using the RNeasy Mini Kit (Qiagen). RNA (1 µg) was reverse-transcribed (BioRad Laboratories) and analyzed by qPCR using IQ SYBR green (BioRad Laboratories), *Eif2a* as reference and

primers listed in **Supplementary Table S1** (n = 5 mice per CT). RNA was also processed to prepare RNA-sequencing (RNA-seq) libraries (TruSeq Stranded mRNA Library Prep Kit; Illumina; n = 3 mice per CT) which were sequenced on an Illumina HiSeq2500. RNA-seq reads were processed with Tuxedo (Trapnell et al., 2010). TopHat v2.10 was used to align reads with no mismatch against the mm10 genome (Langmead and Salzberg, 2012). Transcript level was estimated using cufflinks v2.2.1 and differential gene expression determined using cuffdiff v2.2.1 (Trapnell et al., 2010). Gene expression plots show mean ± SD relative expression levels (for RT-qPCR data) or FPKM (fragments per kilobase of exon model per million reads mapped; RNA-seq data) at each CT, as indicated, with single data points. A gene was ascribed to a LAD if its transcription start site overlapped with the LAD.

MetaCycle Analysis

We used MetaCycle (Wu et al., 2016) to identify genes with periodic expression patterns. MetaCycle measures the goodness-of-fit between RNA-seq, FPKM, and theoretical cosine curves with varying periods and phases. The extrapolated periodic function best fitting the RNA-seq data is selected and the significance of a given periodicity is determined by assigning *P* values after scrambling FPKM values. MetaCycle was applied to the entire range of CTs in the study (30 h). To fit RNA-seq data with periodic functions, MetaCycle normalizes FPKM values by computing z-scores. Our time series data are integer intervals with even sampling and do not include missing values. Given the features of our time series data, MetaCycle incorporated both the JTK_CYCLE (JTK) and the Lomb-Scargle (LS) methods for periodic signal detection. Based on our data and time resolution, available period values are integers (0, 6, 12, 18, 24, 30, and 36 h) for JTK and real numbers ranging from 12 to 48 h for LS. Periods are the mean of JTK and LS period values. Thus we focused our analyses on oscillations with 12, 18, 24, and 30 h periods, each ± 3 h, i.e. half the time resolution in our study. Moreover, the restricted 12 ± 3 h period group was not able to distinguish groups of 12 h periodic genes oscillating in positive ($\Phi\_\pi/2$) or negative ($\Phi\_{-\pi/2}$) quadrature of phase, but only those oscillating in phase or opposition of phase. MetaCycle was also applied to identify periodicity in LAD coverage (see below).

Liver Extracts and Immunoblotting

Mouse liver samples were homogenized in ice-cold phosphate buffered saline (PBS) with 1× protease inhibitor cocktail (Sigma-Aldrich) and 1 mM phenylmethylsulfonide fluoride (PMSF; Sigma-Aldrich), using a Dounce tissue grinder with an A-type glass pestle, followed by centrifugation at 200 g for 5 min at 4°C. Supernatants were discarded, and pellets washed once in ice-cold PBS with 1× protease inhibitor cocktail and 1 mM PMSF and centrifuged at 200 g for 5 min at 4°C. Cells were lysed in RIPA buffer (140 mM NaCl, 10 mM Tris–HCl pH 8.0, 1 mM EDTA, 0.5 mM EGTA, 1% Triton X-100, 0.1% SDS, 0.1% sodium deoxycholate, 1 mM PMSF, protease inhibitors) with 1× protease inhibitor cocktail and 1 mM PMSF, sonicated twice with 30 s on/off in a Bioruptor (Diagenode), and incubated under rotation at 25 rpm for 30 min at 4°C. Lysates were centrifuged at 10,000 g for 10 min at 4°C and supernatants collected for immunoblotting analysis. Proteins were separated by 7.5% SDS-PAGE, transferred onto an Immobilon-FL membrane (Millipore) and membranes blocked with 3% BSA in TBST (0.15 M NaCl, 50 mM Tris–HCl pH 7.6, 0.05% Tween®20). Membranes were incubated with antibodies against CLOCK (1:500; Abcam ab3517), LMNB1 (1:1,000; Santa Cruz Biotechnology sc6216), and β-actin (1:2,000; Sigma-Aldrich A5441) in TBST with 3% BSA. Secondary horseradish peroxidase-conjugated anti-mouse (Jackson ImmunoResearch #115-035-174) and anti-goat (Rockland #605-4302) antibodies were used at 1:10,000 dilutions in TBST with 3% BSA.

Chromatin Immunoprecipitation (ChIP)

ChIP of LMNB1 was done as described earlier (Rønningen et al., 2015) and adapted for liver pieces. Snap-frozen liver tissue pieces (40–50 mg, in liquid nitrogen) were thawed on ice and minced on ice for 30 s. Minced tissue was resuspended in PBS containing 1 mM PMSF and protease inhibitors, and homogenized by 7–10 strokes in a 2-ml Dounce homogenizer using a pestle B (tight-fitting). Samples were centrifuged at 400 g and supernatants discarded. Pellets were resuspended in PBS containing 1% formaldehyde (Sigma-Aldrich) and cross-linking was allowed to occur for 10 min at room temperature. Cross-linked samples were sedimented and lysed in RIPA buffer. Chromatin was fragmented by sonication (4 times 10 min) in a Bioruptor (Diagenode). After sedimentation, the supernatant was diluted 10-fold in RIPA buffer and incubated with anti-LMNB1 antibodies (10 μg; Abcam ab16048) coupled to Dynabeads Protein G (Invitrogen) overnight at 4 °C. ChIP samples were washed 3 times in ice-cold RIPA buffer. Cross-links were reversed and DNA eluted for 6 h at 68°C in 50 mM NaCl, 20 mM Tris–HCl pH 7.5, 5 mM EDTA, 1% SDS and 50 ng/μl proteinase K. DNA was purified by phenol-chloroform-isoamylalcohol extraction and used for qPCR (see **Supplementary Table S1** for primer information) or to prepare libraries (Illumina) for sequencing on an Illumina HiSeq2500. Input ChIP DNA consisted of fragmented chromatin aliquots (as above) incubated overnight at 4 °C with no antibodies or beads and subsequently processed as, and in parallel with, the ChIP samples.

LMNB1 ChIP-Seq Data Processing

LMNB1 ChIP-seq and input reads were mapped to the mm10 genome using Bowtie v2.25.0 (Langmead et al., 2009) with default parameters after removing duplicates using Picard's MarkDuplicates. To avoid normalization bias, we ensured that each pair of mapped ChIP and input read files had the same read depth by down-sampling reads for each chromosome individually. Mapped reads were used to call LADs using Enriched Domain Detector (EDD) (Lund et al., 2014) with the following alterations (Forsberg et al., 2019) as described here. To account for technical variation occurring in LAD calling, we first ran EDD 10 times on each LMNB1 ChIP-seq dataset in auto-estimation mode for GapPenalty (GP) and BinSize (BS). Average GP standard deviation was ≤ 1.6 units while BS did not vary (**Supplementary Table S2**). GP variations elicited minimal alterations in LAD calls, allowing estimation of technical variability. For all LADs, median length of these variations was 0.32 Mb; this is < 1% of total LAD coverage, and 3–15 times smaller than median LAD sizes for each CT and replicate. Thus intrinsic EDD variability did not significantly impact LAD calling. Average GP and BS

values from the 10 runs were used to set GP and BS before a final EDD run with each ChIP-seq dataset (**Supplementary Table S2**). Intersects between LADs and genes were determined using BEDTools v2.21.0 (Quinlan and Hall, 2010) and BEDOPS v2.4.27 (Neph et al., 2012). Scripts were written in Bash, Perl, or R and ggplot2 in R was used for plots. Browser files were generated by calculating ChIP/input ratios in 10-kb bins with input normalized to the ratio of total ChIP reads over total input reads.

Determination of Periodic Lads With MetaCycle

To quantify the genomic coverage of variation in the length of LADs during the circadian cycle, we determined for each LAD its "maximal coverage" (cov_{max}) as the union of LAD coverage across all replicates and CTs, and attributed to this cov_{max} a reference value of 1. The cov_{max} 5′ and 3′ limits provided genomic coordinates for measures of variations in LAD length within cov_{max}. For each CT and replicate, variable 5′ and 3′ genomic lengths (in base pairs) were extracted and standardized from 0 to 1, 0 referring to the complete disappearance of a LAD and 1 being the cov_{max} value of the LAD. MetaCycle was applied to determine the periodicity of LAD extensions and shortenings at the 5′ and 3′ borders. Period groups were defined as for RNA-seq analysis (12, 18, 24, and 30 h, each ± 3 h). The method is described in more detail as part of the *Results* section.

Randomization to Validate Periodic LAD Significance

A randomization test was done as additional validation of extrapolated MetaCycle LAD periodicity. To this end, we shuffled the measured experimental variations in 5′ and 3′ LAD lengths within the cov_{max} area for all datasets across CTs and replicates; this was done 3 times. MetaCycle was applied to each randomized order of CTs to identify any periodicity in the variations in LAD lengths across these randomized CTs. The extrapolated periodicity given by MetaCycle was compared with the periodicity found for the experimental order of CTs. If experimental LAD periodicity was different from at least two randomized CTs, it was considered as imposed by the order of CT and not due to random lamin–chromatin interactions.

Determination of Gene-LAD Distance

Gene-to-nearest LAD distance was calculated as the distance from the 5′ and 3′ end of a gene to, respectively, the nearest 3′ and 5′ LAD border. Gene strand was respected and LAD intersects were used at each CT. If a gene was entirely in a LAD, gene-to-nearest LAD distance was the distance from the 5′ and 3′ end of the gene to the first neighboring LAD, both upstream and downstream. In our approach, internal LAD configuration within the cov_{max} area, such as a LAD split or fusion, was not considered in the determination of periodicity at the 5′ and 3′ borders.

Data Viewing

Genome browser views were produced with the Integrated Genomics Viewer (Robinson et al., 2011) using the mm10 genome annotation to illustrate LADs in regions of interest.

Statistics

MetaCycle used its built-in statistical method to assign *P* values from Fisher's exact tests. The JTK and LS methods used in MetaCycle assign a *P* value for each fitted data type, i.e. gene expression variation for RNA-seq and RT-qPCR, protein expression level for Western blot quantification or LAD size variation for LMNB1 ChIP-seq data. These multiple *P* values are combined into a one-test Chi-square statistics assuming a Chi-squared distribution with 2 k degrees of freedom (where k is the number of *P* values; here k = 3 for RNA-seq data, k = 5 for RT-qPCR, k = 3 for Western blot data and k = 2 for LAD data), when all null-hypotheses are true and each *P* value is independent. The combined *P* value was determined by the Chi-square *P* value and was used to determine the significance of oscillating patterns. Protein levels in Western blots were compared pair-wise between time-points using paired t-tests generating two-tailed *P* values; P < 0.01 was considered significant.

RESULTS

Hepatic Genes Exhibit Distinct Periodic Transcript Levels in Liver

To entrain the circadian clock, mice were subjected to 24 h fasting and refed *ad libitum* from circadian time CT0 (Tahara et al., 2011). Livers were collected every 6 h until CT30, and from non-synchronized (NS) mice 18 h before the fasting period (**Figure 1A**). Entrainment of the clock was confirmed by periodic expression of the core clock genes *Clock*, *Arntl* (*Bmal1*), *Cry1*, *Per1*, and *Nr1d1*, assessed by RT-qPCR and analysis of their periodicity using MetaCycle (**Supplementary Figure 1**; **Supplementary Table S3**). We used MetaCycle to identify genes with periodic expression patterns from RNA-seq data generated in biological triplicates at each CT. MetaCycle measures the goodness-of-fit between RNA-seq FPKM and cosine curves with varying periods and phases. The extrapolated periodic function best fitting the data is selected and significance is determined (Fisher's exact tests) after scrambling FPKM values. From the period distribution for all 17,330 expressed genes in liver (expressed at least at one time point), we focused on oscillations with 12, 18, 24, and 30 h periods (each ± 3 h, half the time resolution in our study) (**Supplementary Figure S2A**). We find that nearly 20% of oscillations are circadian (24 h period; 3,046 genes), and thousands of genes oscillate with periods within the circadian rhythm and beyond (**Figure 1B**), in line with previous reports (Hughes et al., 2009; Korencic et al., 2014; Zhu et al., 2017). Among these, a subset displays highly significantly oscillating transcripts (*P* < 0.005; **Figures 1B** and **C**). Within a given period, mRNA oscillations occurred with distinct phases (**Supplementary Figure S2B**): oscillations are in phase (Φ = 0, time at first maxima) and opposition of phase (Φ = π), and for 18, 24, and 30 h periods, are also offset by one-quarter cycle (Φ = ½ π and Φ = −½ π) (**Figure 1C**; **Supplementary Figures S2C** and **D**). Significantly periodic genes include the core clock genes (**Figure 1D**; **Supplementary Figure S2E**), confirming entrainment of the clock. Genes (644) also display significant (*P* < 0.005) mRNA oscillations with periods outside 12, 18, 24, or 30 h. We also defined a set of 204 "non-periodic" genes with mRNA
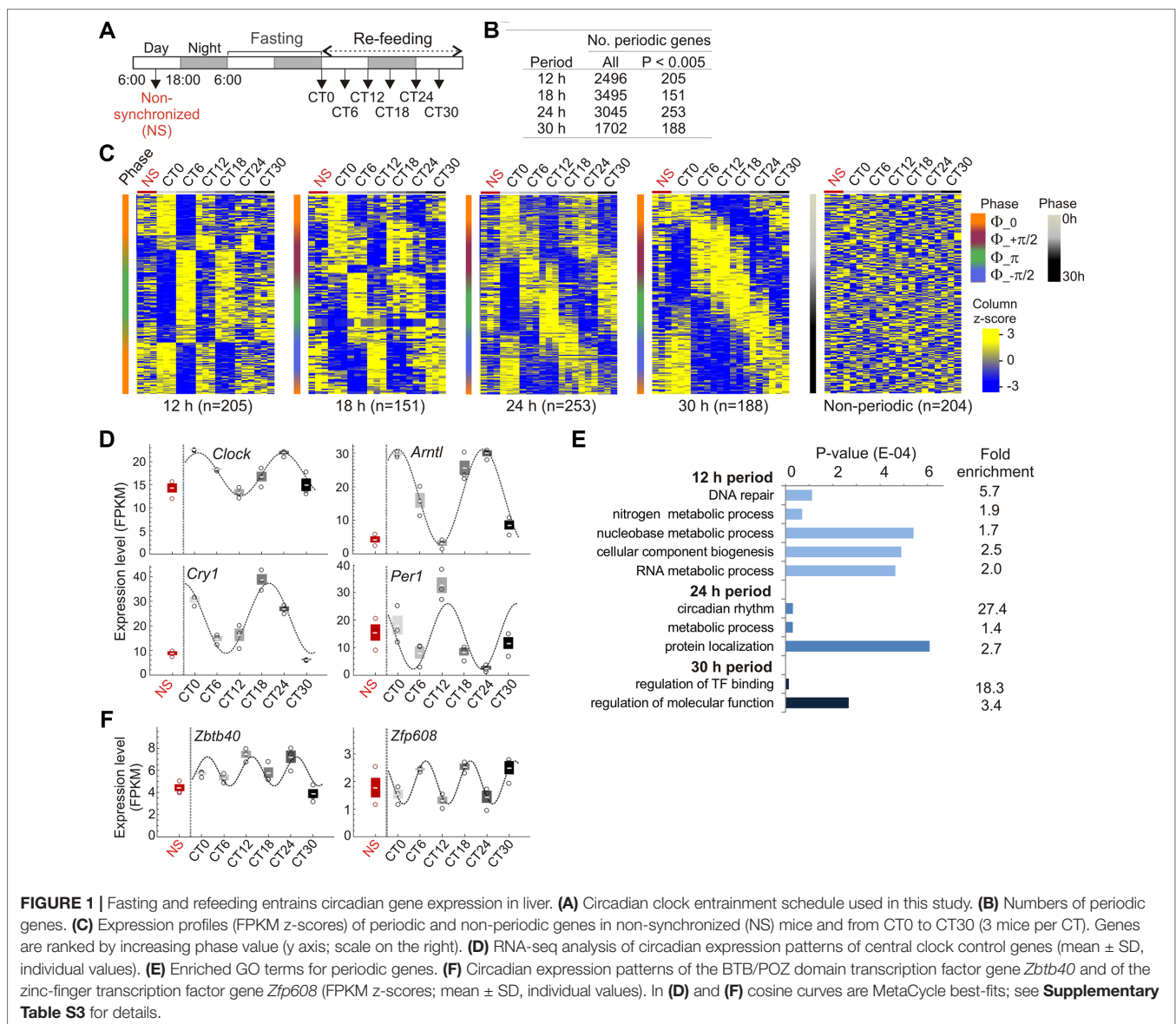
FIGURE 1 | Fasting and refeeding entrains circadian gene expression in liver. **(A)** Circadian clock entrainment schedule used in this study. **(B)** Numbers of periodic genes. **(C)** Expression profiles (FPKM z-scores) of periodic and non-periodic genes in non-synchronized (NS) mice and from CT0 to CT30 (3 mice per CT). Genes are ranked by increasing phase value (y axis; scale on the right). **(D)** RNA-seq analysis of circadian expression patterns of central clock control genes (mean ± SD, individual values). **(E)** Enriched GO terms for periodic genes. **(F)** Circadian expression patterns of the BTB/POZ domain transcription factor gene *Zbtb40* and of the zinc-finger transcription factor gene *Zfp608* (FPKM z-scores; mean ± SD, individual values). In **(D)** and **(F)** cosine curves are MetaCycle best-fits; see **Supplementary Table S3** for details.

levels discordant (1 > P > 0.9999) with any cosine curve tentatively fitted by MetaCycle (**Figure 1B**). Lists of periodic and non-periodic genes are provided in **Supplementary Tables S4** and **S5**.

Gene ontology analysis confirms enrichment of 24 h periodic genes in rhythmic and circadian processes, including key metabolic functions (**Figure 1E**; **Supplementary Table S6**). A number of periodic genes encode BTB/POZ domain TFs, some of which are involved in targeting chromatin to the nuclear lamina (Zullo et al., 2012) (**Supplementary Table S4**). Some of these genes are CLOCK or BMAL1 targets (e.g. *Zbtb40*, *Zbtb7b/cKrox*, and *Zfp608*; **Figure 1F**) and could tentatively be involved in associations of chromatin with the nuclear envelope.

Entrainment of the Circadian Clock Resets LMNB1–Chromatin Interactions

We therefore examined chromatin association with nuclear lamins in liver during the circadian cycle. We first established

that LMNB1 protein levels vary moderately over time but do not significantly oscillate (P = 0.61; Fisher's exact test), and that *Lmnb1* transcripts analyzed by RNA-seq and verified by RT-qPCR do not periodically oscillate (**Figures 2A–C**; **Supplementary Figure S3A**). Moreover, chromatin immunoprecipitation (ChIP)-qPCR of LMNB1 from liver confirmed LMNB1 enrichment in LADs found in several other mouse cell types (constitutive LADs; cLADs) (Meuleman et al., 2013) (**Figure 2D**).

Thus, we determined to what extent LADs varied during the circadian cycle. We performed a ChIP-seq analysis of LMNB1 from livers of NS mice and at each CT in biological replicates (i.e. two mice per CT) and mapped LADs (**Figure 3A**; see **Supplementary Table S2**). We find that LAD sizes are overall constant and LADs display low gene density (**Supplementary Figures S3B** and **C**). LADs also show robust overlap between replicates (**Figure 3A** and **B**), as shown by Jaccard indices (**Figure 3C**) and by minimal variations between intersect coverage and

FIGURE 2 | Expression of LMNB1 protein and transcripts during the circadian cycle. **(A)** Western blots of LMNB1 and CLOCK expression; β-actin was used as loading control; see **Supplementary Figure S3A** for all biological replicates. **(B)** Quantification of Western blots from biological triplicates, relative to β-actin; mean ± SD, individual values; *P < 0.01 (paired t-tests, two tailed P values). Note the difference in variation of expression of CLOCK protein and *Clock* transcripts expected from the regulation of protein expression at the transcriptional and protein degradation levels). **(C)** Levels of *Lmnb1* transcripts determined by RNA-seq (FPKM; n = 3) and RT-qPCR (n = 5; expression relative to *Eif2a* levels); means ± SD, individual values. Cosine curves are MetaCycle best-fits. *Lmnb1* is not significantly periodic (RNA-seq P = 0.16; RT-qPCR P = 0.98; MetaCycle Fisher's exact tests). RT-qPCR graph: blue line, MetaCycle best-fit from RT-qPCR data; black line, MetaCycle best-fit from RNA-seq data; note the overlap between the two, indicating strong concordance between the two datasets. Amplitude and base values used for both fits are from RT-qPCR MetaCycle analysis. **(D)** ChIP-qPCR analysis of LMNB1 occupancy in constitutive LADs and in non-LAD regions (mean ± SD of % of input chromatin analyzed by qPCR; n = 3 NS mice); ChIP using an irrelevant IgG was done as negative control.

FIGURE 3 | Characterization of LADs during the circadian cycle. **(A)** Genome browser view of LADs in biological replicate (r1, r2) and at each CT for the indicated region on chromosome 10. **(B)** Genome browser view of LAD intersects between replicates for each CT in the same region as in **(A)**. **(C)** Jaccard indices of LAD overlap between replicates. **(D)** Venn diagram of LAD overlap between NS mice and CT0 (intersect of replicates); bottom, schematic representation of genome coverage by LADs gained or lost at CT0 relative to NS, for stand-alone LADs and LAD extension or shortening. **(E)** Radar plot of genome coverage by LADs. **(F)** Distribution and median of LAD size. **(G)** Jaccard indices of LAD overlap between consecutive CTs.

replicates (< 1 Mb, or 0.05–0.21% of LAD coverage per replicate; **Supplementary Table S7**). Thus unless specified otherwise, LADs were subsequently analyzed at each time point as intersects between replicates.

We next assessed to what extent entrainment of the circadian clock did reset LADs. We find that entrainment of the clock is manifested by a LAD gain of 126.7 Mb at CT0 relative to NS, as stand-alone LADs or as extensions of existing LADs (**Figure 3D**). This increase in LMNB1–chromatin interactions was confirmed by ChIP-qPCR (**Supplementary Figures S3D** and **E**). We also note a LAD loss of 46 Mb at CT0 relative to NS, mostly as stand-alone LADs (**Figure 3D**). Thus, entrainment of the clock is associated with a net gain of LMNB1–chromatin interactions.

Comparison of LAD coverage over time reveals an increase from CT0 (339 Mb) to CT12 (496 Mb), followed by a decrease to CT30 (312 Mb) (**Figure 3E**), likely resulting from variations in LAD numbers rather than LAD size (**Figure 3F**). LADs nevertheless display robust overlap across CTs (**Figure 3G; Supplementary Figure S3F**), indicating that they are overall conserved in liver during the circadian cycle. However, the data also indicate that some changes in LMNB1–chromatin interactions do occur, and underline the detection of variable LADs. Of note, although LMMB1 is predominantly found at the nuclear lamina at the nuclear periphery, a fraction of LMNB1 has also been reported in the nucleoplasm, in association with nucleoli in heterochromatin domains (Sen Gupta and Sengupta, 2017) and with domains of euchromatin (Pascual-Reguant et al., 2018). Moreover, our ChIP approach to identify LMNB1 LADs does not *a priori* discriminate between the nuclear peripheral and internal pools of LMNB1. Thus we do not at present exclude that a subset of LMNB1–chromatin interactions detected during the circadian cycle in our study potentially involves a nucleoplasmic LMNB1 pool.

Periodic Oscillations in LMNB1–Chromatin Interactions Constitute a Minor Proportion of LADs

We next examined variations in LADs more closely during the circadian cycle. These occur by LAD extension or shortening, sometimes resulting in a fusion or splitting of LADs, or by formation and dissociation of entire LADs (see **Figures 3A** and **B**). We therefore devised a strategy to quantitatively characterize the genomic coverage of these variable LADs over time. We determined for each LAD the maximal genome coverage (cov_{max}) in the CT0–CT30 time course as the union of LAD coverage across all replicates and CTs, and ascribed to cov_{max} a reference value of 1 (**Figure 4A**, left panel). The 5′ and 3′ boundaries of this cov_{max} area provided genomic coordinates for measures of variations in LAD length within this area. For each CT and replicate, variable 5′ and 3′ LAD lengths were extracted and standardized from 0 to 1 (cov_{max}), 0 referring to the complete disappearance of a LAD, and 1 corresponding to the entire LAD being present over the whole cov_{max} area (**Figure 4A**, middle panel). We then used MetaCycle to identify any periodicity in the extension or shortening of LADs within the cov_{max} area (**Figure 4A**, right panel), where MetaCycle applied a cosine curve best-fitting genome coverage variations at the 5′ and 3′ end of LADs.

We applied MetaCycle to 626 variable LAD borders (at 313 LADs) to identify periodically oscillating lengths of these LADs over the CT0–CT30 time course (**Figure 4B**). Among these, MetaCycle tentatively identifies 5′ and/or 3′ end oscillations with 12, 18, 24, or 30 h (± 3 h) periods in 420 LAD borders (among 240 LADs; **Figure 4B**; **Supplementary Table S8**). Ascribing a stringent P value of < 0.005 (Fisher's exact test; as in our MetaCycle RNA-seq analysis) returns 10 highly significantly periodic LADs with periods distributed throughout the circadian cycle (**Figure 4B**; **Table 1**; **Supplementary Table S8**). Relaxing the P value to $P < 0.05$ expectedly increases the number of periodic LAD borders to 77 (30 5′-periodic, 47 3′-periodic, and 13 both 5′- and 3′-periodic) among 64 distinct LADs (**Figure 4B**; **Supplementary Table S8**). However, inspection of the profiles of these LADs revealed, for some of them, discrepancy with the best curve fitted by MetaCycle. This led us to focus our subsequent analysis on the 10 LADs identified above at $P < 0.005$, which we henceforth refer to as "periodic LADs" (**Figures 4C** and **D**). Periodic LADs therefore constitute a subset of variable LADs with highly significant periodic oscillations in the genomic coverage in their 5′ or 3′ ends. These LADs withstand a randomization test of all replicates and CTs (see Materials and Methods section), suggesting that LAD periodicity observed in our data is imposed by the order of CTs. Periodic LADs include LADs with a stable core and variable borders, and LADs that entirely appear or disappear (**Figures 4C** and **D**). Altogether, our data indicate that significant periodicity in LAD border interactions with LMNB1 only concerns a minor set of LADs. Thus, the majority of LMNB1–chromatin interactions are conserved during the circadian cycle.

Periodic Gene Expression Is Uncoupled From Rhythmic LMNB1–Chromatin Interactions

We then examined the relationship between periodic LADs and gene expression. Out of 430 genes found in periodic LADs, only 68 genes are expressed, albeit with no periodicity (**Figures 5A** and **B**; **Supplementary Figure S4A**). Moreover, we find that the vast majority of periodic genes are outside LADs at any time point during the circadian cycle (only < 2% are in LADs; **Figure 5C**). We then examined genes located within 2.5 Mb of the 5′ or 3′ end of periodic LADs (523 genes). Most of these genes are expressed (437 genes), among which ~10% are periodic, yet again with no dominant period and no temporal relationship to LAD periodicity (**Figure 5A**). Thus, since most genes reside outside LADs during the circadian cycle and no specific feature was identified in periodic LADs, we then determined at each CT the relationship between genes, and in particular periodic genes, and gene distance to the nearest LAD (see Materials and Methods). We find that the minimal distance occurred at CT12 while the maximal distance was detected at CT0 and CT24/30 (**Supplementary Figure S4B**). We thus examined the magnitude of variations in gene-to-nearest-LAD distance occurring between CT0 and CT12 and between CT12 and CT24 (to maintain 12-h intervals in both cases during a 24 h circadian time). Consistent with this transient gain in LAD coverage (see **Figure 3E**) and with the gene-poor content of LADs, we observe
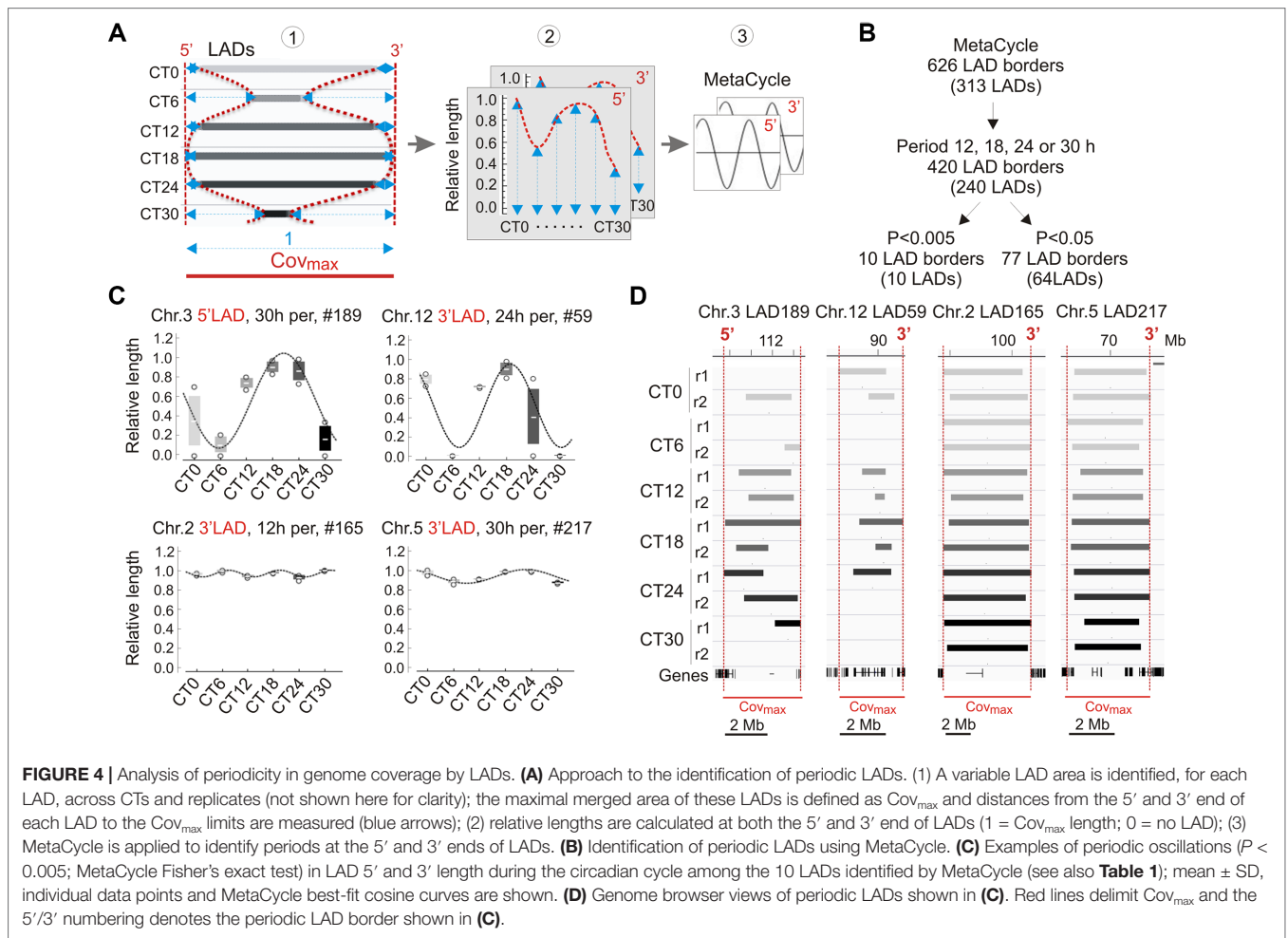
FIGURE 4 | Analysis of periodicity in genome coverage by LADs. **(A)** Approach to the identification of periodic LADs. (1) A variable LAD area is identified, for each LAD, across CTs and replicates (not shown here for clarity); the maximal merged area of these LADs is defined as Cov$_{max}$ and distances from the 5′ and 3′ end of each LAD to the Cov$_{max}$ limits are measured (blue arrows); (2) relative lengths are calculated at both the 5′ and 3′ end of LADs (1 = Cov$_{max}$ length; 0 = no LAD); (3) MetaCycle is applied to identify periods at the 5′ and 3′ ends of LADs. **(B)** Identification of periodic LADs using MetaCycle. **(C)** Examples of periodic oscillations ($P <$ 0.005; MetaCycle Fisher's exact test) in LAD 5′ and 3′ length during the circadian cycle among the 10 LADs identified by MetaCycle (see also **Table 1**); mean ± SD, individual data points and MetaCycle best-fit cosine curves are shown. **(D)** Genome browser views of periodic LADs shown in **(C)**. Red lines delimit Cov$_{max}$ and the 5′/3′ numbering denotes the periodic LAD border shown in **(C)**.

an overall decrease in gene-to-nearest LAD distance between CT0 and CT12 (**Figure 5D**; data points in quadrants 1 and 2 and along the y axis, negative values), and for most genes, an increase thereafter, between CT12 and CT24 (data points in quadrant 2). These changes concern both periodic genes (*left panel*, green data points) and all other genes (*right panel*) regardless of the magnitude of this variation (**Figure 5D**; y axis negative values). Of note, the magnitude of this variation (**Figure 5E**) is larger than that of the intrinsic cumulated EDD error at each CT

involved (see **Supplementary Table S2**, EDD error) and larger than the LAD variation between LAD intersects and replicates (see **Supplementary Table S7**, LAD variation).

We conclude that there is no correlation between periodicity in gene expression and variation in gene-to-nearest LAD distance. This variation appears to be caused by a transient gain in the number of LADs, the functional significance of which remains to be examined. Similarly, the central clock-regulating genes are typically megabases away from the nearest LAD (**Supplementary Table S9**; **Supplementary Figure S4C**), and promoter regions of these genes are also essentially devoid of LMNB1 interaction at any CT (**Supplementary Figure S4D**).

Altogether, our results argue for a constitutive localization of circadian genes, including clock regulators, in a chromatin environment essentially devoid of B-type lamin interactions, providing permissiveness for periodic transcriptional activation during the circadian cycle (Koike et al., 2012; Kim et al., 2018). Our findings argue that oscillatory expression of periodic genes, including central clock-control genes, is uncoupled from a direct association with the nuclear lamina or from their localization in the vicinity of periodic LADs.

TABLE 1 | Period of 5′ and 3′ significantly periodic LAD borders.

LAD no.	Chr.	5′ period (h)	3′ period (h)
15	1	–	12
165	2	–	12
167	2	24	–
189	3	30	–
194	3	–	12
217	5	–	30
239	7	–	18
262	8	12	–
36	10	18	–
59	12	24	–
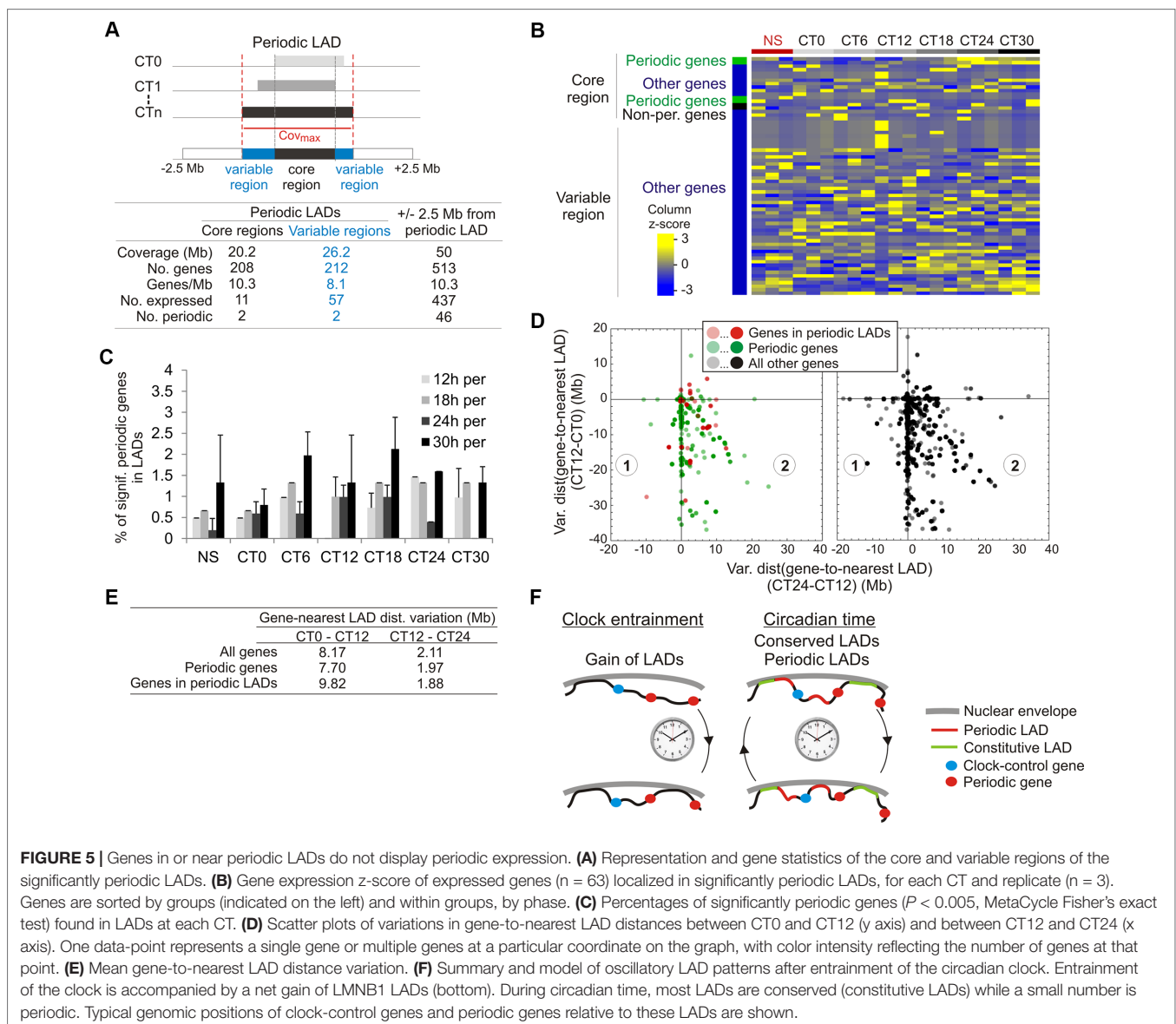
FIGURE 5 | Genes in or near periodic LADs do not display periodic expression. **(A)** Representation and gene statistics of the core and variable regions of the significantly periodic LADs. **(B)** Gene expression z-score of expressed genes (n = 63) localized in significantly periodic LADs, for each CT and replicate (n = 3). Genes are sorted by groups (indicated on the left) and within groups, by phase. **(C)** Percentages of significantly periodic genes (*P* < 0.005, MetaCycle Fisher's exact test) found in LADs at each CT. **(D)** Scatter plots of variations in gene-to-nearest LAD distances between CT0 and CT12 (y axis) and between CT12 and CT24 (x axis). One data-point represents a single gene or multiple genes at a particular coordinate on the graph, with color intensity reflecting the number of genes at that point. **(E)** Mean gene-to-nearest LAD distance variation. **(F)** Summary and model of oscillatory LAD patterns after entrainment of the circadian clock. Entrainment of the clock is accompanied by a net gain of LMNB1 LADs (bottom). During circadian time, most LADs are conserved (constitutive LADs) while a small number is periodic. Typical genomic positions of clock-control genes and periodic genes relative to these LADs are shown.

DISCUSSION

Oscillations in chromatin conformation mediated by rhythmic chromosomal interactions contribute to the regulation of circadian gene expression (Aguilar-Arnal et al., 2013; Xu et al., 2016; Kim et al., 2018; Mermet et al., 2018; Yeung et al., 2018). We now provide evidence of a net gain of lamin–chromatin interactions following entrainment of the circadian clock (NS-CT0 transition), which speculatively may reinforce the robustness of segregation of chromatin domains in the nucleus space.

Given the overall repressive chromatin environment at the nuclear periphery (van Steensel and Belmont, 2017), and evidence of cyclic recruitment and silencing of specific genes at the nuclear envelope in a human cancer cell line (Zhao et al., 2015), we reasoned that periodic gene expression could at least in part be regulated by periodic interactions with the nuclear lamina. We applied MetaCycle, a tool designed to identify

periodic transcript oscillations (Wu et al., 2016), to identify periodic changes in genome coverage by LMNB1. Our approach distinguishes 5′ and 3′ LAD extension or shortening from entire LAD emergence or disappearance (**Figure 5F**). The gain of lamin–chromatin interactions between NS to CT0 is followed by periodic interactions of specific genomic regions with LMNB1, suggestive of discrete rhythmic associations with the nuclear lamina. Our ChIP approach would notably detect interactions of chromatin with nucleoplasmic LMNB1, which appear to be more euchromatic than peripheral LADs (Pascual-Reguant et al., 2018), suggesting that periodic LADs may also be nucleoplasmic. The detection of periodic LADs in our study adds to mounting evidence that chromatin is able to display oscillations in its 3-dimensional conformation (Kim et al., 2018).

Counterintuitively however, several points in our data argue that in the mouse liver, periodic gene expression is not directly

coupled to oscillating or periodic chromatin associations with the nuclear lamina. (1) Genes with periodic transcript levels reside outside LADs at any time point during the circadian cycle. This notably includes *Pard3*, which has been found to be periodically recruited to the nuclear envelope in human colon cancer cells (Zhao et al., 2015), but in mouse liver is localized 15 Mb away from the nearest (and conserved) LAD. (2) Similarly, our analysis reveals that central clock-control genes reside megabases away from the nearest LAD and show no promoter association with LMNB1. This configuration may keep these genes in a transcriptionally permissive ("lamin-free") environment throughout the circadian cycle, compatible with a regulation of circadian transcription by rhythmic TF binding and activity (Koike et al., 2012; Masri et al., 2014; Zhang et al., 2015). Our results also suggest that rhythmic chromatin looping activity which may regulate gene expression within TADs (Kim et al., 2018) take place in an environment where chromatin is not restrained by nuclear lamins (Bronshtein et al., 2015). (3) Periodic genes can also flank constitutive LADs and conversely, genes with stable (high or low) expression levels may flank periodic LADs. (4) Lastly, there is no relationship between periodic gene expression and gene-nearest LAD distance during the circadian cycle. We find that periodic genes are primarily involved in chromatin regulation, transcription regulation and several metabolic functions. Our data strongly suggest therefore that the periodic LAD patterns identified here in liver cannot readily explain these oscillatory gene expression patterns. In fact, periodic hepatic gene expression as a whole appears to be uncoupled from periodic chromatin association with the nuclear lamina.

Concurring with our results, other chromatin-linked processes are uncoupled from gene expression patterns. For example, many oscillatory genes display stable chromosomal interactions (Kim et al., 2018), including promoter–enhancer contacts (Beytebiere et al., 2019) during the circadian cycle. Conversely, many expressed genes display circadian oscillations in promoter and enhancer histone modification patterns that are irrespective of whether or not these genes are periodic or not (Koike et al., 2012). These observations highlight a complex and in some instances enigmatic cross-talk between circadian transcription and rhythmic changes in chromatin states.

Our findings raise several important issues. First, periodic LADs are not a prominent feature of LMNB1–chromatin interactions during the circadian cycle. Sixty-four LADs display variations in their 5′ and/or 3′ end coverage, but we only find, using our stringent approach, ten highly significantly periodic LADs, with asynchronous oscillations between their 5′ and 3′ borders. Yet, these variations withstand a randomization test, suggesting that rhythmicity is elicited by the underlying order of CTs (i.e. circadian time) rather than by random lamin–chromatin interactions. Our findings suggest therefore that the periodic LMNB1–chromatin interactions identified here represent a small subset of all variable interactions. Nevertheless, although we find no evidence of punctual interactions of LMNB1 with individual clock-control genes or promoters, it remains possible that a subset of genes, including periodic genes, display discrete circadian interactions with LMNB1 reminiscent

of those shown in cancer cells (Zhao et al., 2015). In addition, periodic LADs do not seem to harbor any evident functional properties. This contrasts with developmentally regulated B-type lamin–chromatin interactions which have been reported during differentiation of mouse embryonic stem cells (Peric-Hupkes et al., 2010). On the other hand, differential LMNB1 LADs have also been reported in hepatocarcinoma cells treated with cyclosporin, albeit with no significant changes in gene expression (Forsberg et al., 2019), akin to what we observe in the liver. It remains to be examined whether LADs, and periodic LADs in particular, described here involve a level of regulation which currently remains unappreciated.

Second, how could periodic lamin–chromatin interactions be regulated? The cistrome of circadian genes can oscillate in a manner concordant with circadian gene expression (Feng et al., 2011; Fang et al., 2014; Zhang et al., 2015), thus factors mediating lamin–chromatin interactions may also be periodically recruited to target loci. Our transcriptome data indicate that several genes encoding BTB/POZ domain proteins oscillate during the circadian cycle. These proteins share DNA binding motifs enriched in LADs (Guelen et al., 2008) and in lamin-associated sequences (Zullo et al., 2012; Lund et al., 2013), and are found in sequences able to re-localize chromatin to the nuclear lamina (Harr et al., 2015). Thus, oscillating LADs could potentially be regulated through the periodic recruitment of factors important for chromatin localization at the nuclear periphery (Shachar et al., 2015). A search for protein binding motifs in the core and variable regions of periodic LADs using several tools including HOMER (Heinz et al., 2010) and the MEME suite (Bailey et al., 2009), however, revealed no significant enrichment in known motifs which could point to protein candidates mediating these periodic lamin–chromatin interactions. Speculatively, proteins of the inner nuclear membrane or bound to the nuclear lamina, through rhythmic post-translational modifications or through their periodic recruitment to these nuclear domains, could also mediate periodic interactions by direct or indirect interactions with chromatin. A discovery of the proteome of the nuclear periphery or of interactome of nuclear lamins during the circadian cycle would be valuable in the identification of periodic association of chromatin with the nuclear lamina.

Third, what would be the significance of oscillating, or taken more broadly, variable lamin–chromatin interactions and their impact on genome architecture? Resetting of LADs immediately after entrainment of the circadian clock may strengthen the robustness of liver-specific gene expression, possibly through a marked segregation of heterochromatin from euchromatin (Solovei et al., 2013; Falk et al., 2019). Oscillations of subsets of LADs, regardless of periodicity, may alter the radial positioning of chromatin and/or confer dynamic changes in chromatin states in regions that are in 3-dimensional proximity, but not necessarily in linear proximity. These changes altogether may affect gene expression in some of these regions (Robson et al., 2016; Paulsen et al., 2019), but not necessarily in all (Forsberg et al., 2019). LAD displacement may also result in radial repositioning of topological chromatin domains (Robson et al., 2016), or of regulatory elements (Robson et al., 2017).

Assessment of periodic LADs in a 3-dimensional context should shed light on the putative long-range impact of LAD dynamics on genome architecture and function.

DATA AVAILABILITY STATEMENT

ETHICS STATEMENT

Animal procedures were approved by the Norwegian Regulatory Authorities (Approval No. 8565).

AUTHOR CONTRIBUTIONS

FF, AB and PC designed the study. FF and QF did wet-lab experiments. TS supervised parts of these experiments. AB did the bioinformatics analyses. AB and PC supervised the work and wrote the manuscript.

ACKNOWLEDGMENTS

SUPPLEMENTARY MATERIAL

The Supplementary Material for this article can be found online at: https://www.frontiersin.org/articles/10.3389/fgene.2019.00917/full#supplementary-material

REFERENCES

Aguilar-Arnal, L., Hakim, O., Patel, V. R., Baldi, P., Hager, G. L., and Sassone-Corsi, P. (2013). Cycles in spatial and temporal chromosomal organization driven by the circadian clock. *Nat. Struct. Mol. Biol.* 20, 1206–1213. doi: 10.1038/nsmb.2667

Aguilar-Arnal, L., Katada, S., Orozco-Solis, R., and Sassone-Corsi, P. (2015). NAD(+)-SIRT1 control of H3K4 trimethylation through circadian deacetylation of MLL1. *Nat. Struct. Mol. Biol.* 22, 312–318. doi: 10.1038/nsmb.2990

Bailey, T. L., Boden, M., Buske, F. A., Frith, M., Grant, C. E., Clementi, L., et al. (2009). MEME Suite: tools for motif discovery and searching. *Nucl. Acids Res.* 37, W202–W208. doi: 10.1093/nar/gkp335

Beytebiere, J. R., Trott, A. J., Greenwell, B. J., Osborne, C. A., Vitet, H., Spence, J., et al. (2019). Tissue-specific BMAL1 cistromes reveal that rhythmic transcription is associated with rhythmic enhancer–enhancer interactions. *Genes Dev.* 33, 294–309. doi: 10.1101/gad.322198.118

Bronshtein, I., Kepten, E., Kanter, I., Berezin, S., Lindner, M., Redwood, A. B., et al. (2015). Loss of lamin A function increases chromatin dynamics in the nuclear interior. *Nat. Commun.* 6, 8044. doi: 10.1038/ncomms9044

Brunet, A., Forsberg, F., and Collas, P. (2019). Rhythmic chromatin interactions with lamin B1 reflect stochasticity in variable lamina-associated domains during the circadian cycle. *bioRxiv*, 584011. doi: 10.1101/584011

Burke, B., and Stewart, C. L. (2013). The nuclear lamins: flexibility in function. *Nat. Rev. Mol. Cell Biol.* 14, 13–24. doi: 10.1038/nrm3488

Demmerle, J., Koch, A. J., and Holaska, J. M. (2013). Emerin and histone deacetylase 3 (HDAC3) cooperatively regulate expression and nuclear positions of MyoD, Myf5, and Pax7 genes during myogenesis. *Chromosome Res.* 21, 765–779. doi: 10.1007/s10577-013-9381-9

Falk, M., Feodorova, Y., Naumova, N., Imakaev, M., Lajoie, B. R., Leonhardt, H., et al. (2019). Heterochromatin drives compartmentalization of inverted and conventional nuclei. *Nature* 570, 395–399. doi: 10.1038/s41586-019-1275-3

Fang, B., Everett, L. J., Jager, J., Briggs, E., Armour, S. M., Feng, D., et al. (2014). Circadian enhancers coordinate multiple phases of rhythmic gene transcription *in vivo*. *Cell* 159, 1140–1152. doi: 10.1016/j.cell.2014.10.022

Feng, D., Liu, T., Sun, Z., Bugge, A., Mullican, S. E., Alenghat, T., et al. (2011). A circadian rhythm orchestrated by histone deacetylase 3 controls hepatic lipid metabolism. *Science* 331, 1315–1319. doi: 10.1126/science.1198125

Forsberg, F., Brunet, A., Ali, T. M. L., and Collas, P. (2019). Interplay of lamin A and lamin B LADs on the radial positioning of chromatin. *Nucleus* 10, 7–20. doi: 10.1080/19491034.2019.1570810

Ghosh, S., Liu, B., Wang, Y., Hao, Q., and Zhou, Z. (2015). Lamin A Is an Endogenous SIRT6 Activator and Promotes SIRT6-Mediated DNA Repair. *Cell Rep.* 13, 1396–1406. doi: 10.1016/j.celrep.2015.10.006

Guelen, L., Pagie, L., Brasset, E., Meuleman, W., Faza, M. B., Talhout, W., et al. (2008). Domain organization of human chromosomes revealed by mapping of nuclear lamina interactions. *Nature* 453, 948–951. doi: 10.1038/nature06947

Harr, J. C., Luperchio, T. R., Wong, X., Cohen, E., Wheelan, S. J., and Reddy, K. L. (2015). Directed targeting of chromatin to the nuclear lamina is mediated by chromatin state and A-type lamins. *J. Cell Biol.* 208, 33–52. doi: 10.1083/jcb.201405110

Hastings, M. H., Maywood, E. S., and Brancaccio, M. (2018). Generation of circadian rhythms in the suprachiasmatic nucleus. *Nat. Rev. Neurosci.* 19, 453–469. doi: 10.1038/s41583-018-0026-z

Heinz, S., Benner, C., Spann, N., Bertolino, E., Lin, Y. C., Laslo, P., et al. (2010). Simple combinations of lineage-determining transcription factors prime cis-regulatory elements required for macrophage and B cell identities. *Mol. Cell* 38, 576–589. doi: 10.1016/j.molcel.2010.05.004

Hughes, M. E., DiTacchio, L., Hayes, K. R., Vollmers, C., Pulivarthy, S., Baggs, J. E., et al. (2009). Harmonics of circadian gene transcription in mammals. *PLoS Genet.* 5, e1000442. doi: 10.1371/journal.pgen.1000442

Kim, Y. H., Marhon, S. A., Zhang, Y., Steger, D. J., Won, K. J., and Lazar, M. A. (2018). Rev-erbalpha dynamically modulates chromatin looping to control circadian gene transcription. *Science* 359, 1274–1277. doi: 10.1126/science.aao6891

Koike, N., Yoo, S. H., Huang, H. C., Kumar, V., Lee, C., Kim, T. K., et al. (2012). Transcriptional architecture and chromatin landscape of the core circadian clock in mammals. *Science* 338, 349–354. doi: 10.1126/science.1226339

Korencic, A., Kosir, R., Bordyugov, G., Lehmann, R., Rozman, D., and Herzel, H. (2014). Timing of circadian genes in mammalian tissues. *Sci. Rep.* 4, 5782. doi: 10.1038/srep05782

Langmead, B., and Salzberg, S. L. (2012). Fast gapped-read alignment with Bowtie 2. *Nat. Methods* 9, 357–359. doi: 10.1038/nmeth.1923

Langmead, B., Trapnell, C., Pop, M., and Salzberg, S. L. (2009). Ultrafast and memory-efficient alignment of short DNA sequences to the human genome. *Genome Biol.* 10, R25. doi: 10.1186/gb-2009-10-3-r25

Lin, S. T., Zhang, L., Lin, X., Zhang, L. C., Garcia, V. E., Tsai, C. W., et al. (2014). Nuclear envelope protein MAN1 regulates clock through BMAL1. *Elife* 3, e02981. doi: 10.7554/eLife.02981

Liu, B., Ghosh, S., Yang, X., Zheng, H., Liu, X., Wang, Z., et al. (2012). Resveratrol rescues SIRT1-dependent adult stem cell decline and alleviates progeroid features in laminopathy-based progeria. *Cell Metab.* 16, 738–750. doi: 10.1016/j.cmet.2012.11.007

Lund, E., Oldenburg, A., Delbarre, E., Freberg, C., Duband-Goulet, I., Eskeland, R., et al. (2013). Lamin A/C-promoter interactions specify chromatin state-dependent transcription outcomes. *Genome Res.* 23, 1580–1589. doi: 10.1101/gr.159400.113

Lund, E. G., Oldenburg, A. R., and Collas, P. (2014). Enriched Domain Detector: a program for detection of wide genomic enrichment domains robust against local variations. *Nucleic Acids Res.* 42, e92. doi: 10.1093/nar/gku324

Masri, S., Rigor, P., Cervantes, M., Ceglia, N., Sebastian, C., Xiao, C., et al. (2014). Partitioning circadian transcription by SIRT6 leads to segregated control of cellular metabolism. *Cell* 158, 659–672. doi: 10.1016/j.cell.2014.06.050

Mermet, J., Yeung, J., Hurni, C., Mauvoisin, D., Gustafson, K., Jouffe, C., et al. (2018). Clock-dependent chromatin topology modulates circadian transcription and behavior. *Genes Dev.* 32, 347–358. doi: 10.1101/gad.312397.118

Meuleman, W., Peric-Hupkes, D., Kind, J., Beaudry, J. B., Pagie, L., Kellis, M., et al. (2013). Constitutive nuclear lamina–genome interactions are highly conserved and associated with A/T-rich sequence. *Genome Res.* 23, 270–280. doi: 10.1101/gr.141028.112

Naetar, N., Ferraioli, S., and Foisner, R. (2017). Lamins in the nuclear interior — life outside the lamina. *J. Cell Sci.* 130, 2087–2096. doi: 10.1242/jcs.203430

Nakahata, Y., Kaluzova, M., Grimaldi, B., Sahar, S., Hirayama, J., Chen, D., et al. (2008). The NAD+-dependent deacetylase SIRT1 modulates CLOCK-mediated chromatin remodeling and circadian control. *Cell* 134, 329–340. doi: 10.1016/j.cell.2008.07.002

Neph, S., Kuehn, M. S., Reynolds, A. P., Haugen, E., Thurman, R. E., Johnson, A. K., et al. (2012). BEDOPS: high-performance genomic feature operations. *Bioinformatics* 28, 1919–1920. doi: 10.1093/bioinformatics/bts277

Pascual-Reguant, L., Blanco, E., Galan, S., Le Dily, F., Cuartero, Y., Serra-Bardenys, G., et al. (2018). Lamin B1 mapping reveals the existence of dynamic and functional euchromatin lamin B1 domains. *Nat. Commun.* 9, 3420. doi: 10.1038/s41467-018-05912-z

Paulsen, J., Liyakat Ali, T. M., Nekrasov, M., Delbarre, E., Baudement, M. O., Kurscheid, S., et al. (2019). Long-range interactions between topologically associating domains shape the four-dimensional genome during differentiation. *Nat. Genet.* 51, 835–843. doi: 10.1038/s41588-019-0392-0

Peric-Hupkes, D., Meuleman, W., Pagie, L., Bruggeman, S. W., Solovei, I., Brugman, W., et al. (2010). Molecular maps of the reorganization of genome–nuclear lamina interactions during differentiation. *Mol. Cell* 38, 603–613. doi: 10.1016/j.molcel.2010.03.016

Poleshko, A., Shah, P. P., Gupta, M., Babu, A., Morley, M. P., Manderfield, L. J., et al. (2017). Genome–nuclear lamina interactions regulate cardiac stem cell lineage restriction. *Cell* 171, 573–587. doi: 10.1016/j.cell.2017.09.018

Quinlan, A. R., and Hall, I. M. (2010). BEDTools: a flexible suite of utilities for comparing genomic features. *Bioinformatics* 26, 841–842. doi: 10.1093/bioinformatics/btq033

Robinson, J. T., Thorvaldsdottir, H., Winckler, W., Guttman, M., Lander, E. S., Getz, G., et al. (2011). Integrative genomics viewer. *Nat. Biotechnol.* 29, 24–26. doi: 10.1038/nbt.1754

Robson, M. I., de Las Heras, J. I., Czapiewski, R., Le Thanh, P., Booth, D. G., Kelly, D. A., et al. (2016). Tissue-specific gene repositioning by muscle nuclear membrane proteins enhances repression of critical developmental genes during myogenesis. *Mol. Cell* 62, 834–847. doi: 10.1016/j.molcel.2016.04.035

Robson, M. I., de Las Heras, J. I., Czapiewski, R., Sivakumar, A., Kerr, A. R. W., and Schirmer, E. C. (2017). Constrained release of lamina-associated enhancers and genes from the nuclear envelope during T-cell activation facilitates their association in chromosome compartments. *Genome Res.* 27, 1126–1138. doi: 10.1101/gr.212308.116

Rønningen, T., Shah, A., Oldenburg, A. R., Vekterud, K., Delbarre, E., Moskaug, J. O., et al. (2015). Prepatterning of differentiation-driven nuclear lamin A/C-associated chromatin domains by GlcNAcylated histone H2B. *Genome Res.* 25, 1825–1835. doi: 10.1101/gr.193748.115

Sen Gupta, A., and Sengupta, K. (2017). Lamin B2 Modulates Nucleolar Morphology, Dynamics, and Function. *Mol. Cell Biol.* 37, e00274–e00217. doi: 10.1128/MCB.00274-17

Shachar, S., Voss, T. C., Pegoraro, G., Sciascia, N., and Misteli, T. (2015). Identification of gene positioning factors using high-throughput imaging mapping. *Cell* 162, 911–923. doi: 10.1016/j.cell.2015.07.035

Shi, G., Xie, P., Qu, Z., Zhang, Z., Dong, Z., An, Y., et al. (2016). Distinct roles of HDAC3 in the core circadian negative feedback loop are critical for clock function. *Cell Rep.* 14, 823–834. doi: 10.1016/j.celrep.2015.12.076

Solovei, I., Wang, A. S., Thanisch, K., Schmidt, C. S., Krebs, S., Zwerger, M., et al. (2013). LBR and lamin A/C sequentially tether peripheral heterochromatin and inversely regulate differentiation. *Cell* 152, 584–598. doi: 10.1016/j.cell.2013.01.009

Somech, R., Shaklai, S., Geller, O., Amariglio, N., Simon, A. J., Rechavi, G., et al. (2005). The nuclear-envelope protein and transcriptional repressor LAP2beta interacts with HDAC3 at the nuclear periphery, and induces histone H4 deacetylation. *J. Cell Sci.* 118, 4017–4025. doi: 10.1242/jcs.02521

Tahara, Y., Otsuka, M., Fuse, Y., Hirao, A., and Shibata, S. (2011). Refeeding after fasting elicits insulin-dependent regulation of Per2 and Rev-erbalpha with shifts in the liver clock. *J. Biol. Rhythms* 26, 230–240. doi: 10.1177/0748730411405958

Takahashi, J. S. (2017). Transcriptional architecture of the mammalian circadian clock. *Nat. Rev. Genet.* 18, 164–179. doi: 10.1038/nrg.2016.150

Trapnell, C., Williams, B. A., Pertea, G., Mortazavi, A., Kwan, G., van Baren, M. J., et al. (2010). Transcript assembly and quantification by RNA-Seq reveals unannotated transcripts and isoform switching during cell differentiation. *Nat. Biotechnol.* 28, 511–515. doi: 10.1038/nbt.1621

van Steensel, B., and Belmont, A. S. (2017). Lamina-associated domains: links with chromosome architecture, heterochromatin, and gene repression. *Cell* 169, 780–791. doi: 10.1016/j.cell.2017.04.022

Vollmers, C., Schmitz, R. J., Nathanson, J., Yeo, G., Ecker, J. R., and Panda, S. (2012). Circadian oscillations of protein-coding and regulatory RNAs in a highly dynamic mammalian liver epigenome. *Cell Metab.* 16, 833–845. doi: 10.1016/j.cmet.2012.11.004

Wu, G., Anafi, R. C., Hughes, M. E., Kornacker, K., and Hogenesch, J. B. (2016). MetaCycle: an integrated R package to evaluate periodicity in large scale data. *Bioinformatics* 32, 3351–3353. doi: 10.1093/bioinformatics/btw405

Xu, Y., Guo, W., Li, P., Zhang, Y., Zhao, M., Fan, Z., et al. (2016). Long-range chromosome interactions mediated by cohesin shape circadian gene expression. *PLoS Genet.* 12, e1005992. doi: 10.1371/journal.pgen.1005992

Yeung, J., Mermet, J., Jouffe, C., Marquis, J., Charpagne, A., Gachon, F., et al. (2018). Transcription factor activity rhythms and tissue-specific chromatin interactions explain circadian gene expression across organs. *Genome Res.* 28, 182–191. doi: 10.1101/gr.222430.117

Yeung, J., and Naef, F. (2018). Rhythms of the Genome: Circadian dynamics from chromatin topology, tissue-specific gene expression, to behavior. *Trends Genet.* 34, 915–926. doi: 10.1016/j.tig.2018.09.005

Zhang, Y., Fang, B., Emmett, M. J., Damle, M., Sun, Z., Feng, D., et al. (2015). Discrete functions of nuclear receptor Rev-erbalpha couple metabolism to the clock. *Science* 348, 1488–1492. doi: 10.1126/science.aab3021

Zhao, H., Sifakis, E. G., Sumida, N., Millan-Arino, L., Scholz, B. A., Svensson, J. P., et al. (2015). PARP1- and CTCF-mediated interactions between active and repressed chromatin at the lamina promote oscillating transcription. *Mol. Cell* 59, 984–997. doi: 10.1016/j.molcel.2015.07.019

Zhu, B., Zhang, Q., Pan, Y., Mace, E. M., York, B., Antoulas, A. C., et al. (2017). A Cell-autonomous mammalian 12 hr clock coordinates metabolic and stress rhythms. *Cell Metab.* 25, 1305–1319 e1309. doi: 10.1016/j.cmet.2017.05.004

Zullo, J. M., Demarco, I. A., Pique-Regi, R., Gaffney, D. J., Epstein, C. B., Spooner, C. J., et al. (2012). DNA sequence-dependent compartmentalization and silencing of chromatin at the nuclear lamina. *Cell* 149, 1474–1487. doi: 10.1016/j.cell.2012.04.035

Supplementary information

Supplementary Table S1. RT-qPCR and ChIP-qPCR primers used in this study.
Supplementary Table S2. LAD detection parameters using EDD.
Supplementary Table S3. MetaCycle analysis of expression of central clock regulators and *Lmnb1* determined by RT-qPCR and RNA-seq.
Supplementary Table S4. Lists of periodic and non-periodic genes. (Excel; classifiable lists-Supplementary Table 4)
Supplementary Table S5. Periodic genes classified by phase within periods. (Excel - Supplementary Table 5)
Supplementary Table S6. Gene ontology terms enriched for periodic genes.
Supplementary Table S7. Analysis of LAD intersects.
Supplementary Table S8. Characterization of periodic LADs by MetaCycle. (Excel; classifiable lists - Supplementary Table 8)
Supplementary Table S9. Distances between central clock-regulating genes and nearest LADs.

Supplementary Table S1. RT-qPCR and ChIP-qPCR primers used in this study.

Amplicon	Chr.	Forward primer (F) / Reverse primer (R)	mm10 Genomic position (nt)
RT-qPCR primers			
Clock	11	F: CCTAGAAAATCTGGCAAAATGTCA R: CCTTTTCCATATTGCATTAAGTGCT	
Per1	1	F: ACCAGCGTGTCATGATGACATA R: GTGCACAGCACCCAGTTCCC	
Arntl	5	F: GCAGTGCCACTGACTACCAAGA R: TCCTGGACATTGCATTGCAT	
Nr1d1	2	F: CTGGAGGGCTGCAGTATAGC R: CGGTCATTCAAACTGGACCT	
Cry1	16	F: CAGACTCACTCACTCAAGCAAGG R: TCAGTTACTGCTCTGCCGCTGGAC	
Eif2a	3	F: CAACGTGGCAGCCTTACA R: TTTCATGTCATAAAGTTGTAGGTTAGG	
ChIP-qPCR primers			
cLAD-1 chr.11	11	F: TAACCACCGTGTCTCTAAGCG R: TCCGGTGTGACTTAGCATGA	chr11:81201226-81201309
cLAD-1 chr.1	1	F: GCCACCAACATGGAGTCAGA R: CAGGCTCTGAATGGAGCCAA	chr1:190487280-190487361
cLAD-1 chr.5	5	F: TGCTGTGAGCATTTGGTCCT R: GCCTCCACCTCAGTCACTTC	chr5:126224330-126224438
cLAD-1 chr.2	2	F:CCTGACTTTTACCGTCCCAATC R: TGCTACTACACAAGGCCCCAA	chr2:156231214-156231331
cLAD-1 chr.16	16	F: GTTTTTCATCGGACGGTGGC R: CCGCCGCTCATACACCATAA	chr16:10796381-10796520
cLAD-2 chr.1	1	F: CCACAGCATCCCAGTTTCCT R: CAGGGACCTTCCAGGTTTCC	chr1:113441259-113441360
cLAD-2 chr.5	5	F: TCTCTGCCACAGACTGCAAG R: GCCTTCTGGTCTCCTGCTTT	chr5:55584684-55584784
cLAD-1 chr.12	12	F: AGCTCCTTGTCTTGCCTGTC R: AGAATAGCGAGTGCCCAACC	chr12:47158301-47158371
cLAD-2 chr.16	16	F: TGGAGTTCTGCAAGGCTGAG R: ACTGCTTGCTGCTCTCCTTT	chr16:82996670-82996796
vLAD chr.1	1	F: GGTGGCATCAGCTCCAAAGT R: AGCTTTTATTTTCTCAAAGGCAGGT	chr1:123423631-123423729
vLAD chr.5	5	F: CAGTTGCTGGGACTGTAGCA R: AAAGTGTGAGCCCAGGATGG	chr5:48143370-48143444
vLAD chr.12	12	F: GAGGAGCAAACCTGTTCCCA R: AGCTTTTACTCTGTGCCCCC	chr12:38104881-38105004
vLAD chr.16	16	F: TCCCCAGCAACATTCCAGAC R: AGCAACAAATGTGCAGGCAG	chr16:39947233-39947346
nonLAD chr.6 (*Gadh* promoter)	6	F: GTTGCACTGGCCTAGCAAAG R: GACCGGGATTCTTCACTCCG	chr6:125166811-125166927
nonLAD chr.7	7	F: CACCGGCTTCACCGAATACT R: GGAGAGAAACGGGGGTTCCG	chr7:25315585-25315719
nonLAD chr.11 (*Ube2b* promoter)	11	F: GCCGAACTTGAAACTAGCGAC R: GTTGCTTGCGGGCAACTACG	chr11:52000592-52000714
nonLAD chr.18 (*Lmnb1* promoter)	18	F: GGTCAAGTCATTGGTGGGCT R: TCATTGGCTATGAACGCGGA	chr18:56707121-56707212

cLAD, constitutive LAD; vLAD, variable LAD.

Supplementary Table S2. LAD detection parameters using EDD.

		NS		T0		T6		T12		T18		T24		T30	
		Rep1	Rep2	Rep1	Rep2	Rep1	Rep2	Rep1	Rep2	Rep1	Rep2	Rep1	Rep2	Rep1	Rep2
EDD parameters	Mean(BinSize) (bp)	61000	4000	47000	4000	35000	11000	1000	5000	19000	6000	14000	18000	31000	46000
	Mean(GapPenalty)	3.70	6.20	3.50	5.00	4.40	4.30	4.10	6.40	3.60	3.60	3.50	4.20	4.00	5.00
	StdDev(GapPenalty)	1.20	0.50	0.40	0.20	0.80	0.50	0.40	0.10	0.40	0.10	0.30	0.30	0.80	1.60
	Edd Error (Mb)	0.98	1.24	0.11	0.16	0.95	0.30	0.11	0.12	0.46	0.19	0.34	0.51	0.78	0.69
# RemovedLADs		0	79	0	39	0	4	4	39	0	13	0	0	0	0
# LADs in replicates		74	372	97	320	130	280	242	300	154	346	179	183	138	127
# LADs in intersect		93		111		153		225		198		163		111	

Supplementary Table S3. MetaCycle analysis of expression of central clock regulators and *Lmnb1* determined by RT-qPCR and RNA-seq.

	Gene	P-value ID	P-value	Period ID	Period	Phase	Base	Amplitude
RT-qPCR	*Lmnb1*	Non-Significant	9.8E-01	12h	13.7	13.2	0.3	0.0
	Clock	Periodic	4.7E-04	24h	23.7	23.6	0.9	0.6
	Arntl	Periodic	3.1E-10	24h	23.1	22.3	0.5	0.5
	Cry1	Periodic	1.7E-06	24h	22.7	19.7	3.9	3.5
	Per1	Non-Significant	7.2E-02	18h	15.0	13.7	0.3	0.4
	Nr1d1	Periodic	5.1E-11	24h	23.8	7.9	0.9	1.1
RNA-seq	*Lmnb1*	Non-Significant	1.6E-01	12h	12.0	6.7	6.5	0.6
	Clock	Periodic	4.6E-06	24h	22.8	1.0	17.3	4.7
	Arntl	Periodic	2.1E-06	24h	23.0	0.0	17.0	14.2
	Cry1	Periodic	1.2E-08	24h	23.0	19.9	23.1	14.3
	Cry2	Non-Significant	1.4E-02	18h	18.0	9.6	26.4	1.6
	Per1	Non-Significant	2.1E-01	18h	18.7	13.6	14.1	11.9
	Per2	Periodic	2.7E-07	30h	29.3	14.3	17.7	11.3
	Per3	Periodic	3.0E-06	24h	23.9	14.1	13.1	10.1
	Nr1d1	Periodic	7.1E-06	24h	24.4	8.2	41.7	39.7
	Nr1d2	Periodic	1.7E-03	24h	24.2	11.3	24.2	10.6
	Rorc	Periodic	3.2E-05	30h	28.0	19.7	50.6	19.9
	Ube2b	Non-Significant	1.3E-01	24h	21.1	15.8	43.6	0.4

For MetaCycle analysis, see Main text; these values are used for best-fits. Function used for best-fit:
$F[x] = Amplitude*Cos[(2\pi/Period)(x - Phase)] + Base$.

Supplementary Table S6. Gene ontology terms enriched for periodic genes.

| PANTHER GO-Slim Biological Process	No. genes in ref. genome	No. genes in GO term	Expected No. genes	Fold Enrichment	P-value	FDR	Over/under representation
12h period							
DNA repair	153	8	1.4	5.73	1.12E-04	9.08E-03	+
regulation of biological process	3320	12	30.27	0.4	9.70E-05	1.18E-02	-
nitrogen compound metabolic process	2462	42	22.45	1.87	7.02E-05	1.71E-02	+
nucleobase-containing metabolic process	2710	42	24.71	1.7	5.41E-04	2.20E-02	+
cellular component biogenesis	733	17	6.68	2.54	4.89E-04	2.39E-02	+
RNA metabolic process	1536	28	14.01	2	4.64E-04	2.83E-02	+
18h period							
None							
24h period							
rhythmic process	13	4	0.15	27.4	3.15E-05	2.57E-03	+
circadian rhythm	13	4	0.15	27.4	3.15E-05	3.85E-03	+
metabolic process	6009	98	67.48	1.45	3.05E-05	7.44E-03	+
sensory perception of smell	699	0	7.85	< 0.01	6.84E-04	2.78E-02	-
sensory perception of chemical stimulus	748	0	8.4	< 0.01	4.84E-04	2.95E-02	-
G-protein coupled receptor signaling pathway	875	1	9.83	0.1	8.52E-04	2.97E-02	-
protein localization	494	15	5.55	2.7	6.09E-04	2.97E-02	+
30h period							
DNA binding transcription factor activity	34	5	0.27	18.29	1.41E-05	3.44E-03	+
regulation of molecular function	436	12	3.51	3.42	2.67E-04	3.25E-02	+
Non-periodic							
None							

+, over-representation; -, under-representation.

Supplementary Table S7. Analysis of LAD intersects.

|	NS		T0		T6		T12		T18		T24		T30	
	Rep1	Rep2	Rep1	Rep2	Rep1	Rep2	Rep1	Rep2	Rep1	Rep2	Rep1	Rep2	Rep1	Rep2
	vs. Intersect	vs. Intersect	vs. Intersect	vs. Intersect	vs. Intersect	vs. Intersect	vs. Intersect	vs. Intersect	vs. Intersect	vs. Intersect	vs. Intersect	vs. Intersect	vs. Intersect	vs. Intersect
LAD size variation (Mb)	001	001	001	001	000	001	000	000	000	001	001	001	001	001
LAD coverage per replicate (Mb)	335.29	526.51	423.75	574.97	495.17	584.04	586.34	553.19	617.87	662.99	631.35	540.44	405.39	392.37
LAD coverage (intersect) (Mb)	258.87		339.59		434.22		496.13		515.81		474.77		311.99	

Supplementary Table S9. Distance between central clock-regulating genes and nearest LADs.

| Gene	Chr.	Dist. 5' end of gene to LAD (Mb)	Dist. 3' end of gene to LAD (Mb)
Clock	5	-4.2	+1.6
Arntl (Bmal1)	7	-5.2	no LAD
Cry1	10	-10.8	+12.6
Per1	11	-20.8	+21.6
Per2	1	-41.4	+2.7
Per3	4	-3.2	no LAD
Nr1d1	11	-5.3	no LAD
Nr1d2	14	-10.5	+19.3
Rorc	3	-1.5	+15.7
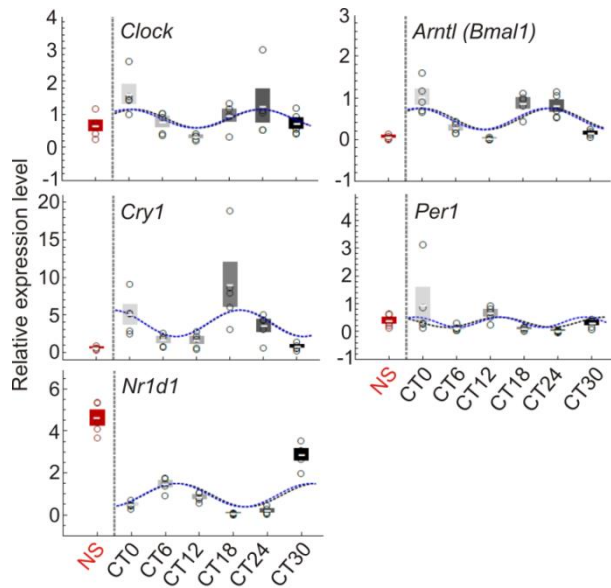
Supplementary Figure S1. Circadian expression of central clock genes. RT-qPCR analysis of expression of clock genes in non-synchronized (NS) mice and from CT0 to CT30 (mean ± SD, single data points; n = 5 mice at NS and per CT). Blue line, MetaCycle best-fit from RT-qPCR data; black line, MetaCycle best-fit from RNA-seq data; note the strong overlap between the two. Amplitude and base values used for both fits are from RT-qPCR MetaCycle analysis.
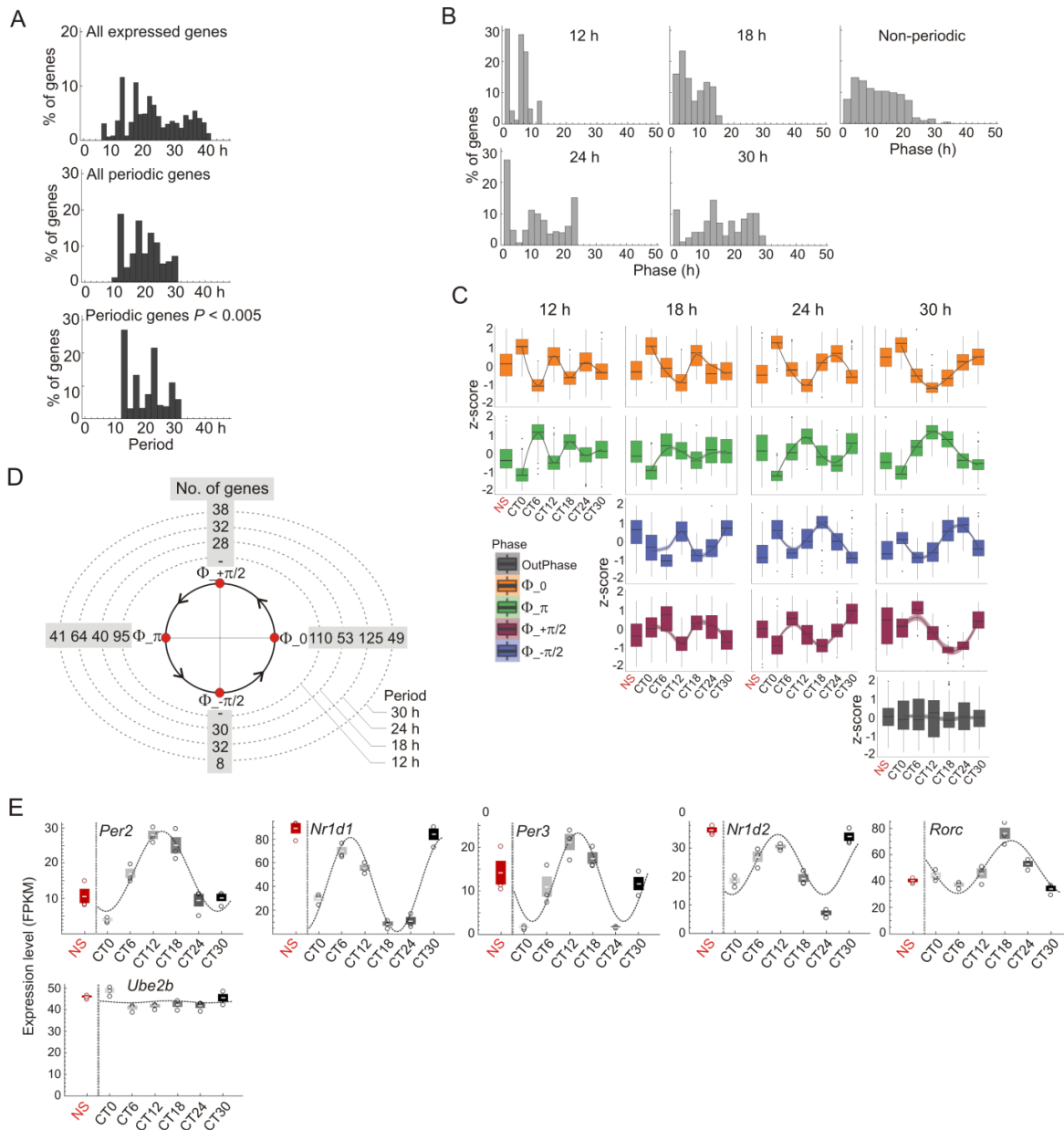
Supplementary Figure S2. Characterization of periodic gene expression in liver. **(A)** Period distribution of all 17,330 expressed genes, all periodic genes and significantly ($P < 0.005$; Fisher's exact test) periodic genes. **(B)** Phase distribution of periodic genes (x axis), shown as % of genes in indicated periods. **(C)** Expression of periodic genes according to their phase (median, upper/lower quartiles, maxima/minima and smoothing of medians ± SD). **(D)** Trigonometric clock and number of significantly ($P < 0.005$) periodic genes with indicated period (circle dotted lines) and phase (central circular axis). **(E)** RNA-seq analysis of circadian expression of central clock genes and the housekeeping gene *Ube2b* (n = 3 mice per CT; mean ± SD, individual data points). Cosine curves in are best-fits from MetaCycle; fitting function F[x] = Amplitude*Cos[(2π/Period) (x - Phase)] + Base; see **Supplementary Table S3**.
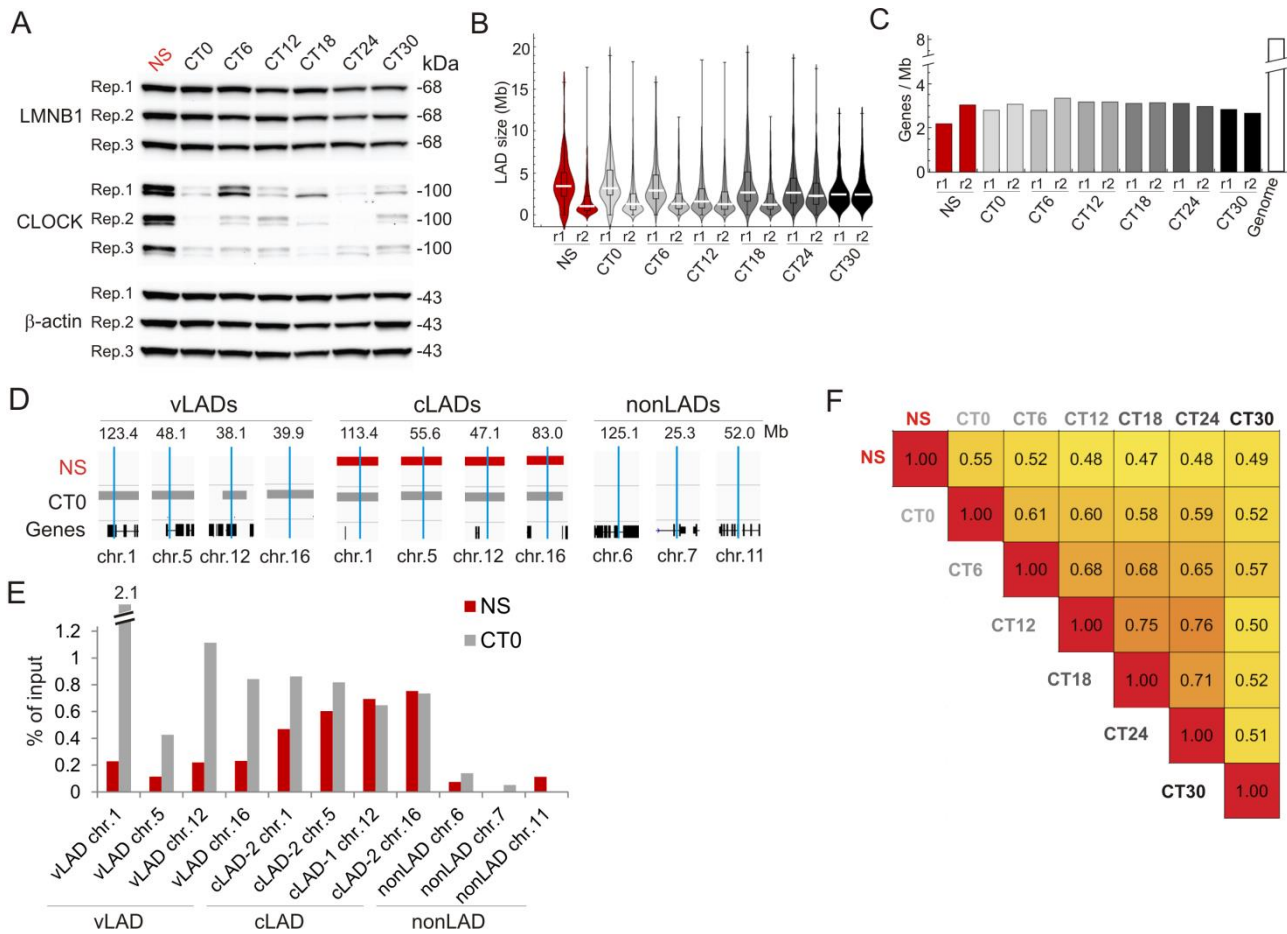
Supplementary Figure S3. Characterization of LMNB1 LADs during the circadian cycle. **(A)** Western blots of LMNB1 and CLOCK expression; β-actin was used as loading control (biological triplicate). Each replicate blot (Rep.1/2/3) is from the liver of one mouse per CT. **(B)** Median (white bars) and violin plot distribution of LAD sizes for each CT and biological replicate (r1, r2). **(C)** Gene density in LADs and in the mm10 genome. **(D)** Genome browser views of variable LAD (vLAD), constitutive LAD (cLAD) and nonLAD regions at NS and CT0, with position of amplicons (blue bars, in Mb on indicated chromosomes; bottom) analyzed by ChIP-qPCR in (E). **(E)** ChIP-qPCR analysis of LMNB1 enrichment in indicated vLAD, cLAD and nonLAD regions; see **Supplementary Table S1** for position of amplicons. **(F)** Jaccard indices of LAD coverage overlap between CTs (values are for for LAD intersects of both replicates at each CT).
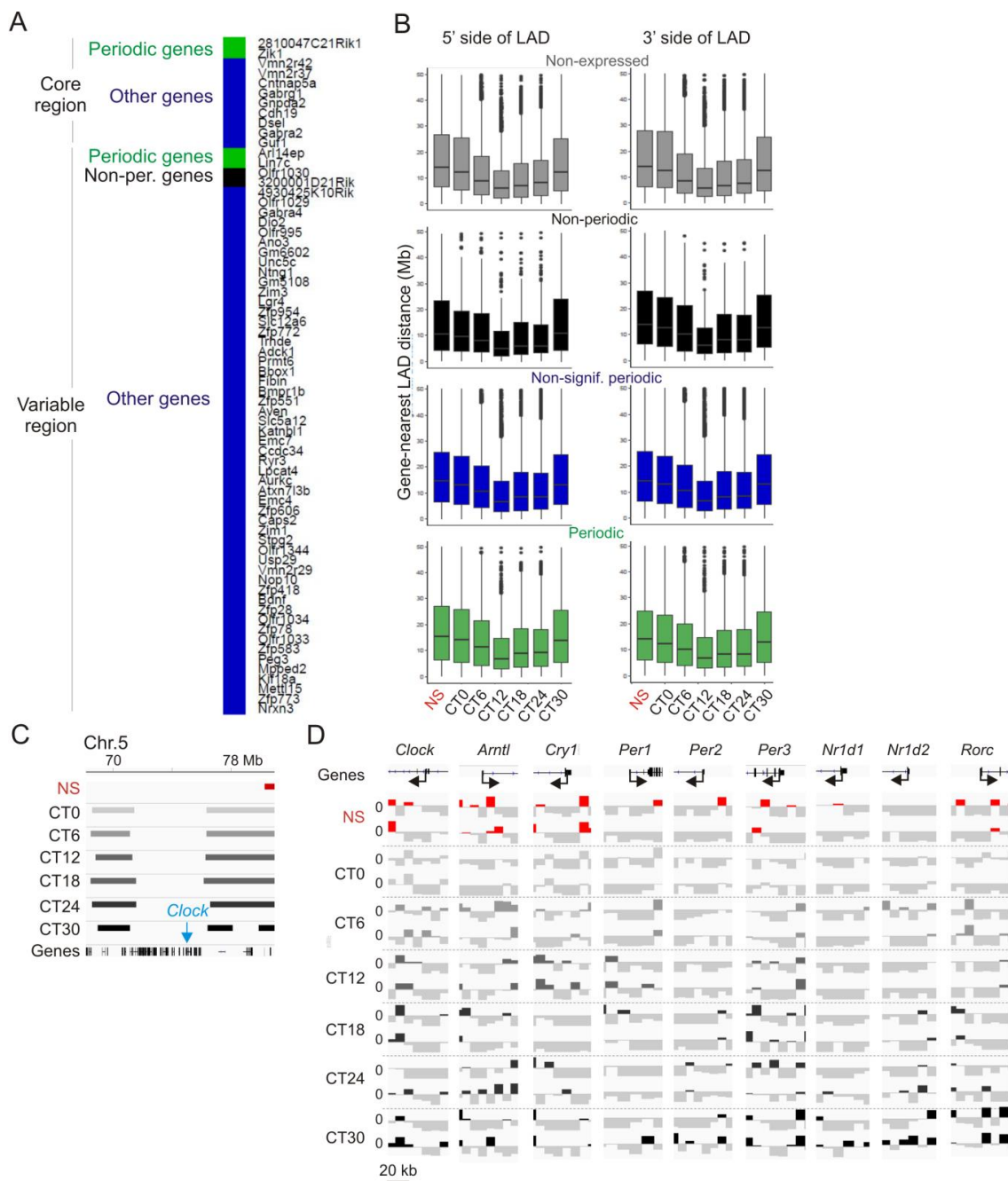
Supplementary Figure S4. Gene-to-nearest LAD distances are uncoupled from periodic gene expression. **(A)** List of genes in periodic LADs, classified in the core and variable regions in **Figure 5B**. **(B)** Box plots of variation in gene-to-nearest LAD distance at the 5' and 3' sides of LADs (median, upper/lower quartiles, maxima/minima); data are shown for non-expressed genes (n = 4820), non-periodic genes (n = 204), non-significantly periodic genes (n = 15685) and periodic genes (n = 1441). **(C)** Genome browser view of LADs in a fragment of chromosome 5 showing *Clock* between two LADs. **(D)** The transcription start site (arrow) of central clock-control genes is devoid of LMNB1 interaction detectable by ChIP. The panel shows genome browser views of LMNB1 enrichment in promoter regions for each ChIP replicate and CT. Data are shown for 10 kb bins, as log2(ChIP/input) ratios (y axis, scale: -0.3 to +0.3).

Errata

Candidate: Anna Frida Forsberg

Title of thesis: Modulation of nuclear lamin-chromatin interactions by external cues

Page	Line	Original text	Corrected text
5	3	From[8].	From[8] by permission of Oxford University Press.
5	3-4	Adapted from[1].	Adapted from[1] with copyright permission.
8	4-5	From[33].	Republished from[33] with copyright permission under the creative commons attribution (CC BY) license.
8	6-7	From[33].	Republished from[33] with copyright permission under the creative commons attribution (CC BY) license.
8	8-9	From[58].	Republished with permission of Annual Reviews, Inc from[58].
10	17-18	From[76].	From[76], reprinted with permission from AAAS.
10	19	From[76].	From[76], reprinted with permission from AAAS.
15	8-9	From[100].	Reprinted with copyright permission by Springer Nature from[100].
15	10	From[104].	Reprinted from[104] with permission from Elsevier.
18	26-27	limiting its application to cell systems	limiting its application in cell systems
30	4	From[234].	From[234], reprinted with permission from AAAS.
44	5-6	From[192].	Republished from[192] with copyright permission under the creative commons attribution (CC BY) license.
46	7	From[189]	Reprinted from[189] with permission from Elsevier.